DOKUZ EYLÜL UNIVERSITY

GARADUATE SCHOLL OF NATURAL AND APPLIED SCIENCES

FINITE ELEMENT ANALYSIS OF A VERTICAL MACHINING CENTER WITH ALUMINUM PROFILE FRAMING

by

Serkan GÜLER

June, 2013

İZMİR

FINITE ELEMENT ANALYSIS OF A VERTICAL MACHINING CENTER WITH ALUMINUM PROFILE FRAMING

A Thesis Submitted to the
Graduate School of Natural and Applied Sciences of Dokuz Eylül University
In Partial Fulfillment of the Requirements for the
Degree of Doctor of Philosophy in
Machine Theory and Dynamics Program

by
Serkan GÜLER

June, 2013
İZMİR

Ph.D. THESIS EXAMINATION RESULT FORM

We have read the thesis entitled **"FINITE ELEMENT ANALYSIS OF A VERTICAL MACHINING CENTER WITH ALUMINUM PROFILE FRAMING"** completed by **SERKAN GÜLER** under supervision of **PROF. DR. HİRA KARAGÜLLE** and we certify that in our opinion it is fully adequate, in scope and in quality, as a thesis for the degree of Doctor of Philosophy.

Prof.Dr. Hira KARAGÜLLE

Supervisor

Assoc.Prof.Dr. Zeki KIRAL

Thesis Committee Member

Assist.Prof.Dr. Ahmet ÖZKURT

Thesis Committee Member

Prof.Dr. Hakan BOYACI

Examining Committee Member

Assoc.Prof.Dr. Hasan ÖZTÜRK

Examining Committee Member

Prof. Dr. Ayşe OKUR

Director

Graduate School of Natural and Applied Sciences

ACKNOWLEDGEMENTS

FINITE ELEMENT ANALYSIS OF AVERTICAL MACHINING CENTER WITH ALUMINUM PROFILE FRAMING

ABSTRACT

Nowadays, vertical machining centers are extensively used in industrial applications. Therefore, importance of design and analysis of vertical machining centers is increasing. Machine designers are commonly used computer aided engineering methods in the design process. In this study, for a vertical machining center with aluminum profile framing, a finite element model developed and finite element analyses are employed.

Vibration analysis is a method which has been widely used in structural engineering for determining structural modal parameters, such as natural frequencies, mode shapes, etc. In this study, vibration analysis of a vertical machining center which constructed with modular aluminum profile systems is considered. For the vibration analysis, finite elements method is used. A finite elements model of the vertical machining center is developed by using ANSYS parametric design language (APDL). Then, vibration analysis results have been obtained. To validate accuracy of the finite element model experimental modal testing is carried out.

Vibrations arisen after the motion is called residual vibrations. Residual vibrations significantly affect positioning achievement of the end point in flexible systems. To control the residual vibrations of the vertical machining center, trapezoidal velocity profile is applied with open loop control both experimentally and numerically.

Keywords: Vertical machining center, aluminum profile, computer aided engineering, finite elements method, residual vibrations.

ALİMİNYUM PROFİL GÖVDELİ BİR DİK İŞLEM MERKEZİNİN SONLU ELEMANLARLA ANALİZİ

ÖZ

Günümüzde, dik işlem merkezleri endüstriyel uygulamalarda yaygın olarak kullanılmaktadır. Bu sebeple dik işlem merkezlerinin tasarım ve analizlerinin önemi artmaktadır. Makina tasarımcıları tasarım işlemlerinde bilgisayar destekli mühendislik yöntemlerini sıklıkla kullanmaktadırlar. Bu çalışmada alüminyum gövdeli bir dik işlem merkezi için bir sonlu eleman modeli geliştirilmiş ve sonlu eleman analizleri yapılmıştır.

Titreşim analizi; doğal frekanslar, titreşim biçimleri vb. gibi yapısal modal parametreleri belirlemek için yapısal mühendislikte yaygın kullanılan bir yöntemdir. Bu çalışmada bir dik işlem merkezinin titreşim analizi ele alınmıştır. Titreşim analizi için sonlu elemanlar yöntemi kullanılmıştır. ANSYS parametrik tasarım dili kullanılarak dik işlem merkezinin bir sonlu elemanlar modeli geliştirilmiştir. Sonra titreşim analizi sonuçları elde edilmiştir. Sonlu eleman modelini doğrulamak için deneysel modal testler yapılmıştır.

Hareket sonrası oluşan titreşimler artık titreşimler olarak adlandırılmaktadır. Artık titreşimler, esnek sistemlerde uç nokta konumlandırılmasında oldukça etkilidir. Dik işlem merkezinin artık titreşimlerini kontrol etmek için açık kontrol ile trapez hız profili hem deneysel hem de numerik olarak uygulanmıştır.

Anahtar Sözcükler: Dik işlem merkezi, alüminyum profil, bilgisayar destekli mühendislik, sonlu elemanlar analizi, artık titreşimler.

CONTENTS

LIST OF FIGURES

LIST OF TABLES

CHAPTER ONE

INTRODUCTION

1.1 Introduction

Numerical control machines first appeared in the fifties and CNC machines in the seventies. There are many applications for CNC machines in the area of material removal. The very early NC machines were simple drilling machines which just provided point-to-point movement in the horizontal plane and linear movement in the vertical plane. Numerically controlled drilling operations are now generally carried out on milling machine or machining centers. Numerically controlled machining centers are available in two configurations: vertical and horizontal as depicted in Figure1.1 (Tizzard, 1994).
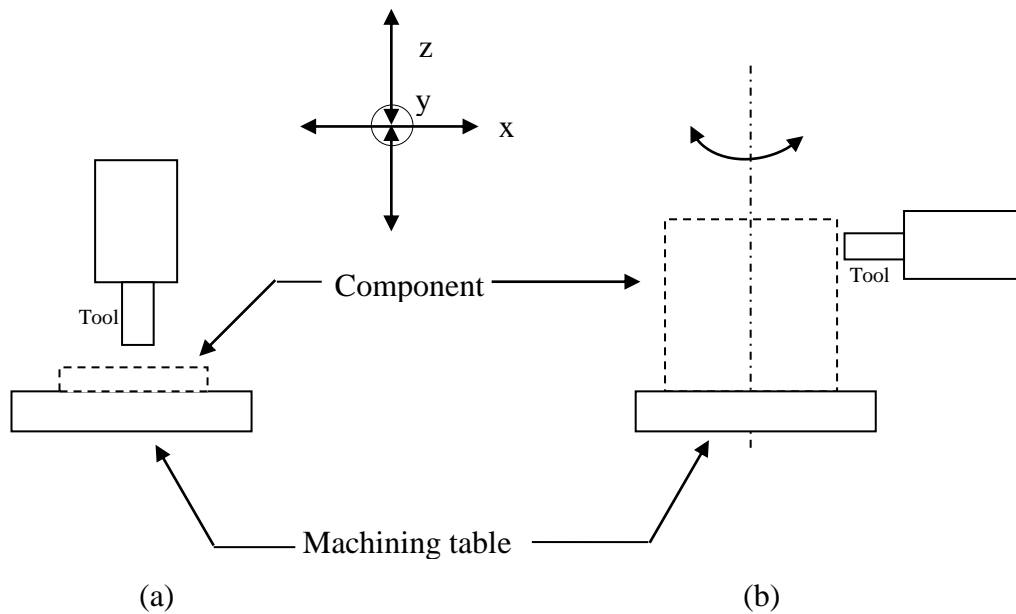
Figure 1.1 CNC machining centers: (a) vertical; (b) horizontal.

In this study, a three-axis vertical machining center which constructed with modular aluminum profile systems to use in medical operations is designed and analyzed.

1.2 CNC Machines

The American Electronics Industries Association describes numerical control (NC) as "A system in which actions are controlled by the direct insertion of numerical data at some point. The system must automatically interpret at least some portion of this data." (Code of Federal Regulations, 1986, p636). CNC machines are extensively used for drilling, milling, turning, laser cutting, water jet cutting, picking and placing, and welding processes.

The metal working equipment industry was slow to catch on. In 1949 the first tape controlled toolmakers lathe was demonstrated, but there was no interest. It was the computation and measurement of the curved surface of a helicopter rotor blade that sparked the original N/C concept. Between 1949 and 1952 The Parsons Corporation and M.I.T., under the sponsorship of the US Air Force, constructed an experimental milling machine to prove the possibility of contour milling. In order for N/C to be made practical it was necessary for the electronics industry to expand and it did at a rapid rate. In 1952 the first successful 3 axis demonstration was made (see in Figure 1.2.) (Anonymous, n.d.).
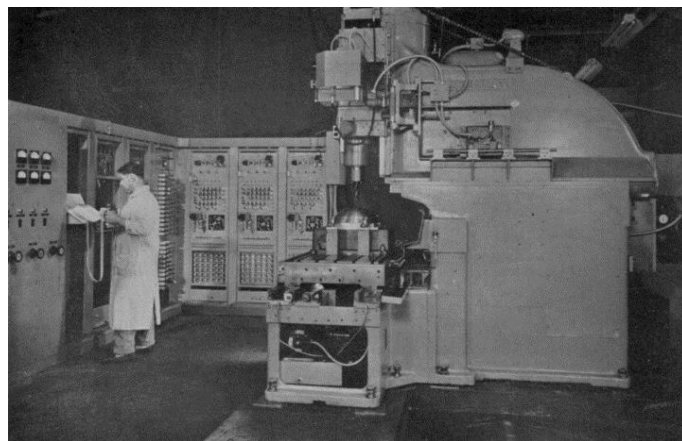
Figure 1.2 The first NC machine was developed by M.I.T.

Therefore, many manufacturers of machine tools began to produce the NC machines. It was necessary to develop the computer technologies for constructing the CNC machines though NC machines were developed. In parallel with developments

in computer technologies, CNC machines showed rapid growth. Today, drilling, milling, turning, laser cutting, water jet cutting, picking and placing, and welding processes can be easily carried out according to developments in the CNC machines.

There are many different types of CNC machines used in industry; some of them are listed below.
- Lathe Machine
- Milling Machine
- Boring Machine
- Grinding Machine
- Vertical Machining Center
- Laser and Water-Jet Cutting Machines

1.2.1 Vertical Machining Centers

Vertical machining center are widely used in many industrial operations such as drilling, milling, laser cutting, and water-jet cutting.

Yamaguchi, S.Y., Nishiyama, N.S., Maeda, K.N., Miyoshi, Y.M. (1989) patented the vertical machining center (see Figure 1.3) in USA. The patent is stated following paragraph.
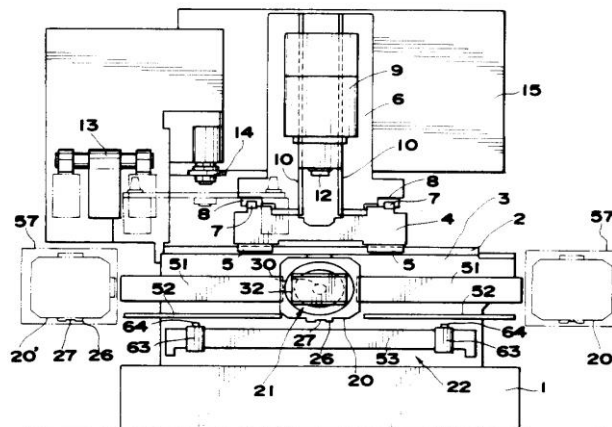
Figure 1.3 Vertical machining center (Vertical machining center patent, 1989).

A vertical machining center, which comprises a pallet clamp unit and a pallet conveyor unit arranged along the front face of the bad. A saddle is provided on the upper surface of the bed, with the saddle being slidable along the X- axis. A column is provided on the top surface of the saddle, with the column slidable along the Y- axis. A headstock is provided on the front face of the column, with the headstock being vertically slidable. A tool magazine and an automatic tool exchange device are both arranged alongside the bed, and a numerical control unit is provided for numerically controlling the saddle, the column, the headstock, the pallet clamp unit, the pallet conveyor, the tool magazine and the automatic tool exchange device (Vertical machining center patent, 1989).

1.2.1.1 Vertical Machining Centers Elements

Basic structure of a vertical machining center (VMC) is occurred machine frame, guides, drive, control systems. Elements of a VMC are depicted in Figure 1.4.
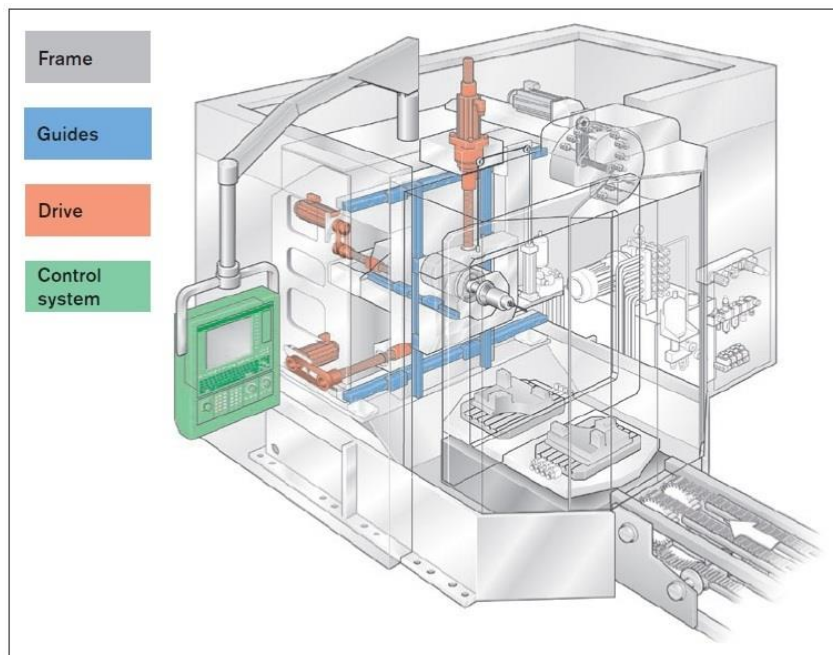
Figure 1.4 Elements of a CNC machining center (Bosch Rexroth AG, 2007).

Frame:

A machine frame consists of fixed components (posts, foundation) and moving components (slides, supports). Aim of the machine frame to support the moving components and to provide the rigidity of the machine.

Many machine frames are made of steel structures due to provide high rigidity. Figure 1.5 shows machine VMC frame and vertical machining center which made of steel.

(a) (b)
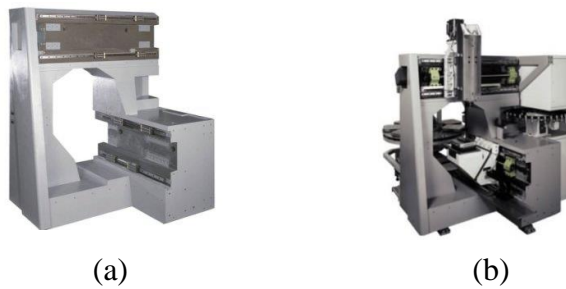
Figure 1.5 VMC frame (a), vertical machining center (b)

For over 30 years, aluminum structural framing systems have used to create machine frames due to provide high strength-to-weight ratios, fast assembly, and easy reconfiguration. There are extensive range of profiles, connectors and accessories on the market. In Figure 1.6, a machine frame which made of aluminum profile systems is shown.
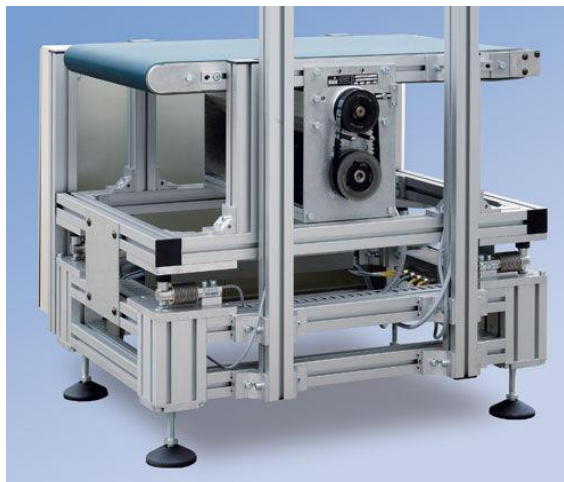
Figure 1.6 Aluminum machine frame.

Guides:

Guides are used for the guidance and power transmission of the moving machine components. Guides are dissociated in rotary guidance and linear guidance based on the movement (Bosch Rexroth AG, 2007). Figure 1.7 shows a linear guide and rotary guide.

(a)   (b)
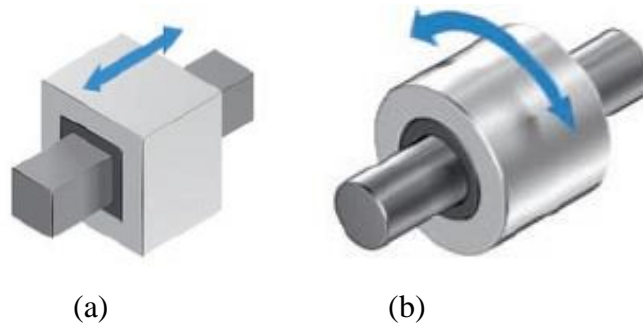
Figure 1.7 Linear guide (a), rotary guide (b). (Bosch Rexroth AG, 2007).

Drive:

Drives convert electrical, hydraulic or pneumatic energy into mechanical energy.

Drive types:

• Electrical drive (e.g. linear motor)

• Electro-mechanical drive

    - Motor (e.g. servomotor)

    - Gearboxes (e.g. planetary gears)

    - Transmission elements (e.g. screw drive, toothed belt drive)

• Pneumatic drive (e.g. pneumatic cylinder)

• Hydraulic drive (e.g. hydraulic cylinder)

CNC driving systems occur from servo driving mechanisms (servo driven linear motion systems) that consist of servomotor and power transmission screws (ball screws). Servomotor rotates with commands coming from NC, the rotation is transmitted to a ball screw via a coupling, and the rotation of the ball screw is transformed into linear movement of a nut, and finally the carriage move linearly. A servo driving mechanism is shown in Figure 1.8.
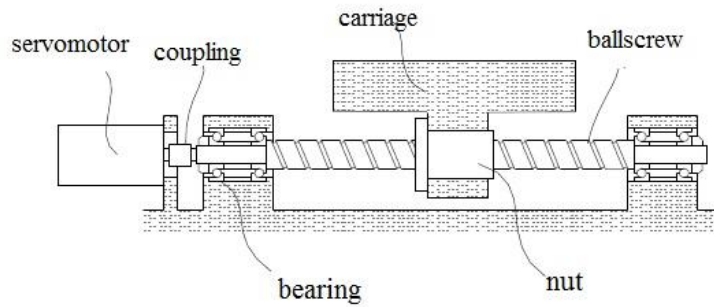
Figure 1.8 Servo driving mechanism (servo driven linear motion system).

Control Systems:

CNC control systems consist of limit switches, measuring systems, field bus systems, servo amplifier, a control unit, a controller and safety circuits. The control unit is programmed with the desired travel profile for the axes movements. The controller and the drive amplifier convert the data the control unit into corresponding signals for the servomotor (Bosch Rexroth AG, 2007).

1.2.1.1.1 Structural Aluminum Framing Systems. Nowadays, aluminum framing systems are applied in variety of environments; from automotive industry to aerospace applications, from electronics to packaging, from medical applications to textiles. Properly, the aluminum framing systems are extensively used in automation systems. They have the advantages such as shorter assembly time, fewer tools, flexible expansion and conversion, providing clean work environment, and reusable components. There are many companies which produce aluminum profiles with hundreds of profile shapes and various assembly components. Figure 1.9 shows several types of aluminum profiles.
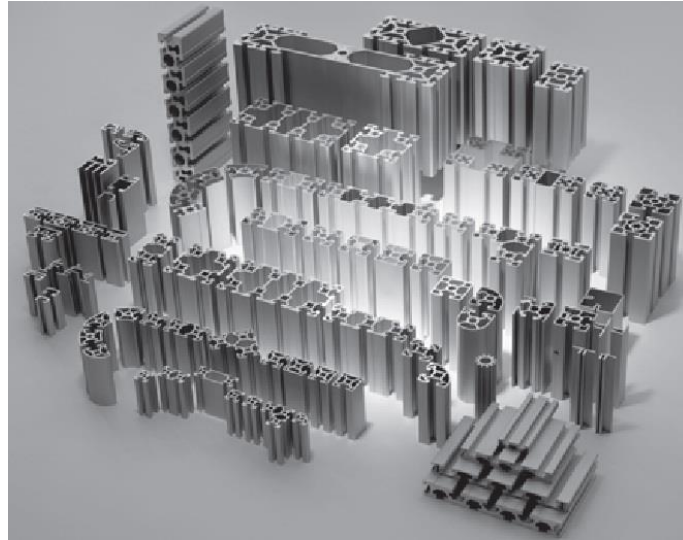
Figure 1.9 Aluminum profiles (Bosch Rexroth AG, 2007).

The machine which made of aluminum profiles is depicted in Figure 1.10.
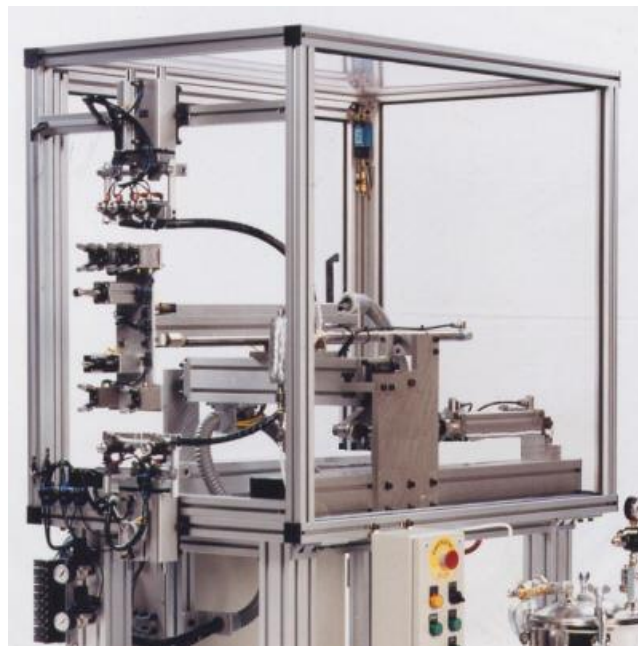
Figure 1.10 The machine which made of aluminum profiles.

1.2.1.1.2 Linear Motion Systems. Linear motion systems are comprised of load bearing profile as frame with guide – rails, carriage with runner – blocks, ball-screw assemblies (consist of end block with bearing, ball-screw, nut, and nut housing). Ball

screw assemblies are the drive components used for converting rotary motion into linear motion. They are suitable for high – speed applications. Both of these functions are combined in linear motion systems (Bosch Rexroth AG, 2007). Figure 1.11 shows a typical linear motion system (also called linear module). A ball – screw assembly system is illustrated in Figure 1.12.
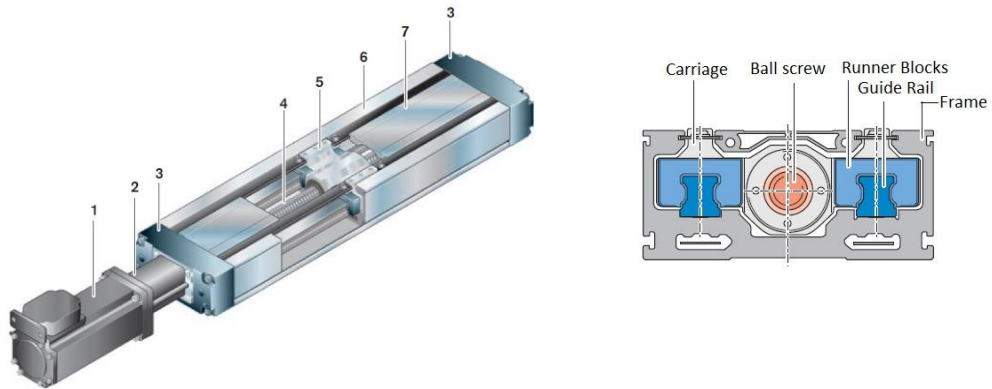
Figure 1.11 Linear motion system; 1: servomotor, 2: flange & coupling, 3: end blocks with bearings, 4: ball – screw drive, 5: carriage with runner blocks, 6: loading profile as frame with guide – rail, 7: cover plate (Bosch Rexroth AG, 2007).
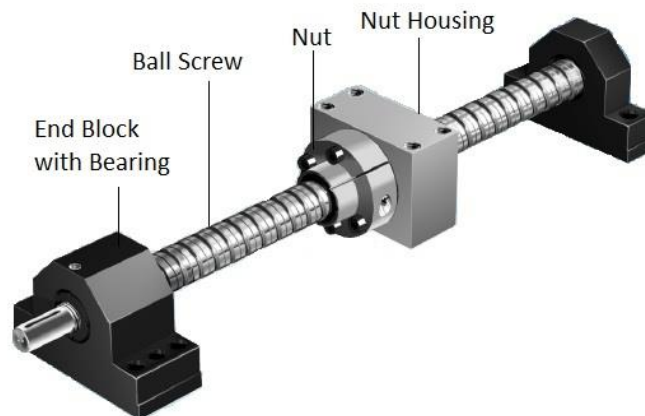
Figure 1.12 Ball – screw assembly system (Bosch Rexroth AG, 2007).

Profiled – rails systems are composed of balls, rollers and cam rollers are used as the rolling elements and guide – rails. They are appropriate for tasks requiring precise linear motion because of their high load bearing capability (Bosch Rexroth AG, 2007). An example guide – rail with its components is depicted in Figure 1.13.
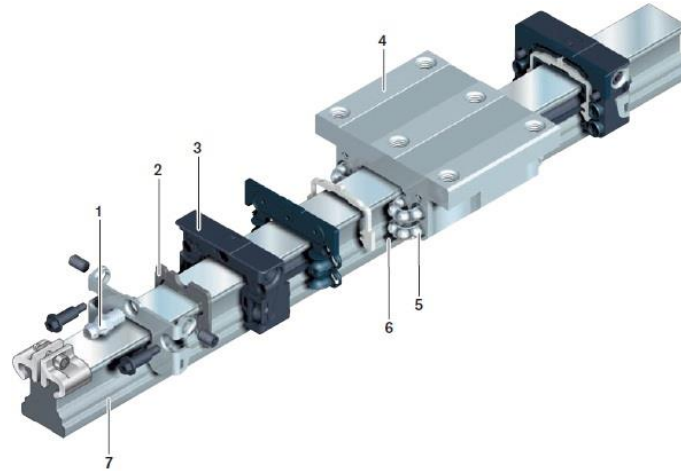
Figure 1.13 Guide – rail; 1: Lube port, 2: end wiper seal, 3: end cap, 4: runner block body, 5: rolling element, 6: side seal, 7: guide rail (Bosch Rexroth AG, 2007).

1.3 Literature Survey

In this section, there are two main parts. First part is related to Computer Aided Engineering studies, the other part is related to Vertical Machining Centers and linear motion systems studies.

1.3.1 Computer Aided Engineering

Early engineers were developed partial differential equations on various engineering systems, then, solution methods for these equations. However, solution of these equations were taken a long time, also, solution results were not precise because of solutions were calculated by manually. In parallel with developments in computer technologies, developed engineering methods have been coded in programs such as FORTRAN, C++, and Visual BASIC. Nowadays, there are many commercial engineering – software such as SolidWORKS, CATIA (Computer Aided Design), ANSYS, ABAQUS (Computer Aided Analysis). They provide to design, analyze, and optimize the engineering systems. Computer aided engineering includes Computer Aided Design (CAD), Computer Aided Analysis (CAA), and Computer Aided Manufacturing (CAM) systems.

Osborne (2006) developed an interactive finite element modeling computer software by using the Microsoft Visual Studio .NET. The software generates a finite element model file, in MSC NASTRAN bulk data file format, of frame assemblies and a vehicle system which occurring beam components. The MSC NASTRAN finite element solver was used to obtain the finite element results.

Bamberg (2000) presented the best structural concepts for Star Technology Grinder five – axis tool and cutter grinder and the three- axis Tube Mill utilizing new finite element analysis (FEA) based concept evaluation technique. The first system was used to define new way of designing machine tool structure. The second system was used optimization process where FEA was used to select size and position structural members. In the finite element models, solid and shell elements were used for modeling the machine frames. Author, also, was modeled guide – rail with runner block system neglecting unnecessary details of the assembly. Beside this, equivalent Young's modulus obtained from static FEA result for the runner – blocks.

Wu (2004) developed a finite element model for a mobile gantry crane by using the finite element software I- DEAS. Author was used beam elements for modeling structure of mobile gantry crane. In this study, also, a 1/10 scale model of the mobile gantry crane was built to validate the finite element model and measured natural frequencies of the system.

Reynoso (1985) proposed dynamical model for predicting vibration response characteristics of a Cartesian robot system. The system was formulated using the Component Mode Synthesis. In order to calculate the vibrations at the end – effector, computer simulations, and experiments were conducted.

Akdağ (2008) proposed an integrated design scheme for robot design including modern CAE procedures. A three – axis serial manipulator (DEU-3X2-550), a two – axis SCARA robot, and a six – axis serial manipulator (DEU-6X5-1500) were designed according to proposed design scheme. Researcher used the finite element

software ABAQUS for finite element models of the robot systems. Joint flexibility definition in the finite element model is important issue according to study. Also, a new concept was defined named as Rigidity Workspace for the robots. This concept includes the end point static deflections and modal behavior of the robots.

Huang & Lee (2001) proposed a computer aided engineering technique to analyze the stiffness of a machine tool. Two methods, a simple module method and a hybrid modeling method, were presented. These techniques were used for analyzing the stiffness of the structure of a vertical machining center contains five modules: the headstock, the column, the table, the saddle, and the bed unit. Authors calculated the stiffness of the five modules by using finite element model of the systems in the finite element software ANSYS.

Garitaonandia, Fernandes & Albizuri (2007) developed a dynamic model of a centerless grinding machine. In the study, numerically obtained mode shapes were correlated with the experimental ones in FEM tools software using the Modal Assurance Criterion (MAC). ANSYS was used to calculate the natural frequencies of the system. Researchers were observed that there were significant differences in the natural frequencies of the mode shapes, so they improved the finite element model of the system under consideration. Improvement included stiffness values of the joint elements connecting the bed to the foundation and the axial stiffness of the lower slide ball – screw. These stiffness values were improved iteratively in order to match finite element results to the experimental ones.

Bais, Gupta, Nakra & Kundra (2004) developed updated FE models of a drilling machine, and conducted experimental modal analysis of the machine. Finite element modeling was done using by a program developed in MATLAB. Beam elements (3 d.o.f. per node) were used for analysis. In the models, there are simplifications such as the joints and boundary conditions were considered to be rigid and influence of structural damping on modal model parameters, was ignored. Apart from, authors developed second finite element model of the machine by using beam mesh elements in I-DEAS software. They compared experimental and FE results by using MAC

technique. Therefore researchers updated the FE model of the drilling machine by using direct matrix methods and indirect (iterative) methods.

Xi & Qin (1998) proposed an integrated approach for design and analysis of a fluid mixer machine. The machine consisted of four − bar linkages. They used Pro/Engineer for design, MATLAB for kinetic analysis and NASTRAN for finite element analysis. Authors optimized their design in order to minimize the vibration using by proposed integrated design approach.

Mahdavinejad (2005) investigated instability of a turning machine. He modeled the machine by using finite element in ANSYS. This model was consisted of machine tool's structure, workpiece and tool. Researcher obtained modal frequencies and mode shapes of the machine by finite element model. In order to validate the finite element results, he conducted experimental modal analysis [16].

Karagülle & Malgaca (2004) studied the effect of flexibility on the trajectory of a planar two-link manipulator by using integrated computer-aided design/analysis (CAD/CAE) procedures. I-DEAS software is used to create solid models and the finite element models of the parts of the manipulator. The end point vibrations and the deviations from the rigid-body trajectory are analyzed for different types of end point acceleration curves. It is observed that the precision of the manipulator can be increased by testing different end point acceleration curves.

1.3.2 Studies on Vertical Machining Centers and Linear Motion Systems

Vertical machining centers are commonly used for various processes such as drilling, milling, laser and water-jet cutting in industry. They consist of linear motion systems. There are limited papers and research on these machines and systems. They are summarized in this part.

Kamalzadeh (2008) investigated a precision ball screw drive system in his doctorate thesis. He established detailed dynamic model of the ball screw

considering rigid body dynamics, nonlinear friction, torque ripples, lead errors, and elastic deformations. Author also designed adaptive sliding mode controller for the system. Besides a finite element model was developed in order to investigate the torsional resonances. Researcher was modeled the ball screw as a rod, the motor shaft as a rigid cylinder with the inertia stated in the motor catalogue, the coupling as two cylinders which including torsional spring representing the coupling flexibility. The effect of table inertia was included as a disc element at the nut position in the model.

Du, Zhang & Hong (2010) proposed a new method to determine the geometric errors of a CNC machine tool. A 3-axis Cincinnati 750 Arrow II vertical machining center was used in order to validate the method proposed in the paper. Comparison experiment was performed on the same machining center by linear measurement system and double bar measurement system.

Yi & et all (2008) investigated the dynamic properties of the linear motion guide system including the steel block carrying the payload both experimentally and theoretically. The natural frequencies of the system and the corresponding mode shapes have been obtained. Authors developed two finite element models for the system. Linear motion block and the steel block were modeled rigid body, the bearing balls as linear spring elements in the first model. In the second model, linear motion block and steel block were modeled as solid brick elements, the bearing balls as the same the first model. In addition, they were investigated hysteresis, which results from micro-scale friction in slowly moving linear motion guide systems, in their study.

Lee, Mayor & Ni (2006) presented dynamic behavior of a miniaturized machine tool (mesoscale machine tool) both experimentally and theoretically. They proposed scaling analysis method to determine the dynamic behavior of the mesoscale machine tool. Authors was used a full-sized vertical machining center to developed scaling analysis method. Experimental modal analysis and finite element analysis were done for the vertical machining center. In the finite element analysis, the finite

element mesh model was created solid elements, and all joints among the machine components were assumed to be rigid. According to comparison between scaling analysis results and experimental results of the mesoscale machine tool, they observed differences between the results. So researchers modeled the joints as equivalent springs and dampers via the FRF (receptance) joint identification method. In conclusion, they increased the accuracy of their method.

Light, Gorlach & Wiens (2011) developed finite element model of a 3-axis gantry CNC machine. They used tetrahedral elements for meshing in PATRAN. Prior to meshing, authors cleaned the geometrical details such as small holes and slots in CAD geometry. Finite element model of the system was established in MD ADAMS. Joints such as bearings linear guideways were modeled as the field connectors with their matrix of stiffness values which obtained from manufacturer documentation. Besides, the ball screw assemblies were represented with one-dimensional beam elements. Experimental modal testing of the machine was conducted. Authors, in order to decrease differences between experimental and simulated results, developed a genetic algorithm in MATLAB, and then rebuild the finite element model of the system via genetic algorithm results.

Si, Yu & Yang (2010) developed a flexible dynamic model of a multi-axis synchronous gantry machining center. They created the CAD model of the machine in Pro Engineer and then CAD model transferred into finite element software SAMCEF Mecano. In the model tetrahedron elements were used. They analyzed the position error and velocity both rigid and flexible bodies.

Lin, Hung & Lo (2010) investigated the influence of linear rolling guides on the vibration characteristics of a vertical column structure using by finite element analysis and vibration tests. They used solid elements (eight node brick element), which were connected with spring elements at the rolling interfaces, for the main bodies of the linear components. The ball screw was modeled as a cylindrical shaft and meshed with 3D solid elements. In addition, the contact between the screw and the nut was simplified as a circular contact mode. Contact stiffness of the ball screw

and nut obtained from technical information. The sliding block and guide rail were connected a series of spring elements by ignoring the effect of the rolling balls. The spindle unit was modeled as a cylindrical body of various sections, but equivalent weight of the original spindle unit.

Okwudire (2005) developed a hybrid finite element model of ball screw feed drive system for control purpose. He modeled the ball screw using by Timoshenko beam elements while the nut was modeled as a 6x6 inertial matrix. Also, he proposed the interface stiffness matrix for the screw-nut interface. The rotor was modeled as single rotary inertia about the axis of rotation. To model the coupling, torsional spring together with rotary inertias was defined. The angular contact bearing was modeled as spring elements in the x, y, and z directions. He obtained natural frequencies of the systems based on position dependent. Author also measured the axial and torsional natural frequencies of the system.

Weiwei (2009) analyzed the dynamics characteristics of a CNC milling machine (named as XK7171) by using the finite element method. Author was established the simplified geometrical CAD model of the machine in Pro Engineer software. And then the CAD model transferred into ANSYS finite element software. SOLID92 element was chosen for meshing of the three dimensional solid units. Linear spring-damper element COMBIN14 was used to simulate the joint surfaces and ball screws. To determine the equivalent damping and stiffness coefficients of the joint surfaces, he was utilized M. Yoshimura integration method. Author reported equivalent spring stiffness and damping values per unit area as long as the average contact pressure is the same according to the method.

Altintas, Verl, Brecher, Uriarte & Pritschow (2011) published a review paper on machine tool feed drives. The paper was organized as follows listed.
- The machine tool guides based on friction, roller bearing, hydrostatic and levitation principles
- The rack-pinion, ball screw and linear drive structures and their dynamical models

- Electric motors and sensors used in feed drives
- The control of rigid and flexible feed drives

Hung, Lai, Lin & Lo (2011) developed a finite element model for the machining stability of a vertical milling under the influence of the preloaded linear guides. They used solid elements (eight node brick element), which were connected with spring elements at the rolling interfaces, for the main bodies of the linear components. The ball screw was modeled as a cylindrical shaft and meshed with 3D solid elements. In addition, the contact between the screw and the nut was simplified as a circular contact mode. Contact stiffness of the ball screw and nut obtained from technical information. The sliding block and guide rail were connected a series of spring elements by ignoring the effect of the rolling balls. The spindle unit was modeled as a cylindrical body of various sections, but equivalent weight of the original spindle unit. They designed a small-scale vertical machine and fabricated to predict cutting stability boundaries. They reported the guides with a high preload that were installed in the spindle feeding mechanism are more effective than the linear guides with low preload in enhancing the dynamic stiffness of the system.

Khim, Park, Shamoto & Kim (2011) studied a linear motion bearing XY table driven by coreless linear motors. Firstly, they constructed a transfer function relating the force acting on a bearing block to the rail form error via Hertz contact theory. And then analytical model was developed to predict the motion error of a table with the multiple bearing blocks, in which the bearing forces were derived from the rail form error using the transfer function.

Ohta & Hayashi (2000) examined the vibration of linear guideway type (LGT) recirculating linear ball bearings. They measured the vibration characteristics such as overall level of vibratory velocity and vibration spectra of the LGT recirculating linear ball bearing at constant linear velocity. They obtained natural frequencies and mode shapes of the LGT recirculating linear ball bearing. Then, authors calculated the natural frequencies of the system by using a finite element model, which was meshed with eight-node solid elements, in COSMOS/M finite element software.

They defined spring elements for the elastic contact between the carriage and each ball, and the profile rail and each ball in the model.

1.4 Scope of the Thesis

Nowadays, vertical machining centers are widely used in industrial applications. There is need to effectively design and analyze of vertical machining centers because of structural complexities and geometrical restrictions. The most popular method for determining the dynamics characteristics of the engineering systems is the vibrations analysis. Nowadays, finite elements method is commonly used in order to obtain the natural frequencies and mode shapes of the engineering structures.

In the scope of this thesis, a new approach to analyze vertical machining centers consisting of aluminum profile framing and linear motion systems is proposed by using finite element program ANSYS. A vertical machining center is analyzed the proposed approach. The vertical machining center is produced and then experimental modal analysis is conducted of the machine.

A VisualBASIC program is developed in this thesis uses the database to transfer the information about the system to the pre-processor of the finite element program ANSYS. The same database is used to obtain solid models in SolidWorks by VisualBASIC commands. SolidWorks has better capability to evaluate solid models which is necessary for design.

Residual vibrations significantly affect positioning achievement of the end point in flexible systems. To control the residual vibrations of the system, trapezoidal velocity profile is applied with open loop control.

1.5 Organization of the Thesis

This thesis consists of five chapters (including the introducing and the conclusions) and the appendices.

Chapter 1 presents the brief history of CNC machines and their elements, literature survey, scope, and organization of the thesis.

Chapter 2 presents finite element modeling of structures with aluminum profiles and modeling of connectors. The program, which is used previously defined databases, is developed to create finite element model macro files. Obtained natural frequencies of the several aluminum framing systems are presented both theoretically and experimentally.

Chapter 3 presents a new approach for the finite element analysis of a vertical machining center which consists of linear motion systems (LMS) by beam elements. The analysis of whole assembly with moving members is given in this chapter.

Chapter 4 presents dynamic analysis of the system with finite element and signal analysis method. Open loop control is applied to control the residual vibrations of LMS with experiments and finite element simulations.

Finally, in Chapter 5, the conclusions and the suggestions for the future works for LMS are presented.

CHAPTER TWO

FINITE ELEMENT MODELING OF STRUCTURES WITH ALUMINUM PROFILES

2.1 Introduction

Modern engineering theories based on advanced engineering mathematics have been developed after the invention of the laws of motion. One of the major areas of modern engineering is the vibration theory. There are many studies in the literature on the vibration analysis of simple structures based on partial differential equations (Rao, 1985). The finite element (FE) method has been developed for modeling of realistic complex engineering systems. This method requires meshing of complex structures to finite elements and constructing mathematical models consisting of a set of differential equations with a large number of degree of freedom. It has been possible to solve these equations after the developments of digital computers. At the beginning, the analyzers would construct these equations and solve them by writing computer codes themselves. A further development on computer software has made it possible that constructing and solving the equations are done by the computer automatically. These user-friendly programs have pre-processors, solvers and post-processors (ANSYS, 2009). The users define the system under the study and the assumptions such as types of finite elements; mesh sizes, etc. using the pre-processor. They select the solution method and obtain the solutions. Finally, they evaluate the results using the post-processor. One of the main research areas of today is to analyze realistic systems using these computer programs by correct assumptions (Akdağ, Karagülle, Malgaca, 2012, Zaeh, Siedl, 2007, Guan, Ren, Su, Mu, 2010). The success of the assumptions must be checked by comparing simulation results with experimental results. Before the information age, simple structures could be analyzed quantitatively and experience was very important for complex structures. However, today, once the assumptions for the simulations are verified by experiments, complex structures can be analyzed quantitatively by simulation and the importance of the experience is decreasing. Engineers can develop complex

engineering systems very rapidly. Vertical machining centers which consist of linear motion systems are widely used in industry. There are many suppliers of their components such as aluminum profiles, ball screws, nuts, guides, cars, bearings, and connecting parts. Aluminum profiles are preferred because they are durable, lightweight, corrosion resistant, and reusable. Fewer tools and lead times are required for the final system. The design is simple, and no welding and painting is required. The manufacturers usually have a large stock of profiles with different shapes and connecting parts. Aluminum profiles are used in automation systems, conveyor frames, automobile body, work tables, interior design, and construction.

This study is a new attempt to analyze vertical machining centers which consists of linear motion systems by using FE programs. Users create a database for the system. A VisualBASIC (VisualBASIC 6.0 Help Documents, 2011) program developed in this study uses the database to transfer the information about the system to the pre-processor of the FE-program. ANSYS is used as the FE-program. The results obtained by ANSYS are transferred to the VisualBASIC program for further evaluations. The same database is used to obtain solid models in SolidWorks (SolidWorks Corp., 2009) by VisualBASIC commands. SolidWorks has better capability to evaluate solid models which is necessary for design. The analysis method developed in this work is explained on a test system. Simulation results are compared with experimental results. The test system is designed to locate a hexapod which can be used for medical operations.

2.2 Structures with Aluminum Profiles

The frame of a test system (Frame-TS-1A) is shown in Figure 2.1. The labels for a beam (b01) and a connector (c01) are shown in the figure. The cross sections of the aluminum profiles and the connecting parts used in the frames studied in this work are shown in Table 2.1 and 2.2. All the parts used are available in the market.
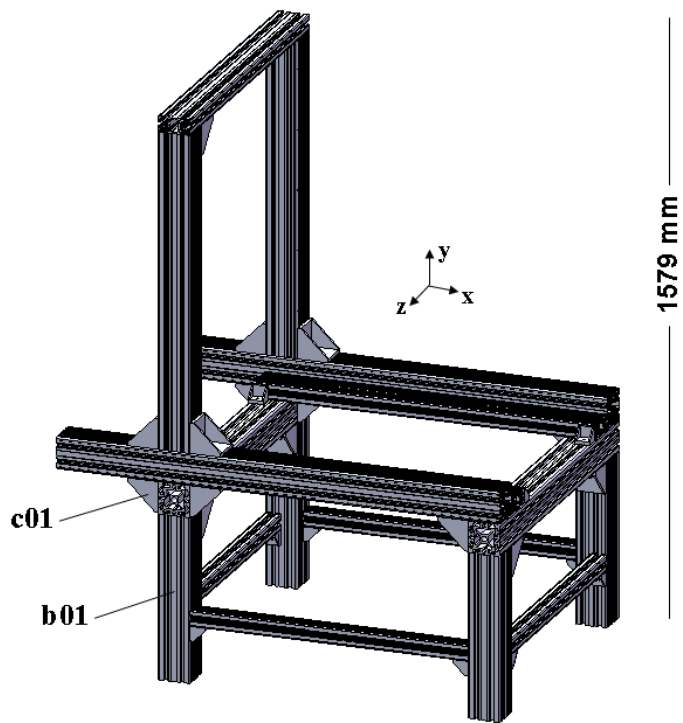
Figure 2.1 Solid model of frame of test system, TS-1A

Table 2.1 Cross sections of profiles (Values are from Bosch-Rexroth)
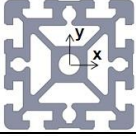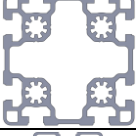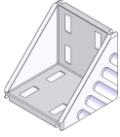
Section	Size (mm)	File name	Weight (kg/m)	Area (cm^2)	Moment of inertia	
					I_x (cm^4)	I_y (cm^4)
	90x90	s90X90	10.5	39.5	302	302
	90x90	s90x90L	6.3	23.6	210	210
	45x45	s45x45L	1.5	5.7	11	11
	90x45	s90x45L	3.1	11.2	23.6	81.9
	30x30	s30x30	0.8	3.1	2.7	2.7

Table 2.2 Connectors (Bosch-Rexroth)

Connector	Weight (gr)	Size (mm)	File name
	314[a]+187[b]	90x90x90	cn90
	56[a]+47[b]	45x45x45	cn45
	20[a]+17[b]	30x30x30	cn30

[a]*Weight of connector,* [b]*Weigth of bolts and nuts*

A database is created in a text file for the information about the structure of the frame. The information about a beam is by the label, the section file name, L_b, and $\mathbf{q}_L$ = [x_0, y_0, z_0, θ_x, θ_y, θ_z]. L_b is the length of the beam; $\mathbf{q}_L$ is the location of the beam. x_0, y_0, and z_0 are the Cartesian coordinates of the local origin of the beam in the global coordinate system. θ_x, θ_y, θ_z are the rotation angles of the beam about the local x, y, and z axes, respectively. The beam is located at the origin and it is oriented in the global z axis for $\mathbf{q}_L = \mathbf{q}_{L0} = [0, 0, 0, 0, 0, 0]$. The distances are given in mm, and the angles are given in degree, unless otherwise stated.

The information about a connector is given by the label, the solid model file name, and $\mathbf{q}_L$. $\mathbf{q}_L$ is the location of the connector. The labels start with the characters b and c for the beams and connectors, respectively. The database for the frame in Figure 2.1 is given in Table 2.3.

Table 2.3 Database for Frame-TS-1A

Label	File name	L_b	q_L
b01	s90x90	464	[0,0,400,-90,0,0]
b02	s90x90	464	[873,0,400,-90,0,0]
b03	s90x90	464	[873,0,-400,-90,0,0]
b04	s90x90	464	[0,0,-400,-90,0,0]
b05	s45x45L	783	[45,182.5,422.5,0,90,0]
b06	s45x45L	710	[895.5,182.5,-355,0,0,0]
b07	s45x45L	783	[45,182.5,-422.5,0,90,0]
b08	s45x45L	710	[-22.5,182.5,-355,0,0,0]
b09	s90x90	890	[873,509,-445,0,0,90]
b10	s90x90	890	[0,509,-445,0,0,90]
b11	s90x90L	1250	[-332,599,-400,90,0,90]
b12	s90x90L	1250	[-332,599,-400,90,0,90]
b13	s45x90L	963	[-45,576.5,310,90,0,90]
b14	s45x90L	963	[-45,576.5,-310,90,0,90]
b15	s90x90L	890	[0,644,400,-90,0,0]
b16	s90x90L	890	[0,644,-400,-90,0,0]
b17	s45x90L	890	[0,1556.5,-445,0,0,90]
c01	cn45		[45,160,422.5,90,90,0]
c02	cn45		[828,160,422.5,0,-90,90]
c03	cn45		[895.5,160,355,90,180,0]
c04	cn45		[895.5,160,-355,90,0,0]
c05	cn45		[828,160,-422.5,0,-90,90]
c06	cn45		[45,160,-422.5,90,90,0]
c07	cn45		[-22.5,160,-355,90,0,0]
c08	cn45		[-22.5,160,355,90,180,0,]
c09	cn90		[45,554,400,0,90,-90]
c10	cn90		[828,554,400,0,-90,90]
c11	cn90		[873,464,355,90,180,0]
c12	cn90		[873,464,-355,90,0,0]
c13	cn90		[828,554,-400,0,-90,90]
c14	cn90		[45,554,-400,0,90,-90]

Table 2.3 continue (Database for Frame-TS-1A)

c15	cn90		[0,464,-355,90,0,0]
c16	cn90		[0,464,355,90,180,0]
c17	cn90		[-45,554,400,0,-90,90]
c18	cn90		[-45,554,-400,0,-90,90]
c19	cn45		[896.5,554,265,-90,0,0]
c20	cn45		[896.5,554,-265,0,0,0]
c21	cn45		[-23.5,554,265,-90,0,0]
c22	cn45		[-23.5,554,-265,0,0,0]
c23	cn90		[0,1534,355,90,180,0]
c24	cn90		[0,1534,-355,90,0,0]
c25	cn90		[45,644,400,0,90,0]
c26	cn90		[-45,644,400,0,-90,0]
c27	cn90		[45,644,-400,0,90,0]

2.3 Finite Element Modeling

2.3.1 Modeling with Solid Finite Elements

The easiest way of FE analysis after constructing solid model of the system is using solid finite elements. ANSYS uses SolidWorks models, considers contacting surfaces, and performs meshing to generate solid finite elements. The user defines the boundary conditions and obtains the solution.

The disadvantages of this approach for complex systems are the resulting number of elements and degrees of freedom are very large, meshing problems may arise, solution times are long, high performance computers are necessary, solutions may not be obtained, and analysis may not be practical.

Small gaps (1 mm) between connected beams are given in the solid model as shown in Figure 2.2 for FE analyses. Gaps are given as decreasing lengths of beams. In this assumption, connected beam faces are mated to connector faces only and there is no direct contact between beams. The solid finite elements are used for obtaining the properties of the cross sections of equivalent beams of connectors in this study.
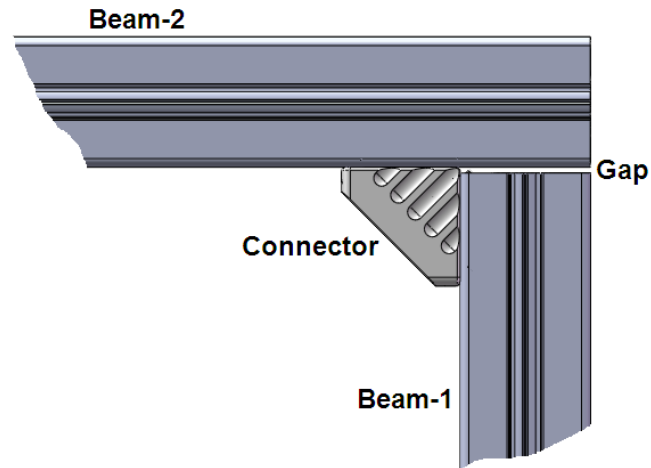
Figure 2.2 Gap given between connected beams

SOLID186 and SOLID187 elements are used in ANSYS. They are 3 dimensional 20-node and 10-node structural finite elements, respectively. Each node has 3 degrees of freedom (nodal translations in x, y, and z directions). The material properties of finite elements are defined by $\mathbf{p}_m = [E, \rho, \upsilon, \beta]$. E is the modulus of elasticity (GPa), ρ is the density (kg/m^3), υ is the Poisson's ratio, and β is the stiffness matrix multiplier for damping. $\mathbf{p}_m=[69,2700,0.3,0]$ for aluminum in this study.

2.3.2 Modeling with Beam Finite Elements

Considering the disadvantages of the solid FE modeling, beam finite elements are used. In this approach, lines are assigned for beams, first. Section attributes are defined for the lines. Two beams with a connector are shown in Figure 2.3 (a). Lines for the beam FE model are shown in Figure 2.3 (b).
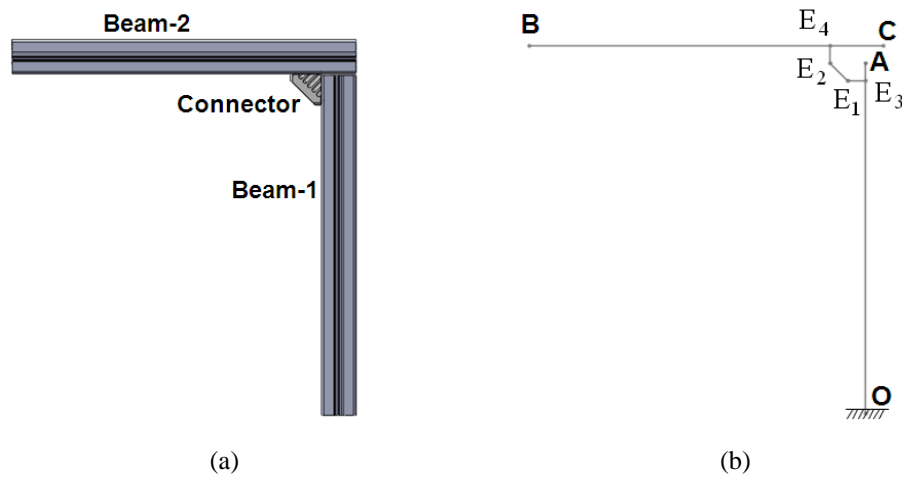
Figure 2.3 (a) Solid model, (b) Line model.

Beam-1 and Beam-2 are created by the extrusions of corresponding cross-sections along the lines AO, and CB respectively.

Extension beams are assumed on the lines E_1E_3 and E_2E_4. An equivalent beam for the connector is assumed on the line E_1E_2. E_1 and E_2 are at the mid-points of mating faces of the connector.

The cross section of an extension beam is assumed to be the same as the adjacent beam. For example, E_1E_3-extension beam is assumed to have the same cross section as OA-beam. A negligible value (1 kg/m^3) is assigned to the densities (ρ) of extension beams.

The properties of the cross sections of the equivalent beams of connectors are assigned by analyzing L-frames as shown in Figure 2.3. Modeling of connectors is discussed in following section "Modeling of Connectors".

Lines for the beam FE model of Frame-TS-1A are shown in Figure 2.4. The location of a point (Point-A) on the line model of a system is defined by $\mathbf{R}_A$ = [x_A, y_A, z_A], where x_A, y_A, and z_A are global Cartesian coordinates. O is the global origin.

27

The locations of the points which are used for the results below are given in the figure. These points are use as excitation or sensor points below.

$$R_A=[0,1485,-400]$$
$$R_B=[0,1485,400]$$
$$R_C=[0,1556.5,0]$$
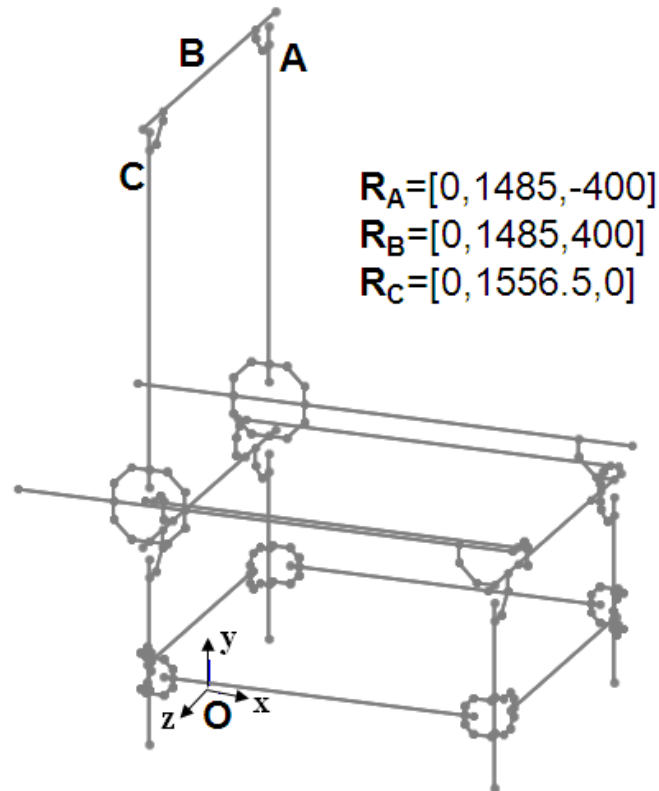
Figure 2.4 Line model of Frame-TS-1A

BEAM44 elements are used in ANSYS for beams. BEAM44 is a uniaxial element with tension, compression, torsion, and bending capabilities (ANYSYS Inc. Theory, 2001). The element has 6 degrees of freedom at each node: translations in the nodal x, y, and z directions and rotations about the nodal x, y, and z-axes. This element allows a different unsymmetrical geometry at each end and permits the end nodes to be offset from the centroidal axis of the beam. The details of the element are given in ANYSYS Inc. Theory. Let a beam element has the nodes at the points I and J. The cross section of an element at I is shown in Figure 2.5, schematically.
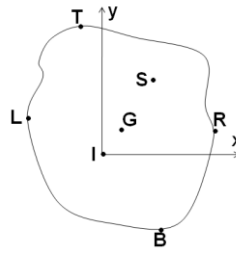
Figure 2.5 Cross section of beam element at Node-I

x and y are the nodal coordinates in the Figure 2.5. G is the area center of gravity. S is the shear center. The geometrical properties of the cross section for the FE analysis is given by $\mathbf{p}_s$ = [A,I_{Gx},I_{Gy},I_{Gz},S_{dx},S_{dy},y_T,y_B,x_L,x_R] and $\mathbf{q}_G$=[x_G,y_G]. Here, A is the area (cm^2), I_{Gx} is the area moment of inertia with respect to the axis with respect to (w.r.t.) the axis in the x direction passing through G. I_{Gy} is the area moment of inertia w.r.t. the axis in the y direction passing through G. I_{Gz} is the moment of inertia w.r.t. the axis in the z direction passing through G. I_{Gz}=I_{Gp} if I_{Gz}=I_{Gx}+I_{Gy}. I_{Gz}=J_{Gt} if I_{Gz} equals to the torsional moment of inertia. The units of area moment of inertias are taken as cm^4 unless otherwise is stated. S_{dx} and S_{dy} are the shear deflection constants. T, B, L, R are the points on the fibers at extreme distances from G. x_G and y_G are the nodal coordinates of G. $\mathbf{q}_G$= [0, 0] if there is no offset between the nodal origin and the area center of gravity of the cross section. It assumed that there is no offset unless it is stated.

The geometrical properties of the beams are given in Table 2.4.

Table 2.4 Geometrical properties of beams

Beam	$\mathbf{p}_s$
s90x90	[38.9,301.9,301.9,152.9,3.25,3.25,45,45,45,45]
s90x90L	[23.56,211.1,211.1,105.4,5.27,5.27,45,45,45,45]
s45x45L	[5.7,11,11,1.7,4.24,4.22,22.5,22.5,22.5,22.5]
s45x90L	[11.29,23.6,81.9,12.9,4.47,3.25,45,45,22.5,22.5]
s30x30	[3.2,2.8,2.8,0.3,3.34,3.34,3.34,15,15,15,15]

The cross-sectional properties of beams are calculated by using Beam Tool in ANSYS. Calculated sample cross-sectional properties of s45x45L are shown in Figure 2.6.
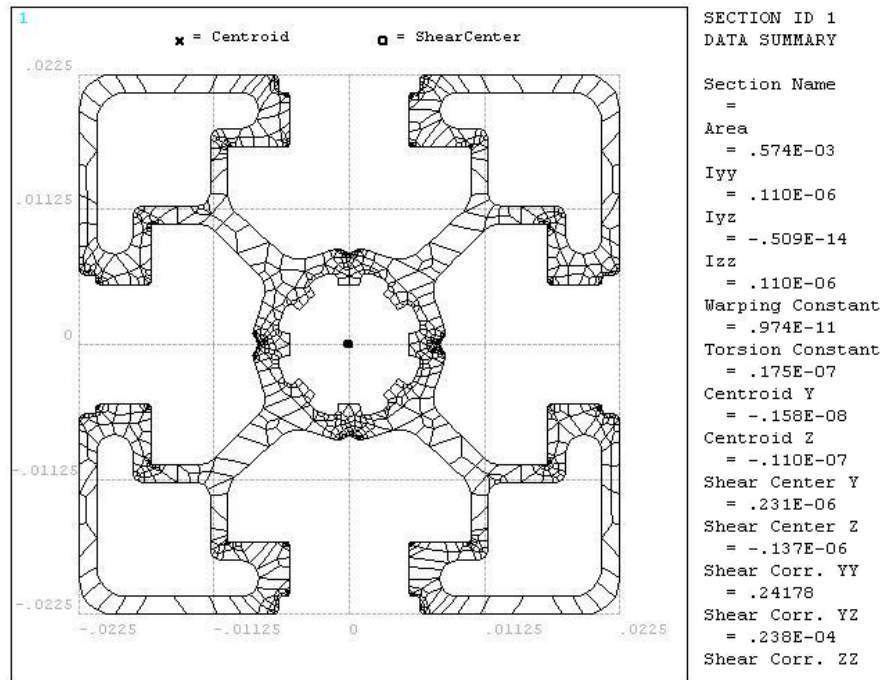
Figure 2.6 Section properties of s45x45L aluminum profile.

2.3.2.1 Modeling of Connectors

In finite element models consist of beam elements, it is commonly assumed that the beams are rigidly articulated at average joint location. According to literature, if the distances of offset are too large between the nodes compared to the lengths of the beams in the finite element models, the offsets have to be modeled. There are three methods used to model the offsets: (i) very stiff element, (ii) rigid element, (iii) multi point constraint equations (Liu & Quek, 2003, p. 265). However, in this study, connectors are modeled instead of the offsets (see Figure 2.7).

In order to define connector elasticity, finite elements model of L-type frames are established by using solid finite elements. The properties of the cross sections of the

equivalent beams of connectors are assigned by analyzing L-frames. Finite element analysis results are obtained by using solid finite elements and beam finite elements.
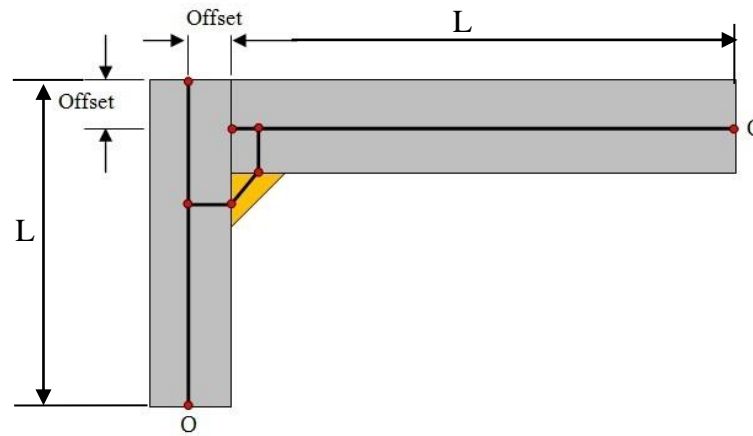
Figure 2.7 Offsets at the L-type frame system.

The structure is fixed at O point. Natural frequencies for the first two modes and the end point deflections at C under static loads are compared. The cross section properties of the connector are found by iteration so that the solid finite element results match with beam finite element results. The value of ρ for an equivalent connector beam is assigned so that the equivalent connector beam has the same mass as the real connector. Modal finite element results of the L-frames with solid and beams elements are depicted in Table 2.5. The geometrical properties of the equivalent beams for connectors are given in Table 2.6.

Table 2.5 Modal finite element results for L-frames structures.

Frame	Element Type	f_{bx} (Hz)	f_{bz} (Hz)	f_{ty} (Hz)
LF-s30x30	SOLID	26.8	56.84	8.68
L=590 mm	BEAM44	26.21	54.63	8.24
LF-s45x45	SOLID	22.53	50.54	113.27
L=450 mm	BEAM44	21.35	54.51	111.28
LF-s90x90	SOLID	17.49	57.15	14.79
L=900 mm	BEAM44	25.06	61.48	17.40

Table 2.6 Geometrical properties of the equivalent beams for connectors.

Connector	$\mathbf{p}_s$
cn90	[3,5.85,7.5,24.21,2.49,1.89,43,43,43,43]
cn45	[1.23,0.87,1.15,1.42,2.12,2.12,11,11,11,11]
cn30	[3.2,2.8,2.8,.3,3.34,3.34,3.34,15,15,15,15]

2.4 Modeling Software

A computer program to model vertical machining center with linear motion systems (LMS) has been developed in VisualBASIC. The user interface of computer program is shown in Figure 2.8. The user creates a database file for LMS. The database contains the following information for FE analysis of frames: The information about the beams, connectors and plates as listed in Table 2.7; the information about the boundary conditions, the meshing size; the geometrical properties of cross sections, and the material properties. The list of the operations is given in Table 2.7. The execution of the operations is activated by clicking the corresponding command options. The operations are achieved by using the input database and Application Programming Interface (API) capabilities of SolidWorks.
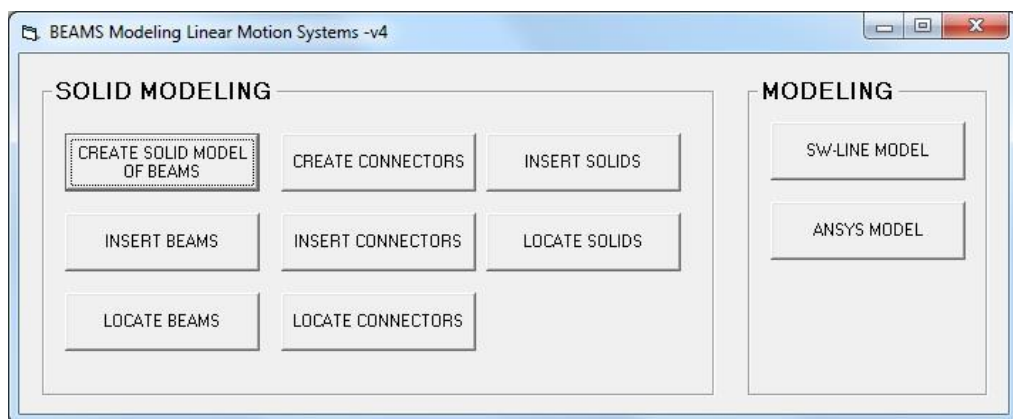
Figure 2.8 User interface of developed computer program.

Table 2.7 List of operations of modeling software

Command label	Operation
Create solid models of beams	Imports cross-section files, extrudes along beam lines, and saves to files named by labels, in SolidWorks.
Insert beams	Inserts beams to assembly file in SolidWorks.
Locate beams	Locates beams in assembly.
Create connectors	Copies connector files to files named by labels, in SolidWorks.
Insert connectors	Inserts connectors to assembly file.
Locate connectors	Locates connectors in assembly.
Insert Solids	Inserts solids previously created to assembly file.
Locate Solids	Locates solids in assembly.
SW-line-model	Displays lines in SolidWorks.
ANSYS model	Creates ANSYS model.

2.5 Measurement System

The wireless vibration sensor is a MicroStrain G-Link tri-axial accelerometer (Accelerometer range: ± 10g, 47 g, 58 mm x 43 mm x 26 mm). The wireless base station is MicroStrain Gateway WSDA-Base-104. The data received by the base station is transmitted to the computer through Universal Serial Bus (USB) and recorded by using Node Commander Software. The sampling rate is 2048 Hz. The frame is excited by a hammer impact. The FFTs (Fast Fourier Transforms) of the recorded signals in the x, y, and z directions are taken in MATLAB. The frequencies where the peaks appear are determined for the natural frequencies. The measurement system for obtaining experimental results is shown in Figure 2.9.
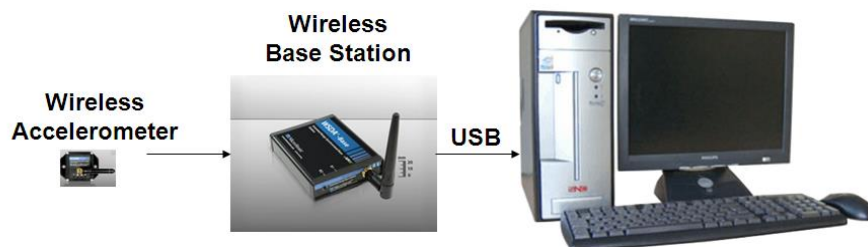
Figure 2.9 Measurement system.

2.6 Results and Discussion

An L-frame and three aluminum profiles framing system are constructed. Their natural frequencies are obtained both experimental and theoretical.

2.6.1 L-Frame (LF-45)

A simple frame (LF-45) as shown in Figure 2.10 is considered.

(a)   (b)
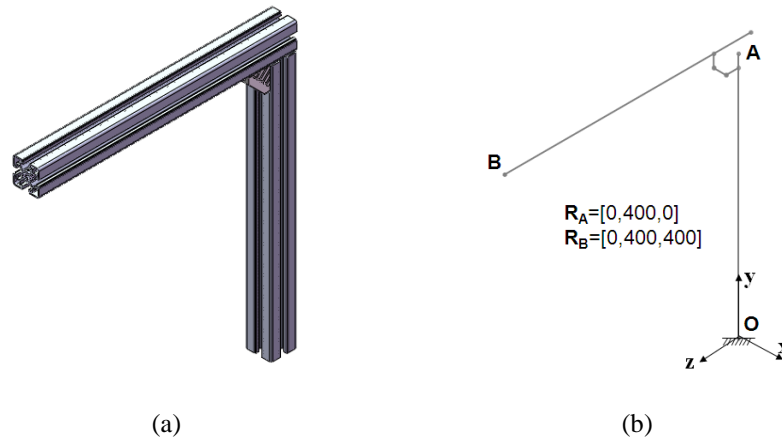
Figure 2.10 L-frame (LF-45) (a) Solid model for simulations, (b) line model.

The database for the LF-45 is given in Table 2.8.

Table 2.8 Database for L-frame (LF-45)

Label	File name	L_b	q_L
b01	s45x45	450	[0,0,0,-90,0,0]
b02	s45x45	450	[0,472.5,-22.5,-0,0,0]
c01	cn45	-	[0,450,22.5,90,0,0]

The properties of the computers used to obtain FE results are given in Table 2.9. The solution time (s) for Type-1 computer is t_1, the solution time (s) for Type-2 computer is t_2, the number of nodes for FE analysis is n_d, and these values are given by $s_p=[t_1,t_2,n_d]$.

Table 2.9 Properties of computers

Computer	Properties
Type-1	WORKSTATION Intel Xeon X5687 3.6 GHz, 24 GB RAM, 64 Bit Win7 Operating System
Type-2	DESKTOP PC AMD PHENOM II X4 955- 3.2 GHz, 8GB RAM, 64 Bit Win7 Operating System

The modal analysis results are given in Table 2.10. f_{ty}, f_{bx}, f_{bz} are natural frequencies corresponding to the mode shapes (see Figure 2.11) where the frame mainly makes torsional vibration about the y-axis (Mode-ty), bending vibration about the x-axis (Mode-bx), and bending vibration about the z-axis (Mode-bz), respectively. The information about the geometrical parameters for a measurement is given by $\mathbf{p}_g$ = [z, A, B] as an example. z is the direction of the excitation and the signal component, A is the excitation point, and B is the sensor point. The excitation is an impact.
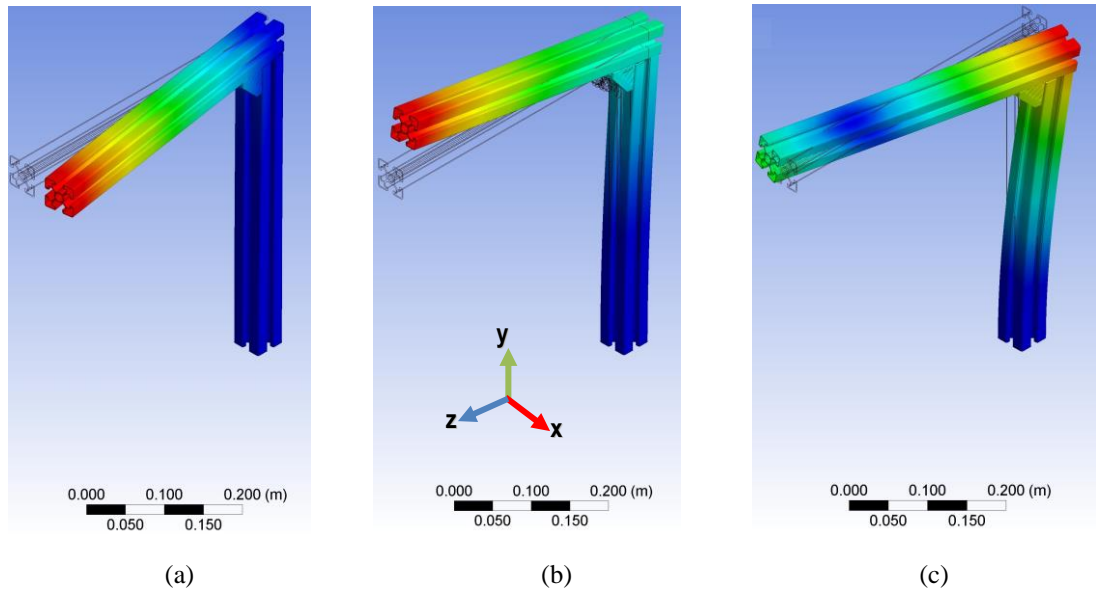
Figure 2.11 Solid finite element results, (a) Mode-ty, (b) Mode-bx, (c) Mode-bz

Table 2.10 Natural frequencies for LF-45

		f_{ty} (Mode-ty)	f_{bx} (Mode-bx)	f_{bz} (Mode-bz)
Simulation	Solid FE $\mathbf{s}_p$=[38,52, 103399]	22.53 Hz	50.54 Hz	113.27 Hz
	Beam FE $(I_{Gz}=I_{Gx}+I_{Gy})$ $\mathbf{s}_p$=[<1,<1,3909]	50.08 Hz[a]	54.51 Hz,	128.65 Hz
	Beam FE $(I_{Gz}=J_{Gt})$ $\mathbf{s}_p$=[<1,<1,3909]	21.35 Hz	54.51 Hz	111.28 Hz
Experiment		21.01 Hz $\mathbf{p}_g$=[x, B, B]	45.03 Hz $\mathbf{p}_g$=[z, A, B]	84.05 Hz $\mathbf{p}_g$=[x, A, B]

[a] *Mode shape is different than torsional vibration about the y-axis*

Signal components and the FFT's of the signal components for the experimental results in Table 2.10 are given in Figure 2.12 to 2.14.
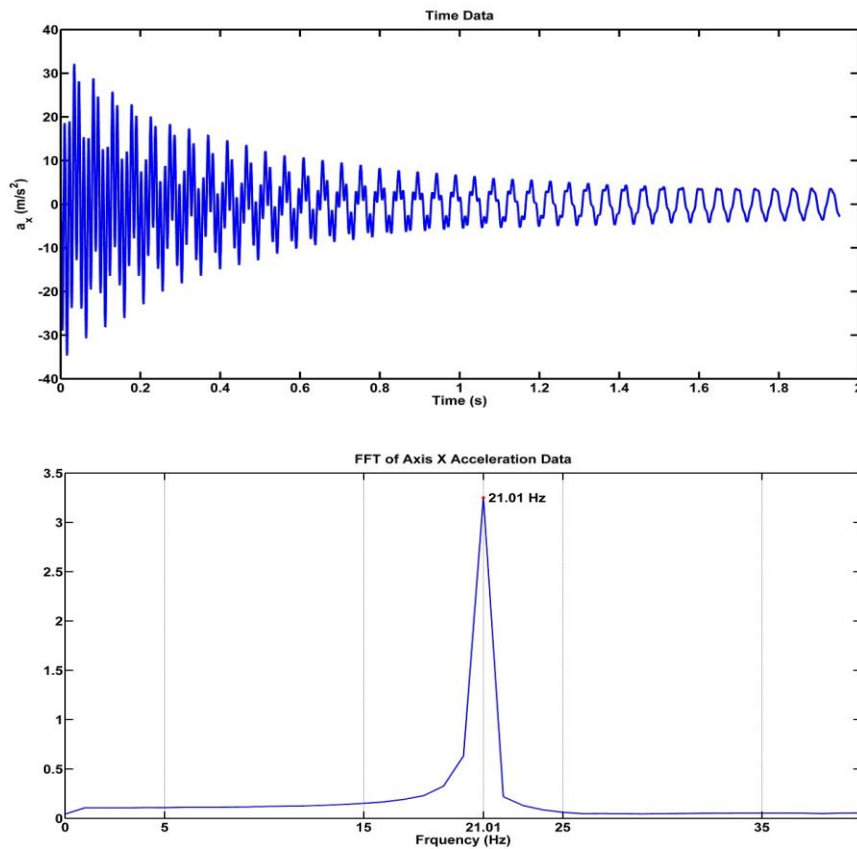
Figure 2.12 Signal and FFT's of signal components for experimental results for Mode-ty.
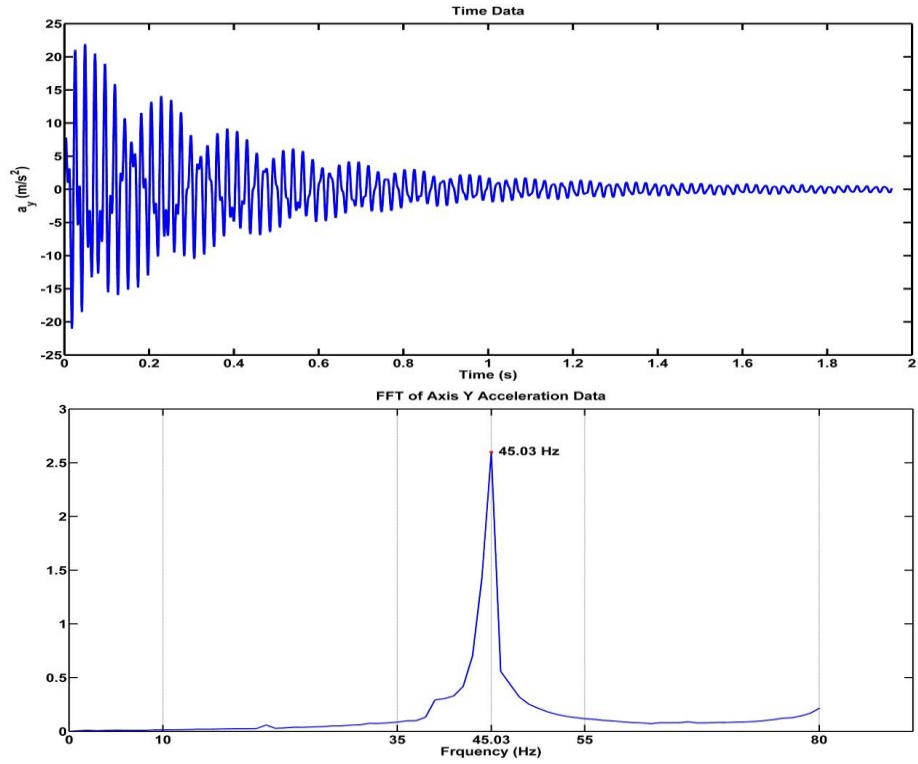
Figure 2.13 Signal and FFT's of signal components for experimental results for Mode-bx.

Figure 2.14 Signal and FFT's of signal components for experimental results for Mode-bz.

2.6.2 Aluminum Profiles Framing Systems

The results are given for Frame TS-1A, Frame TS-1B, and Frame TS-1C in this section. The database for Frame TS-1A shown in Figure 2.1 is given in Table 2.3. Frame TS-1B is obtained by reinforcing Frame TS-1A. Frame TS-1C is obtained by reinforcing TS-1B. Added components are given in Table 2.11 and 2.12. Reinforcing is done considering the mode shapes.
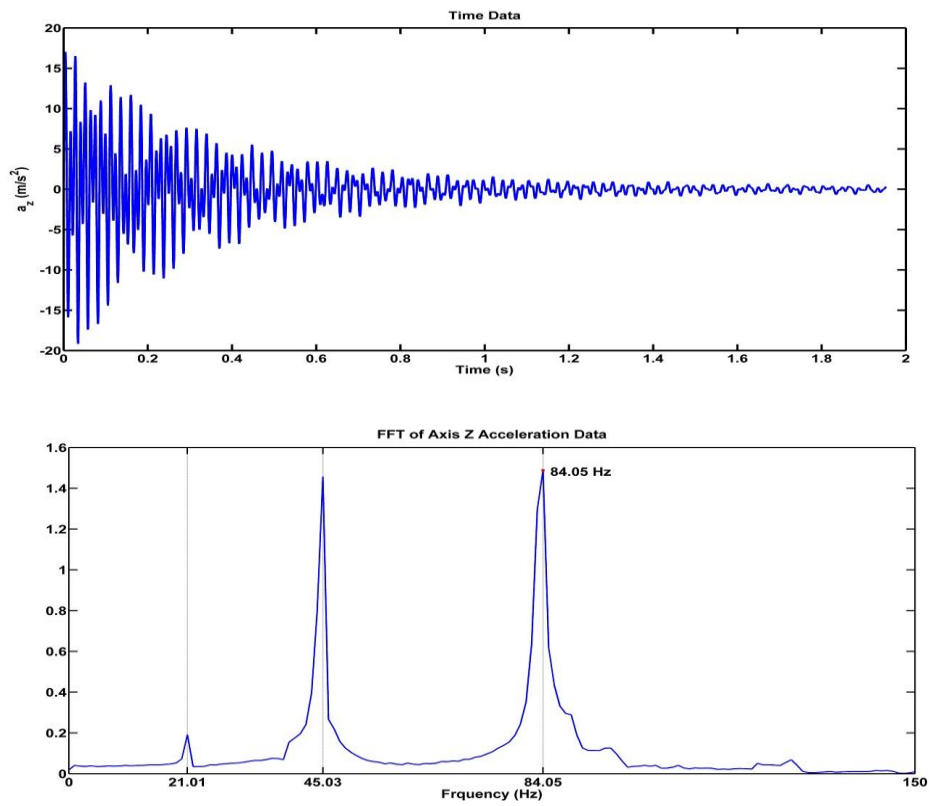
Table 2.11 Added component to TS-1A for TS-1B

Label	File name	L_b	$\mathbf{q}_L$
bt01	s90x90L	L	[0,h,490,-90,0,0]
bt02	s90x90L	L	[0,h,-490,-90,0,0]
ct01	cn90		[0,h,445,90,0,0]
ct02	cn90		[0,h+L,445,0,0,0]
ct03	cn90		[0,h,-445,180,0,0]
ct04	cn90		[0,h+L,-445,-90,0,0]
ct05	cn90		[45,599,445,0,0,-90]
ct06	cn90		[-45,599,445,0,0,90]
ct07	cn90		[45,599,-445,-90,0,-90]
ct08	cn90		[-45,599,-445,-90,0,90]

[a] h is changed. L=530, h=240 unless otherwise stated

Table 2.12 Added component to TS-1B for TS-1C

| Label	File name	L_b	$\mathbf{q}_L$
bt03	s90x90L	355	[-188.5,644,400,-90,0,0]
bt04	s90x90L	188.5	[-233.5,1044,400,0,90,0]
bt05	s90x90L	355	[-188.5,644,-400,-90,0,0]
bt06	s90x90L	188.5	[-233.5,1044,-400,0,90,0]
bt07	s90x90L	355	[188.5,644,400,-90,0,0]
bt08	s90x90L	188.5	[233.5,1044,400,0,-90,0]
bt09	s90x90L	355	[188.5,644,-400,-90,0,0]
bt10	s90x90L	188.5	[233.5,1044,-400,0,-90,0]
ct09	cn90		[45,1089,400,0,90,0]
ct10	cn90		[143.5,999,400,0,-90,90]
ct11	cn90		[233.5,644,400,0,90,0]
ct12	cn90		[45,1089,-400,0,90,0]
ct13	cn90		[143.5,999,-400,0,-90,90]
ct14	cn90		[233.5,644,-400,0,90,0]

The photos Frame TS-1A and solid models and photos of TS-1B, and TS-1C are depicted in Figure 2.14 to 2.16.

Figure 2.15 Photo of Frame TS-1A and measurement system.
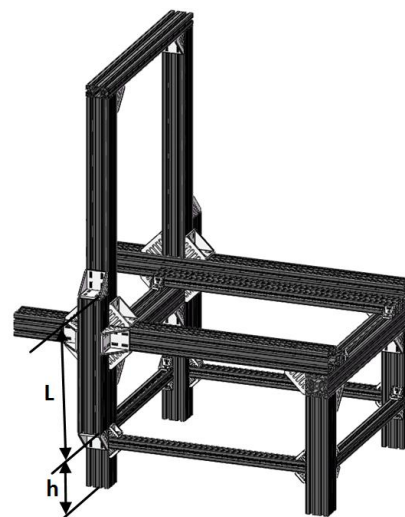
(a)   (b)

Figure 2.16 Photo of Frame TS-1B (a) and solid model of Frame TS-1B (b).
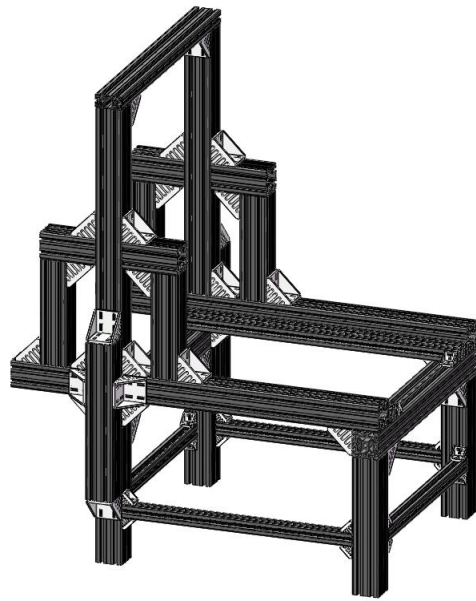
(a)   (b)

Figure 2.17 Photo of Frame TS-1B (a) and solid model of Frame TS-1C (b).

The results are given in Table 2.13, 2.14, and 2.15 for Frame TS-1A, TS-1B, and TS-1C, respectively. See Figure 2.4 for the locations of the excitation and the sensor points.

Table 2.13 Natural frequencies for Frame TS-1A

		f_{bx} (Mode-bx)	f_{bz} (Mode-bz)	f_{ty} (Mode-ty)
Simulation	Beam FE ($I_{Gz}=J_{Gt}$) s_p=[15,19,149317]	31.52	40.34	58.06
Experiment		30.74 p_g=[z, A, C]	39.42 p_g=[x, B, C]	56.35 p_g=[x, A, C]

Table 2.14 Natural frequencies for Frame TS-1B

		f_{bx} (Mode-bx)	f_{bz} (Mode-bz)	f_{ty} (Mode-ty)
Simulation	Beam FE ($I_{Gz}=J_{Gt}$) s_p=[16,23,166911]	43.72	42.88	61.22
Experiment		38.91 p_g=[z, A, C]	41.98 p_g=[x, B, C]	61.46 p_g=[x, A, C]

Table 2.15 Natural frequencies for Frame TS-1C

		f_{bx} (Mode-bx)	f_{bz} (Mode-bz)	f_{ty} (Mode-ty)
Simulation	Beam FE ($I_{Gz}=J_{Gt}$) $\mathbf{s}_p$=[19,27,199059]	36.83	50.62	61.25
Experiment		33.29 $\mathbf{p}_g$=[z, A, C]	43.53 $\mathbf{p}_g$=[x, B, C]	58.89 $\mathbf{p}_g$=[x, A, C]

The mode shapes are given in Figure 2.17, 2.18, and 2.19 for Frame TS-1A, TS-1B, and TS-1C, respectively.
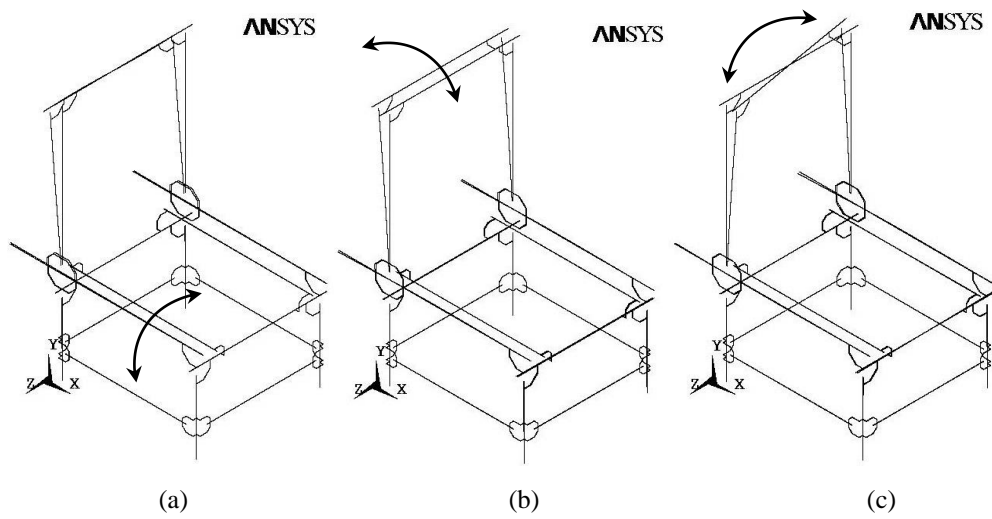

Figure 2.18 Mode-bx (a), Mode-bz (b), and Mode-ty (c) for TS-1A.
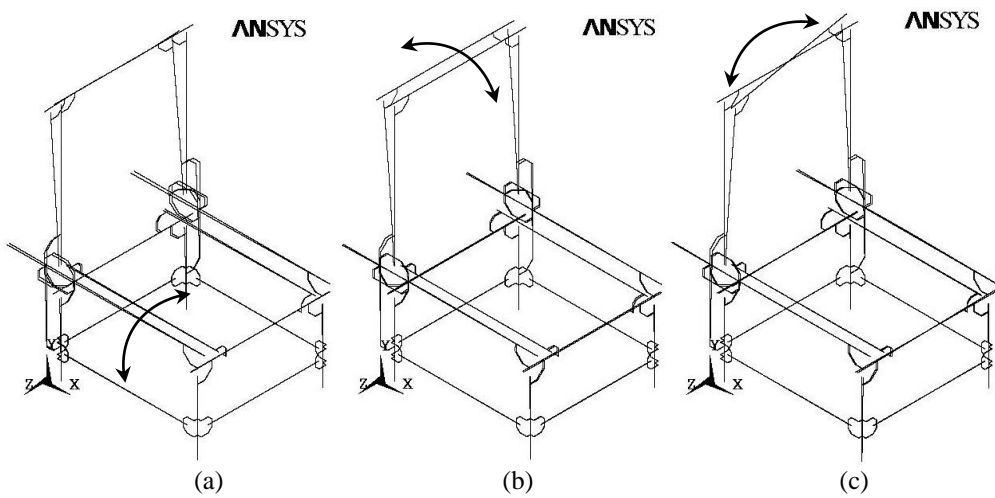

Figure 2.19 Mode-bx (a), Mode-bz (b), and Mode-ty (c) for TS-1B.
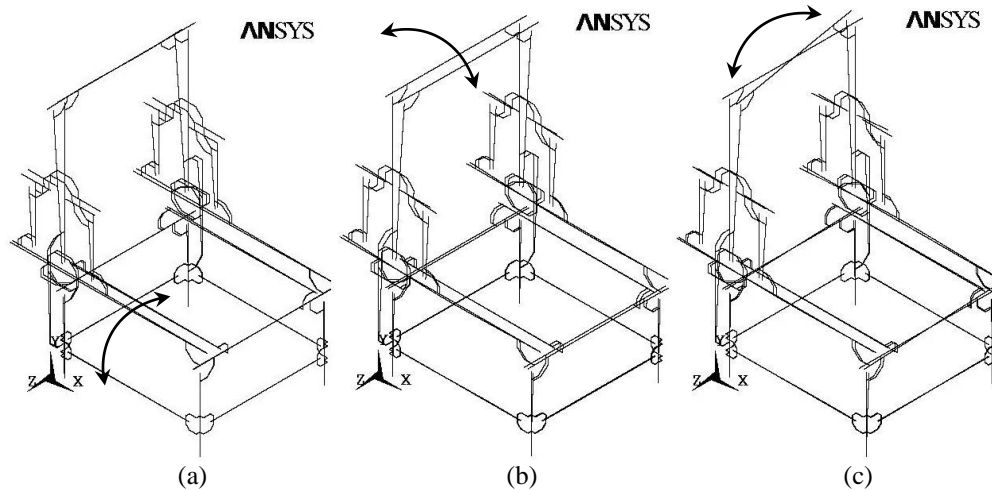
Figure 2.20 Mode-bx (a), Mode-bz (b), and Mode-ty (c) for TS-1C.

Simulation results given in Table 2.13 show that Mode-bx, Mode-bz, and Mode-ty have natural frequencies of 31.52, 40.34, and 58.06 Hz. These frequencies increase by 12.20, 2.54, and 3.16 Hz, respectively, for TS-1B as observed in Table 2.14. These frequencies increase by 5.31, 10.28, and 3.19 Hz, respectively, for TS-1C as observed in Table 2.15.

Experimental results given in Table 2.13 show that Mode-bx, Mode-bz, and Mode-ty have natural frequencies of 30.74, 39.42, and 56.35 Hz. These frequencies increase by 8.17, 2.56, and 5.11 Hz, respectively, for TS-1B as observed in Table 2.14. These frequencies increase by 2.55, 4.11, and 2.54 Hz, respectively, for TS-1C as observed in Table 2.15.

Simulation and experimental results show similar trend for increasing natural frequencies with reinforcing. Reinforcing in TS-1B is more effective to increase the natural frequencies. Natural frequencies increase as stiffness/mass ratio effect of reinforcing increase.

42

CHAPTER THREE

MODELING OF AXES AND FINITE ELEMENT ANALYSIS OF VERTICAL MACHINING CENTER

3.1 Introduction

This work introduces a new approach for the finite element analysis of a vertical machining center which consists of linear motion systems (LMS) by beam elements. Frames with aluminum profiles and connecting parts are discussed in Chapter 2. Analysis of whole assembly with moving members is given in this chapter. Beam elements are used because finite element analysis of vertical machining center which consist of linear motion systems by solid elements is generally not possible because of complicated shapes of cross sections of aluminum profiles or other parts. BEAM44 element in ANSYS is used.

Vertical machining center is designed so that it meets kinematic (the workspace and velocity of the end-point), kinetic (gravity forces, inertial forces due to accelerations, and end-point work forces), and rigidity (permissible end-point deflections due to flexibilities) requirements. Kinematic, kinetic, and rigidity evaluation charts are used to evaluate vertical machining center when a task is assigned.

The finite element analysis of vertical machining center developed in this study is explained on an example system (LMS-1A) shown in Figure 3.1. The system locates a hexapod which can be used for medical operations.
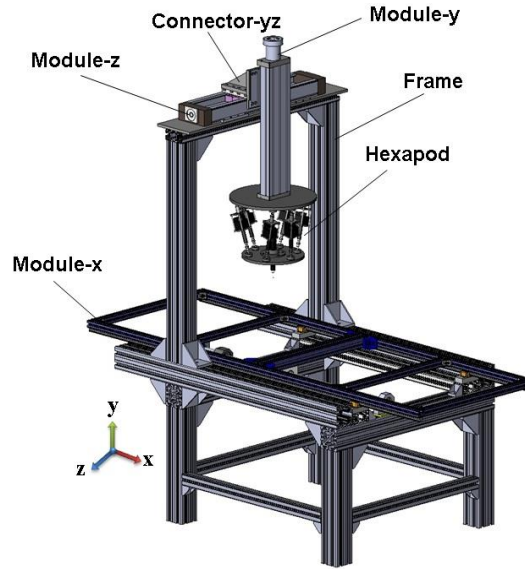
Figure 3.1 The vertical machining center (LMS-1A) for locating hexapod.

The frame (TS-1A) of the system is considered in Chapter 2 of this study. In order to provide high-precision performance, ball-screw driven servomechanisms (linear modules) are used for each of the axes. The linear modules (LM-x, LM-y and LM-z) and Connector-yz are shown in Figure 3.2. The strokes are 700 mm, 280 mm and 400 mm for LM-x, LM-y and LM-z, respectively.

(a)   (b)   (c)   (d)

Figure 3.2 (a) LM-x, (b) LM-y, (c) LM-z, (d) Connector-yz.

3.2 Modeling of Linear Modules

Module-z (LM-z) is explored for modeling as an example. It is manufactured by Bosch-Rexroth (Model CKK20-145, see Figure 3.3). Solid model of LM-z is shown

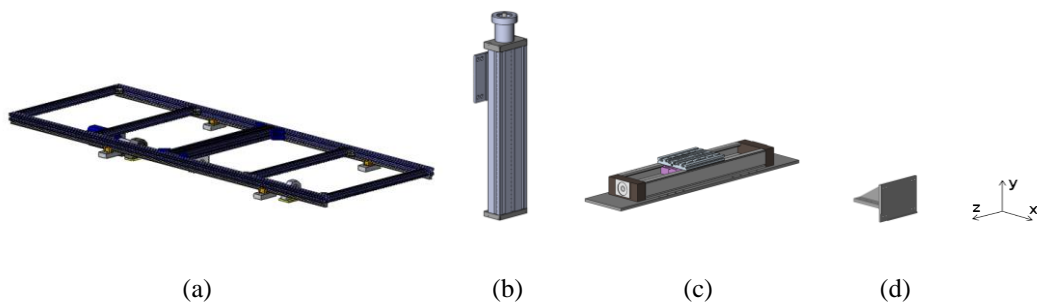in Figure 3.4. The module is composed of two members. They are called Module member-1 and Module member-2. The members have relative sliding motion in the linear motion direction (z axis). Number of 4 cars (runner-blocks) in Module member-2 can slide along number of 2 guides in Module member-1. The motor actuates through the ball screw and the nut. Module member-2 moves if Module member-1 is fixed, or Module member-1 moves if Module member-2 is fixed. z_e is the movement position. Module member-2 is the moving member in this work. The module has 400 mm stroke.

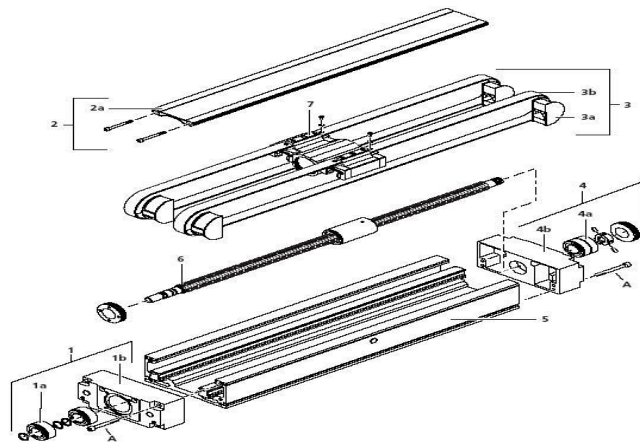Figure 3.3 Exploded view of CKK20-145 (Bosch-Rexroth AG, 2007).

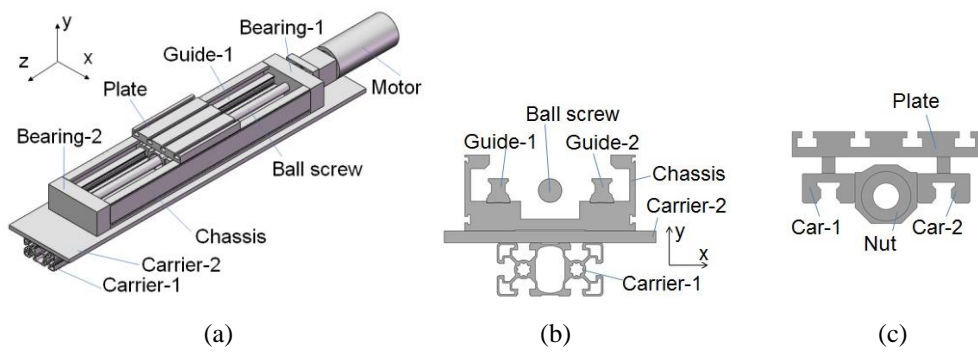(a)   (b)   (c)

Figure 3.4 LM-z (a), cross section of Module member-1 (b), and cross section of Module member-2 (c).

As explained in Chapter 2 of this thesis, beam lines are defined for the beam finite element analysis. Beam cross section attributes are assigned to the beam lines. The

section properties of the profiles and the other parts are defined by $\mathbf{p}_s$ and $\mathbf{q}_G$. $\mathbf{p}_s$=[A, I_{Gx}, I_{Gy}, I_{Gt}, S_{dx}, S_{dy}, y_T, y_B, x_L, x_R] and $\mathbf{q}_G$=[x_G,y_G].The material properties are defined by $\mathbf{p}_m$ = [E, ρ, υ, β]. $\mathbf{p}_s$ and $\mathbf{q}_G$ are used for BEAM44 finite element in ANSYS. The nodes have 6 degrees of freedom, defined by $\mathbf{u}$=[d_x,d_y,d_z,r_x,r_y,r_z]. d_x,d_y,d_z are translational displacements in the global x,y, and z directions, respectively. r_x,r_y,r_z are rotational displacements about the local x,y, and z axes respectively. The displacements are given in mm, the rotations are given in degree (deg) unless otherwise stated.

The geometrical properties of sections used in linear modules in this study are given in Table 3.1. The database for LM-z is given in Table 3.2. The line model of LM-z is shown in Figure 3.5. There are two main axes in the line model of modules, Axis-AB and Axis-CD. The local origin is A. The local z axis is on Axis-AB. Axis-CD is parallel to Axis-AB. The local coordinates of C is given as x_C=0, y_C=66.5, z_C=0. The axes of the beam lines are Axis-AB or Axis-CD. The nodal center of the cross section of a beam is on its beam line. The location of the area center of gravity of a beam cross section is defined by $\mathbf{q}_G$=[x_G,y_G] (Figure 2.5 in Chapter 2) . L_b is the length of a beam. z_O is the local z component of the origin of a beam line. There are extension beams which labeled like Ext.-B1. The information about the extension beams is given below.

Table 3.1 Geometrical properties of sections

Section	File name	$\mathbf{p}_s$
	brx15_ray	[2,.5,.3,.4,1.21,1.42,1.42,8.5,7.7,7.5,7.5]
	bscrew_D25	[4.9,1.9,1.9,3.8,1.17,1.17,1.17,12.5,12.5,12.5,12.5]
	bscrew25_end	[1.8,.2,.2,.5,1.17,1.17,1.17,7.5,7.5,7.5,7.5]
	lx_coupling	[22,44.7,44.7,89.3,1.38,1.38,1.38,27.5,27.5,27.5,27.5]
	motor200w	[9.7,36,36,72,1.97,1.97,1.97,30,30,30,30]
	motor200w_mil	[1.5,.2,.2,.4,1.17,1.17,1.17,7,7,7,7]
	lx_flans	[47.9,285.6,424.9,563,1.96,1.72,1.72,37.5,37.5,45,45]
	lx_fixed_bear	[45.4,198.4,358.8,323,1.53,2.08,2.08,44.4,27.6,54,54]

46

Table 3.1 continue (Geometrical properties of sections)
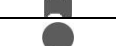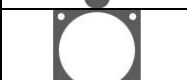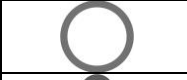
	lx_floating_bear	[42.7,185.9,352.2,306.8,1.57,2.21,2.21,45.4,26.6,54,54]
	brx_rb15	[5.3,1.7,6.1,1.5,2.57,1.57,1.57,8.8,11,17,17]
	x_axis_car_base	[18,6,121.5,20.7,1.2,1.19,1.19,10,10,45,45]
	x_axis_nut_housing	[43.9,183.9,322.4,390.3,1.79,1.6,1.6,32.1,32.9,42.5,42.5]
	x_nuta	[25.3,70.6,70.6,141.2,1.57,1.57,1.57,31,31,31,31]
	x_nutb	[6.4,8.3,8.3,16.6,1.87,1.87,1.87,19,19,19,19]
	lx_bear_base	[16.8,1.4,395.1,5.4,1.2,1.19,1.19,5,5,84,84]
	ly_p54x120	[19.1,46,352.6,3.8,2.95,3.68,3.68,35.8,24.2,60,60]
	ly_brx15_ray1	[2,.3,.5,.4,1.42,1.21,1.21,7.5,7.5,7.7,8.5]
	ly_brx15_ray2	[2,.3,.5,.4,1.42,1.21,1.21,7.5,7.5,8.5,7.7]
	bscrew15	[1.8,.2,.2,.5,1.17,1.17,1.17,7.5,7.5,7.5,7.5]
	brx_rb15_1	[5.3,6.1,1.7,1.5,1.57,2.57,2.57,17,17,11,8.8]
	brx_rb15_2	[5.3,6.1,1.7,1.5,1.57,2.57,2.57,17,17,8.8,11]
	p_bear10x30	[77.1,337.2,1003.9,846.2,1.48,1.4,1.4,35.3,34.7,60,60]
	bear10x30	[6.1,3.8,3.8,7.5,1.47,1.47,1.47,14.8,14.8,14.8,14.8]
	ly_flans_a	[15.7,51,51,102.1,1.88,1.88,1.88,30,30,30,30]
	ly_flans_b	[30.6,170.3,170.3,340.6,1.84,1.84,1.84,40,40,40,40]
	motor400w	[11.9,42.2,42.2,84.4,1.94,1.94,1.94,30,30,30,30]
	motor400w_mil	[1.5,.2,.2,.4,1.17,1.17,1.17,7,7,7,7]
	brx_nut15a	[16.3,25.8,25.8,51.6,1.44,1.44,1.44,24,24,24,24]
	brx_nut15b	[4.4,2.8,2.8,5.5,1.74,1.74,1.74,14,14,14,14]
	lynut2rblock	[7.1,12.9,61.2,.3,2.3,3.15,3.15,13,34,60,60]
	lymodul2ckk_cpart	[16.9,1,563.3,3.9,1.2,1.19,1.19,4.2,4.2,100,100]
	ly_coupling	[5.2,3.6,3.6,7.1,1.7,1.7,1.7,14.8,14.8,14.8,14.8]
	lz_p64x145	[34.2,111.1,880.3,30.2,2.49,5.02,5.02,44.6,29.4,72.5,72.5]

Table 3.1 continue (Geometrical properties of sections)

	s10x180	[18,1.5,486,5.8,1.2,1.19,1.19,5,5,90,90]
	lz_brx20_ray1	[3.1,1.2,.7,1,1.24,1.43,1.43,10.8,9.7,10,10]
	bscrew20	[3.1,.8,.8,1.6,1.17,1.17,1.17,10,10,10,10]
	ckk20_145_rb_a	[6.9,3.1,12,2.3,3.27,1.66,1.66,12.9,12.4,20.2,20.2]
	ckk_cap	[92.8,316.8,1625.9,918.4,1.2,1.19,1.19,32,32,72.5, 72.5]
	bscrew20_end	[1.5,.2,.2,.4,1.17,1.17,1.17,7,7,7,7]
	ckk_flans_a	[20.1,150.4,187.4,222.7,3.04,2.14,2.14,37.5,37.5,4 0,40]
	ckk_flans_b	[17.7,55.9,86.5,103.1,2.48,1.81,1.81,26,26,31,31]
	motor750w	[21.7,136,136,272,1.94,1.94,1.94,40,40,40,40]
	motor750w_mil	[2.8,.6,.6,1.3,1.17,1.17,1.17,9.5,9.5,9.5,9.5]
	lz_coupling	[5.4,3.6,3.6,7.3,1.66,1.66,1.66,14.8,14.8,14.8,14.8]
	ckk_plate	[22.2,7.6,365.3,12,1.89,1.76,1.76,10.5,9,72,72.2]
	ckk_rb2plate_a	[1.2,.2,.1,.2,1.2,1.2,1.2,6.2,6.2,5,5]
	ckk_nut	[8.2,9.4,9.4,18.9,1.73,1.73,1.73,19,19,19,19]
	ckk_car2nut	[7.4,14.9,20.1,30.3,2.18,1.94,1.94,19.5,25.5,23.8,2 3.8]

Cars, guides, ball screws, nuts, bearings, motor assembly parts are steel. The other elements are aluminum. $\mathbf{p}_m$=[69,2700,0.3,0] for aluminum (Al-6063-T6), and $\mathbf{p}_m$=[210,7800,0.29,0] for steel.
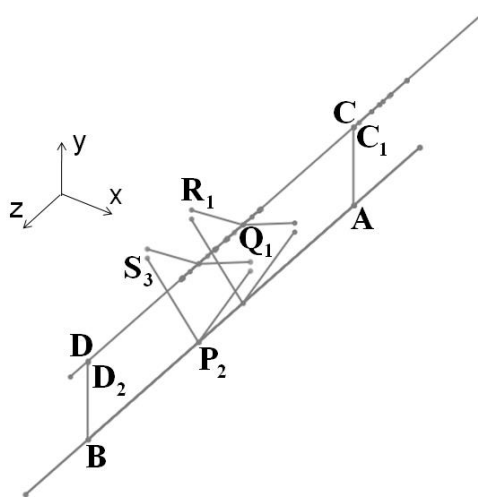
Figure 3.5 Line model of LM-z.

48

Table 3.2 Database for LM-z

Beam label	Section file name	Beam axis	z_O	$\mathbf{q}_G$	L_b
Chassis[a]	s145x64	AB	0	[0,51.94]	600
Carrier-1	s90x45L	AB	-149	[0,0]	890
Carrier-2	s10x180	AB	-149	[0,27.5]	890
Guide-1	lz_brx20_ray1	AB	0	[-44,65.83]	600
Guide-2	lz_brx20_ray2	AB	0	[44,65.83]	600
Bearing-1	ckk_cap	AB	-40	[0,-2]	40
Bearing-2	ckk_cap	AB	600	[0,-2]	40
Ball screw	bscrew20	CD[b]	0	[0,0]	600
Ball screw end	bscrew20_end	CD	-66	[0,0]	66
Car-1	ckk20_145_rb_a	CD	z_e	[-44,7.07]	72.5
Car-2	ckk20_145_rb_b	CD	z_e	[44,7.07]	72.5
Car-3	ckk20_145_rb_a	CD	z_e +100	[-44,7.07]	72.5
Car-4	ckk20_145_rb_b	CD	z_e +100	[44,7.07]	72.5
Plate	ckk_plate	CD	z_e -3.75	[0,38.97]	180
Nut1	ckk_nut	CD	z_e +16.25	[0,0]	40
Nut2	ckk_nut	CD	z_e +116.25	[0,0]	40
Motor	motor750w	CD	-297.5	[0,0]	177.5
Motor shaft	Motor750w_mil	CD	-120	[0,0]	40
Coupling	lz_coupling	CD	-84	[0,0]	72
Flange1	ckk_flans_a	CD	-58	[0,0]	18
Flange2	ckk_flans_b	CD	-120	[0,0]	62
Connector Car-1	ckk_rb2plate_a	CD	z_e	[-44,23.77]	72.5
Connector Car-2	ckk_rb2plate_b	CD	z_e	[44,23.77]	72.5
Connector Car-3	ckk_rb2plate_a	CD	z_e +100	[-44,23.77]	72.5
Connector Car-4	ckk_rb2plate_b	CD	z_e +100	[44,23.77]	72.5
Nut case-1	ckk_car2nut	CD	z_e -3.75	[0,4.56]	80
Nut case-2	ckk_car2nut	CD	z_e +96.25	[0,4.56]	80

[a] *The modul is located with* $\mathbf{q}_L$=[45,1556.5,-741,0,0,0]
[b] y_C = 66.5 mm

Line-AC$_1$ and Line-BD$_2$ in Figure 3.5 are defined as the extension beam lines for Ext.-B1 and Ext.-B2. C$_1$ has the same x and z coordinates of C. The y component of C$_1$ is 1 mm smaller than the y component of C. D$_2$ has the same x and z coordinates of D. The y component of D$_2$ is 1 mm smaller than the y component of D. The 1 mm gaps are used to model bearings. The cross section of an extension beam is assumed

to be the same as the adjacent beam. A negligible value (1 kg/m^3) is assigned to the densities (ρ) of extension beams. The constraints are assigned to model bearings. The nodal displacements d_x, d_y, d_z, r_x, r_y are assigned as coupled for C and C_1 to model Bearing-1, which is a fixed bearing. The nodal displacements d_x, d_y, r_x, r_y are assigned as coupled for D and D_2 to model Bearing-2, which is a slider bearing.

The cross section with Carrier-1, Ball screw, Car-1, Car-2, Guide-1, Guide-2 only is shown in Figure 3.6.
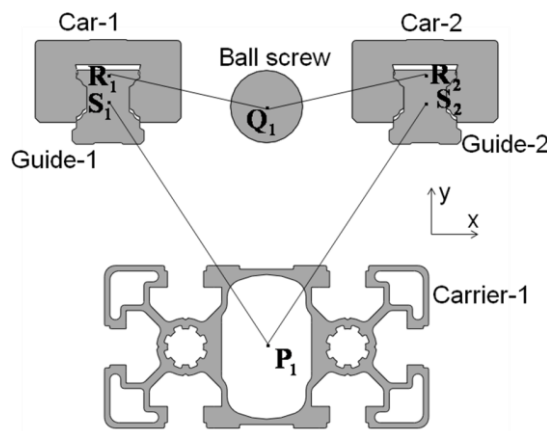
Figure 3.6 Cross section with Carrier-1, Ball screw, Car-1, Car-2, Guide-1, and Guide-2 only.

The nodal centers of Carrier-1, Guide-1, and Guide-2 are located at P_1, which is on Axis-AB. The area centers of gravity of Carrier-1, Guide-1, and Guide-2 are at P_1, S_1, and S_2, respectively. The nodal centers of Ball screw, Car-1, and Car-2 are located at Q_1, which is on Axis-CD. The area centers of gravity of Ball screw, Car-1, and Car-2 are at Q_1, R_1, and R_2, respectively. R_1 and R_2 are at the mid-points of the beam lines for Car-1 and Car-2, respectively. The extension beam lines are defined as Line-P_1S_1, Line-P_1S_2, Line-Q_1R_1, and Line-Q_1R_2. These extension beam lines are for the beams labeled as Ext.-G1-C1, Ext.-G2-C2, Ext.-C1-G1, and Ext.-C2-G2, respectively. The cross sectional properties of Ext.-G1-C1, Ext.-G2-C2, Ext.-C1-G1, and Ext.-C2-G2 are assumed to be the same as Guide-1, Guide-2, Car-1 and Car-2, respectively.

Similarly, the cross section with Carrier-1, Ball screw, Car-3 and Car-4 are considered and the extension beam lines for Ext.-G1-C3, Ext.-G2-C4, Ext.-C3-G1, and Ext.-C4-G2 extension beams.

The nodal displacements d_x,d_y,r_x,r_y,r_z are assigned as coupled for R_1 and S_1 to allow sliding between Car-1 and Guide-1 in the z direction. Similar constraints are assigned to model sliding between all the cars and guides. The constraints are listed in Table 3.3.

Table 3.3 Constraints for LM-z

Points	Coupled nodal displacements	
A and C_1	d_x,d_y,d_z,r_x,r_y	Bearing-1
B and D_2	d_x,d_y,r_x,r_y	Bearing-2
R_1 and S_1	d_x,d_y,r_x,r_y,r_z	Car-1/Guide-1
R_2 and S_2	d_x,d_y,r_x,r_y,r_z	Car-2/Guide-2
R_3 and S_3	d_x,d_y,r_x,r_y,r_z	Car-3/Guide-1
R_4 and S_4	d_x,d_y,r_x,r_y,r_z	Car-4/Guide-2

The motor and its connection parts are modeled approximately by equivalent beams. The section properties of the equivalent beams assigned so that the equivalent assembly has the same inertia as the real motor assembly.

A finite element size L_e is defined. ANSYS generates beam finite elements with a size of L_e. The nodes of the elements on separate lines are not bonded although they occupy a common space. They are merged by the command *nummrg*. L_e is chosen so that the divisions of all the lengths to L_e give integers without remainders. So, the attached or connected beams are modeled.

Nodal forces are given by $\mathbf{f}=[f_x,f_y,f_z,T_x,T_y,T_z]$, where f_x, f_y, and f_z are the forces in the global x, y and z directions respectively; T_x,T_y, and T_z are the moments about the global x, y and z axes respectively. Metric units are used for forces unless otherwise stated. The nodal forces at C_1, D_2, R_1, R_2, R_3, and R_4 are evaluated for the loadings of Bearing-1, Bearing-2, Car-1, Car-2, Car-3, and Car-4 respectively. Let the nodal

force component f_z be f_1 and f_2 at Q_1 and Q_2, respectively. $T_e=f_e h/(2\pi)$, where T_e is the motor moment, $f_e=f_1+f_2$, and h is the pitch of the ball screw.

The database for a module is given as its origin is at the global origin and its chassis is in the z direction first. Then the module can be moved to any location by defining the location of the chassis beam line by $\mathbf{q}_L$ (defined in Section 2.2 of Chapter 2).

The database for LM-y is given in Table 3.4. Solid model of LM-y and its line model are presented in Figure 3.7. Module member-2 with cars is the moving member. y_e is the movement position. The stroke of LM-y is 200 mm.

Table 3.4 Database for LM-y

Beam label	Section file name	Beam axis	z_O	$\mathbf{q}_G$	L_b
Chassis[a]	s120x54	AB	0	[0,0]	518
Guide-1	ly_brx15_ray1	AB	0	[-37.34,21.78]	518
Guide-2	ly_brx15_ray2	AB	0	[37.34,21.78]	518
Bearing-1	p_bear10x30	AB	-15	[0,-2]	15
Bearing-2	p_bear10x30	AB	518	[0,-2]	15
Ball screw	bscrew15	CD[b]	-15	[0,0]	548
Ball screw end	bscrew15	CD	-39	[0,0]	24
Car-1	brx_rb15_1	CD	y_e+15	[-29.77,0.0045]	60
Car-2	brx_rb15_2	CD	y_e +15	[29.77,0.0045]	60
Car-3	brx_rb15_1	CD	y_e +107	[-29.77,0.0045]	60
Car-4	brx_rb15_2	CD	y_e +107	[29.77,0.0045]	60
Plate	lynut2rblock	CD	y_e +15	[0,13.20]	150
Nut1	brx_nut15a	CD	y_e +3	[0,0]	12
Nut2	brx_nut15b	CD	y_e +15	[0,0]	26
Motor	motor750w	CD	-251.5	[0,0]	156.5
Motor shaft	motor200w_mil	CD	-95	[0,0]	30
Coupling	ly_coupling	CD	-84	[0,0]	64
Flange1	ly_flans_a	CD	-75	[0,0]	60
Flange1	ly_flans_b	CD	-95	[0,0]	20
Bear1	bear10x30	CD	-15	[0,0]	15
Bear2	bear10x30	CD	518	[0,0]	15
Connector part	lymodul2ckk_cpart	CD	y_e +15	[0,28.38]	150

[a] *The module is located with* $\mathbf{q}_L$=[215.4865, y_e+1783.5001, z_e -661.75,90,-90,0]
[b] y_C=21.77 mm

(a)   (b)
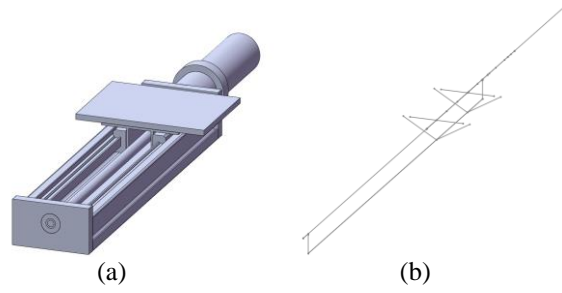
Figure 3.7 (a) Solid model, and (b) line model of LM-y

The database for LM-x is given in Table 3.5. LM-x and its line model are shown in Figure 3.8. Module member-1 with guides is the moving member. x_e is the movement position. The stroke is 700 mm.

Table 3.5 Database for LM-x[a]

Beam Label	Section file name	L_b	q_L	q_G
b51	s30x30	1865	[x_e-496,658,310, 90,0,90]	[0,0,0]
b52	s30x30	1865	[x_e -496,658,-310, 90,0,90]	[0,0,0]
b53	s30x30	590	[x_e +1354,658,295,180,0,0]	[0,0,0]
b54	s30x30	590	[x_e +892.5,658,295,180,0,0]	[0,0,0]
b55	s90x45L	590	[x_e +437,658,295,180,0,90]	[0,0,0]
b56	s30x30	590	[x_e -19.5,658,295,180,0,0]	[0,0,0]
b57	s30x30	590	[x_e -481,658,295,180,0,0]	[0,0,0]
lx_ray1	brx15_ray	1865	[x_e -496,658,310,90,-90,90]	[0,22.6625,0]
lx_ray2	brx15_ray	1865	[x_e -496,658,-310,90,-90,90]	[0,22.6625,0]
lx_bscrew	bscrew_D25	918	[0,600,145,90,0,90]	[0,0,0]
lx_bscrew_end	bscrew25_end	30	[-30,600,145,0,90,0]	[0,0,0]
lx_coupling	lx_coupling	72	[-97,600,145,0,90,0]	[0,0,0]
lx_motor	motor200w	131.5	[-244.5,600,145,0,90,0]	[0,0,0]
lx_motor_mil	motor200w_mil	30	[-113,600,145,0,90,0]	[0,0,0]
lx_flans	lx_flans	16	[-113,600,145,0,90,0]	[0,0,0]
lx_fixed_bear	lx_fixed_bear	46	[0,600,145,0,90,0]	[0,-11.427,0]
lx_floating_bear	lx_floating_bear	28	[890,600,145,0,90,0]	[0,-12.3712,0]
lx_car1	brx_rb15	40.5	[875.25,576.5,310,90,-90,90]	[0,-51.2607,0]
lx_car2	brx_rb15	40.5	[875.25,576.5,-310,90,-90,90]	[0,-51.2607,0]
lx_car3	brx_rb15	40.5	[-42.75,576.5,-310,90,-90,90]	[0,-51.2607,0]
lx_car4	brx_rb15	40.5	[-42.75,576.5,310,90,-90,90]	[0,-51.2607,0]
lx_car1_base	x_axis_car_base	45	[873,576.5,310,0,90,0]	[0,32.5,0]
lx_car2_base	x_axis_car_base	45	[873,576.5,-310,0,90,0]	[0,32.5,0]
lx_car3_base	x_axis_car_base	45	[-45,576.5,-310,0,90,0]	[0,32.5,0]
lx_car4_base	x_axis_car_base	45	[-45,576.5,310,0,90,0]	[0,32.5,0]
lx_nut_housing	x_axis_nut_housing	40	[x_e +437,600,145,0,90,0]	[0,1.8874,0]
lx_nut_a	x_nuta	12	[x_e +425,600,145,0,90,0]	[0,0,0]
lx_nut_b	x_nutb	33	[x_e +437,600,145,0,90,0]	[0,0,0]

53

Table 3.5 continue (Database for LM-x[a])

lx_flb_base	lx_bear_base	79.5	[838.5,600,145,0,90,0]	[0,-41,0]
lx_fxb_base	lx_bear_base	210.5	[-134.5,600,145,0,90,0]	[0,-41,0]
cx51	cn330		[x_e +1339,658,295,-90,0,90]	
cx52	cn30		[x_e +1339,658,-295.5,0,0,90]	
cx53	cn30		[x_e +907.5,658,295,0,180,-90]	
cx54	cn30		[x_e +907.5,658,-295.5,0,0,-90]	
cx55	cn30		[x_e +877.5,658,295,-90,0,90]	
cx56	cn30		[x_e +877.5,658,-295.5,0,0,90]	
cx57	cn30		[x_e +482,658,295,0,180,-90]	
cx58	cn30		[x_e +482,658,-295,0,0,-90]	
cx59	cn30		[x_e +392,658,295,-90,0,90]	
cx60	cn30		[x_e +392,658,-295,0,0,90]	
cx61	cn30		[x_e -4.5,658,295,0,180,-90]	
cx62	cn30		[x_e -4.5,658,-295.5,0,0,-90]	
cx63	cn30		[x_e -34.5,658,295,-90,0,90]	
cx64	cn30		[x_e -34.5,658,-295.5,0,0,90]	
cx65	cn30		[x_e -466,658,295,0,180,-90]	
cx66	cn30		[x_e -466,658,-295.5,0,0,-90]	

[a] The data is given in global coordinates

(a)   (b)
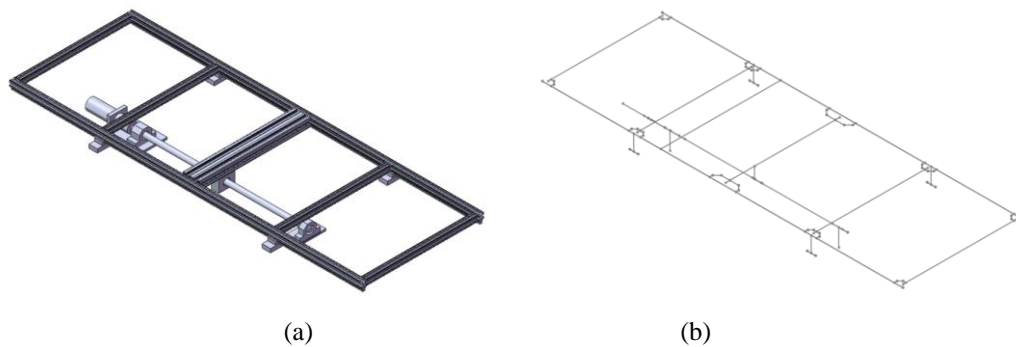
Figure 3.8 (a) Solid model, and (b) line model of LM-x.

Extension beams and constraints are defined for LM-y and LM-x as defined for LM-z above.

3.3 Modeling of Connector-yz

LM-z and LM-y are connected by Connector-yz as shown in Figure 3.1 and 3.2. The solid and line models of Connector-yz are shown in Figure 3.9.

(a)	(b)
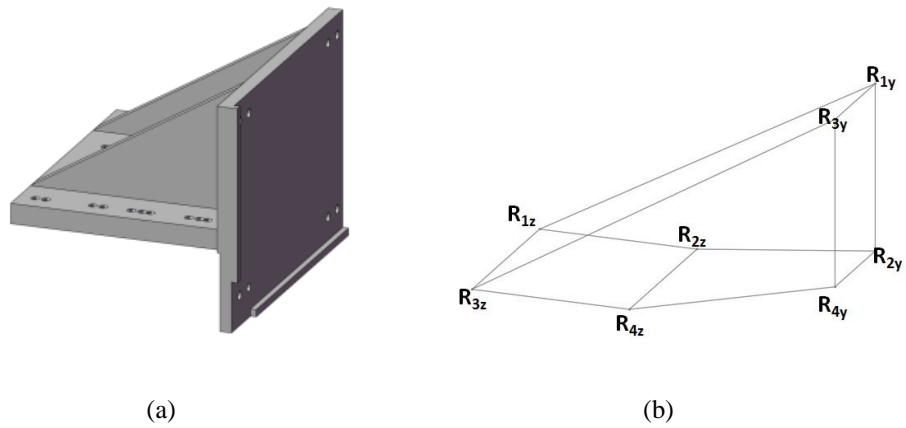
Figure 3.9 (a) Solid model, and (b) line model of Connector-yz.

4 nodal centers of the cars in LM-z are connected to 4 nodal centers of the cars in LM-y by the beams defined on the beam lines. R_{3z} is the nodal center of Car-3 of LM-z for example. Beam section properties are assigned by trial so that the mass and stiffness properties of the solid model are approximately equal to the beam model. The density value for the beam materials is assigned so that the total mass of the solid model is equal to the total mass of the beam model. The total mass of Connector-yz is 5.49 kg. The cross sectional properties of the beams have the same value in the line model of Connector-yz. The beam model is assigned so that the solid model has approximately the same deformation under static loading. Static analysis result obtained by using solid elements and applied loads ($f_x=f_y=f_z=1N$) are shown in Figure 3.10.

(a)	(b)
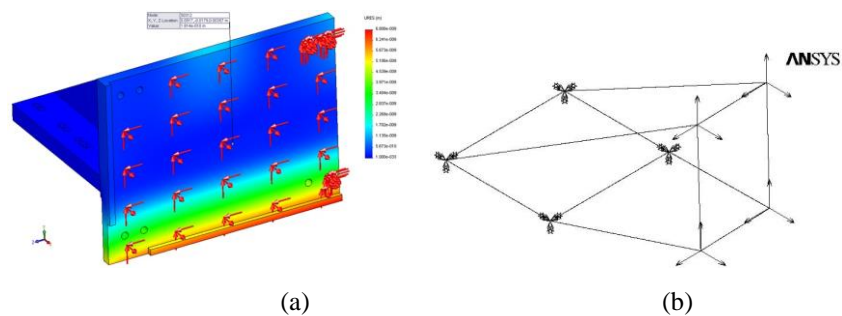
Figure 3.10 Static analysis results for Connector-yz, $u_{sum}=1.814 \times 10^{-10}$ m (a), $u_{sum}=1.814 \times 10^{-10}$ m (b).

The cross sectional properties of the beams are obtained as $\mathbf{p}_s$=[243.30,1700000,1700000,152.7,3.26,3.26,45,45,45,45].

3.4 Modeling of Linear Motion System

The line model of the complete linear motion system (LMS) is shown in Figure 3.11.The line models of the frame, LM-x, LM-y, and LM-z are assembled. In the finite element model and experiments, an end-point mass, which is approximately equal weight (18 kg) of hexapod, is used instead of the hexapod. The end-point mass which represented with Line-EL (EL=70 mm) as beam is attached to LM-y in the model. Section properties of the end-point mass are given as

$\mathbf{p}_s$= [360.3,11492,10716,10267,1.18,2.55,2.55,220,109.7,107.2,220].
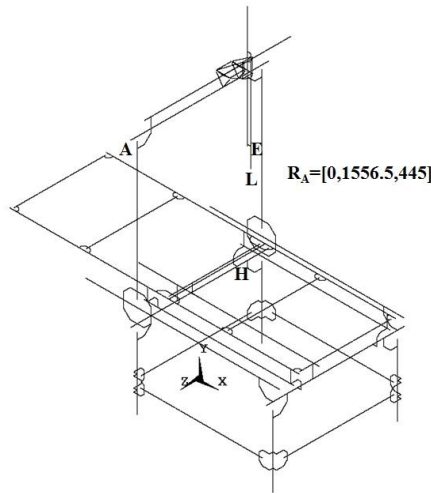
Figure 3.11 Line model of LMS

The end point, E, is located at x=134.8865+x_e, y=1272.5+y_e, and z= −195+z_e in the global coordinates. The end point location is defined by $\mathbf{q}_e$=[x_e, y_e, z_e].

LMS can be used for milling or pick and place operations. Cutting forces in milling, and inertia forces in pick and place applications are applied. Milling application is considered in this study. It is assumed that a work-piece is placed between E and H. H is on LM-x (see Figure 3.8). External nodal forces are applied to the nodes at E and H for the analysis. The cutting forces are transmitted through the

work-piece, and thus if $\mathbf{f_c}$ is applied to E, -$\mathbf{f_c}$ is applied to H. $\mathbf{f_c}$ is assigned as $\mathbf{f_c}$=[50,350,50,0,0,0], considering the forces required to cut materials like bone, wood, and plastics.

ANSYS constructs the following mathematical model of LMS for a given end point location, $\mathbf{q_e}$.

$$[\mathbf{M}]\{\ddot{\mathbf{d}}\}+[\mathbf{C}]\{\dot{\mathbf{d}}\}+[\mathbf{K}]\{\mathbf{d}\}=\{\mathbf{f}\}$$

Here, [M], [C], and [K] are the global mass, damping and stiffness square matrixes. {d} is the nodal displacement column matrix, {f} is the external nodal force column matrix. The distributed gravity forces in the −y direction is defined in ANSYS by using ACEL command.

The end point location changes during the milling operation, and thus the square matrices change. The system is time dependent. The force matrix may also change during the milling.

3.5 Engineering Analysis of Linear Motion System

Engineering analyses are performed after modeling the linear motion system (LMS). Modal analysis is performed first. The following equation is solved for the modal analysis, and the mode shapes and the natural frequencies are found.

$$[\mathbf{M}]\{\ddot{\mathbf{d}}\}+[\mathbf{K}]\{\mathbf{d}\}=\{\mathbf{0}\}$$

The inertia forces are ignored for the milling application and static analysis is performed. The following equation is solved for the static analysis; and the stresses, deformations, and internal nodal forces are evaluated.

$$[\mathbf{K}]\{\mathbf{d}\}=\{\mathbf{f}\}$$

The output quantities considered for the evaluation of LMS is listed in Table 3.6.

Table 3.6 Output quantities and their limit values

Output quantity	Limit value
sten: Maximum tension stress	80 MPa
scom: Maximum compression stress	80 MPa
uend: End point displacement	1 mm
[fy,fz,mx,my,mz]: Nodal forces for cars[a] LM-x	[5400,5400,52,19,19]
[fx,fz,mx,my,mz]: Nodal forces for cars[a] LM-y	[5400,5400,19,52,19]
[fx,fy,mx,my,mz]: Nodal forces for cars[b] of LM-z	[14500,14500,100,100,190]
lx-te:Motor moment for LM-x[c]	0.64 Nm
ly-te:Motor moment for LM-y[d]	1.30 Nm
lz-te:Motor moment for LM-z[e]	2.40 Nm

[a] *Bosch-Rexroth, BOSCH-R166619420-RB15*
[b] *Bosch-Rexroth, BOSCH-R169481411-RB20*
[c] *Mitsubishi,HCKFS-23B*
[d] *Mitsubishi,HCKFS-43B*
[e] *Mitsubishi,HCKFS-73B*

The percentages of the calculated output quantities to the corresponding limit values are shown in the evaluation charts below. The percentages must be below 100.

3.6 Results and Discussion

The vertical machining center under consideration is produced. The photo of vertical machining center under consideration is shown in Figure 3.12.
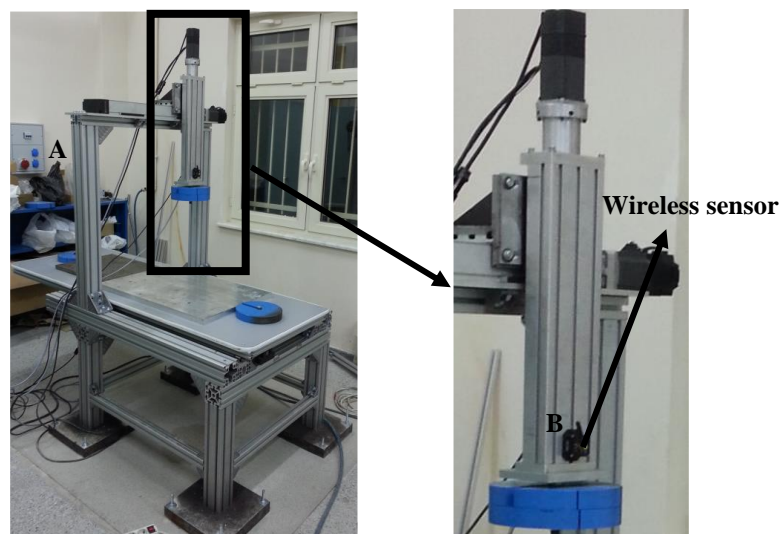
Figure 3.12 The vertical machining center and end point mass.

The finite element analyses and experiments are conducted in different positions of the axes (LM-x, LM-y, LM-z) for obtaining natural frequencies of the system. It is also, static finite element analysis is performed to evaluate the loading on the moving components and frame of LMS.

3.6.1 Modal Analysis

Experiments and finite element analysis are conducted in different three positions of the system. The position vectors of the end point are defined with $\mathbf{q_e} = [x_e, y_e, z_e]$ in local coordinates of the axes. The experimental results were obtained using a wireless vibration sensor (MicroStrain G-Link tri-axial accelerometer). The FFTs (Fast Fourier Transforms) of the recorded signals in the x, y, and z directions are taken. fty, fbx, fbz are natural frequencies corresponding to the mode shapes where the frame mainly makes torsional vibration about the y-axis (Mode-ty), bending vibration about the x-axis (Mode-bx), and bending vibration about the z-axis (Mode-bz), respectively. The information about the geometrical parameters for a measurement is given by $p_g = [z, A, B]$ as an example. z is the direction of the excitation and the signal component, A is the excitation point, and B is the sensor point (see Figure 3.12). The excitation is an impact.

The solid model and finite element model of the system are given in Figure 3.13 to 3.15. The number of nodes in the finite element analysis (FEA) is 289385. The translational displacements and rotational angles of ground nodes are assumed to be equal to zero in the finite element models.

(a)   (b)
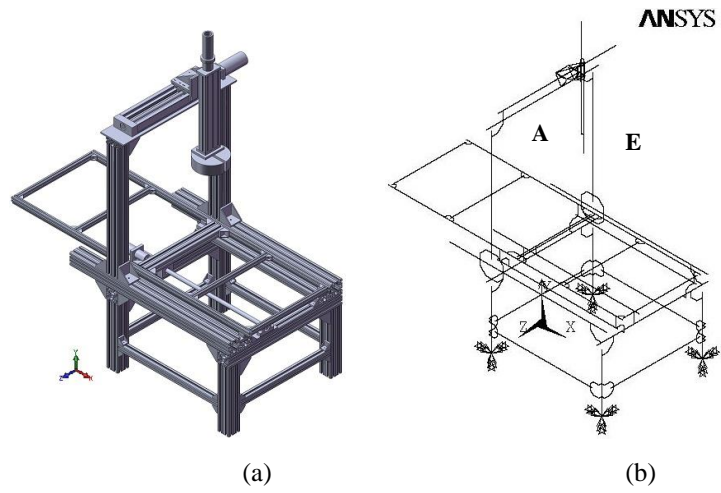
Figure 3.13 Solid model and finite element model of the system at position $\mathbf{q_e}$ =[0,0,0].

(a)   (b)
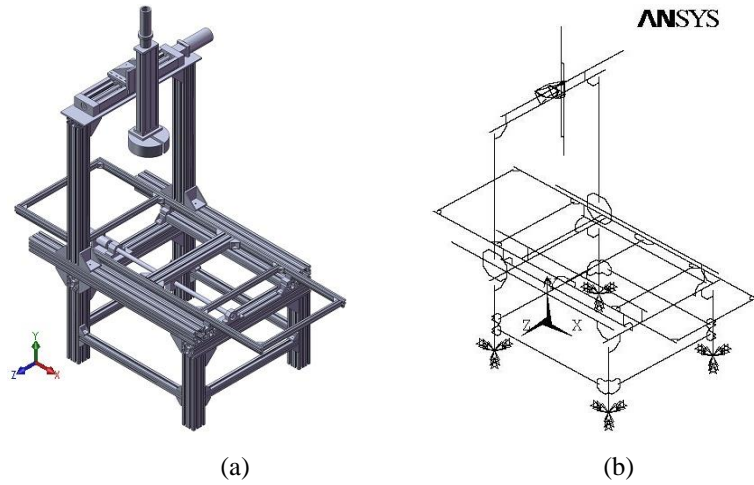
Figure 3.14 Solid model and finite element model of the system at position $\mathbf{q_e}$ =[350,100,200].

(a)   (b)
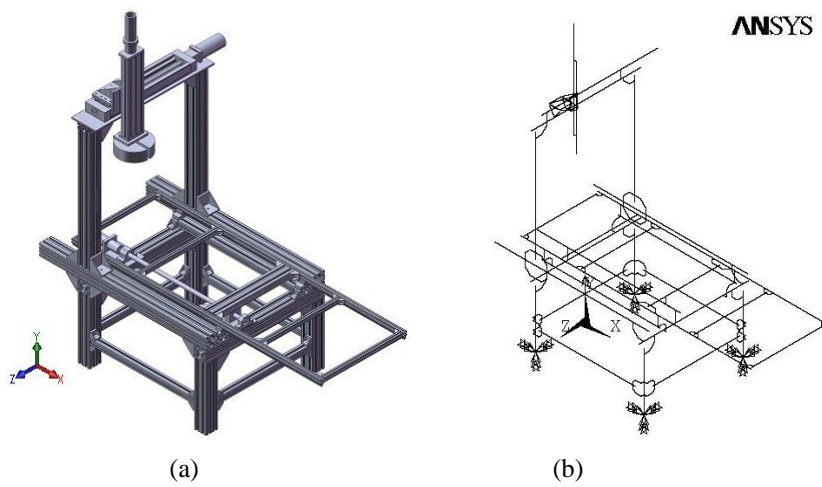
Figure 3.15 Solid model and finite element model of the system at position $\mathbf{q_e}$ =[700,200,400].

Natural frequencies of the system are given in Table 3.7. The mode shapes of the system are given in Figure 3.16, 3.17, and 3.18 for position q_e =[0,0,0], q_e =[350,100,200] and q_e =[700,200,400], respectively.

Table 3.7 Natural frequencies for the vertical machining center.

q_e (mm)	f_{bx} (Hz) p_g=[z,A,E]		f_{bz} (Hz) p_g=[x,A,E]		f_{ty} (Hz)	
	Simulation	Experiment	Simulation	Experiment	Simulation	Experiment
[0,0,0]	10.73	10.12	11.39	11.09	19.98	-
[350,100,200]	10.82	10.54	11.16	12.11	19.11	-
[700,200,400]	11.01	10.82	10.49	11.45	18.89	-

(a)　　　　　　　　　　(b)　　　　　　　　　　(c)
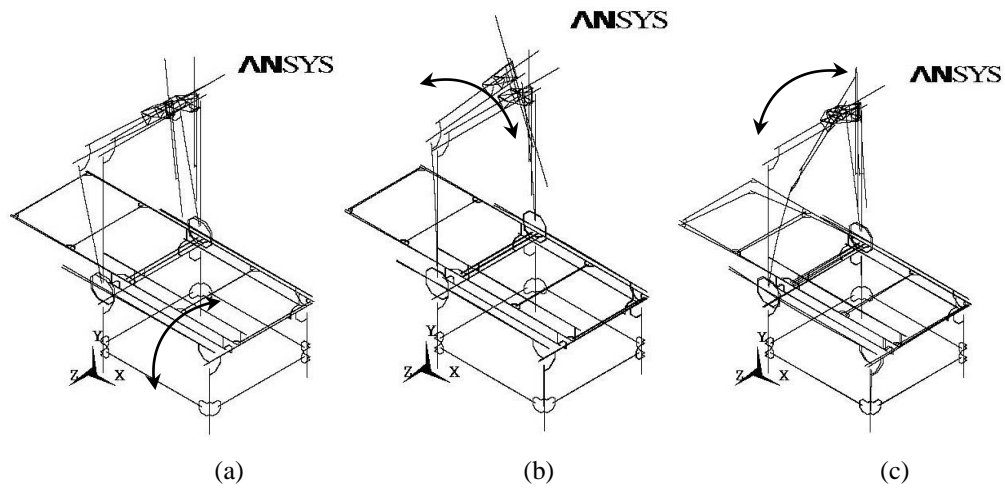
Figure 3.16 Mode-bx (a), Mode-bz (b), and Mode-ty (c) for q_e =[0,0,0].

(a)　　　　　　　　　　(b)　　　　　　　　　　(c)
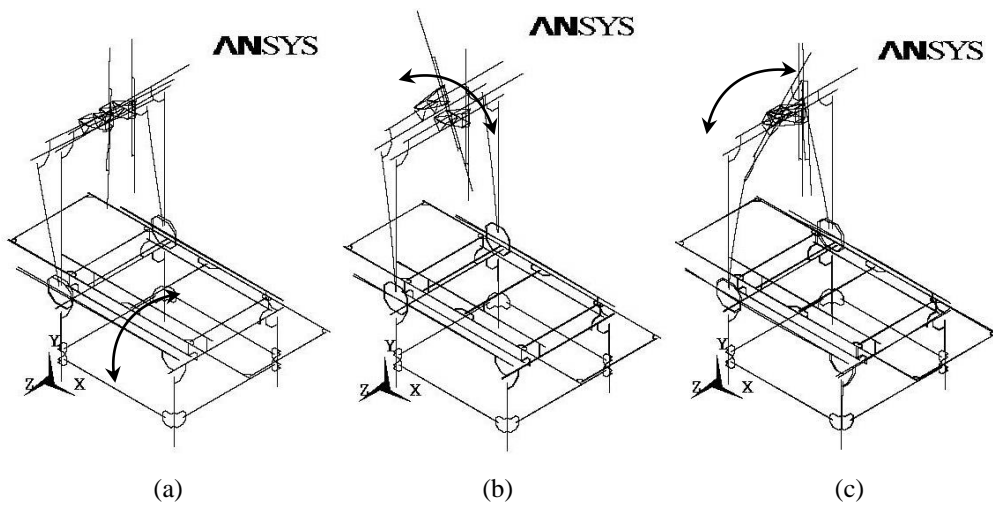
Figure 3.17 Mode-bx (a), Mode-bz (b), and Mode-ty (c) for q_e =[350,100,200].
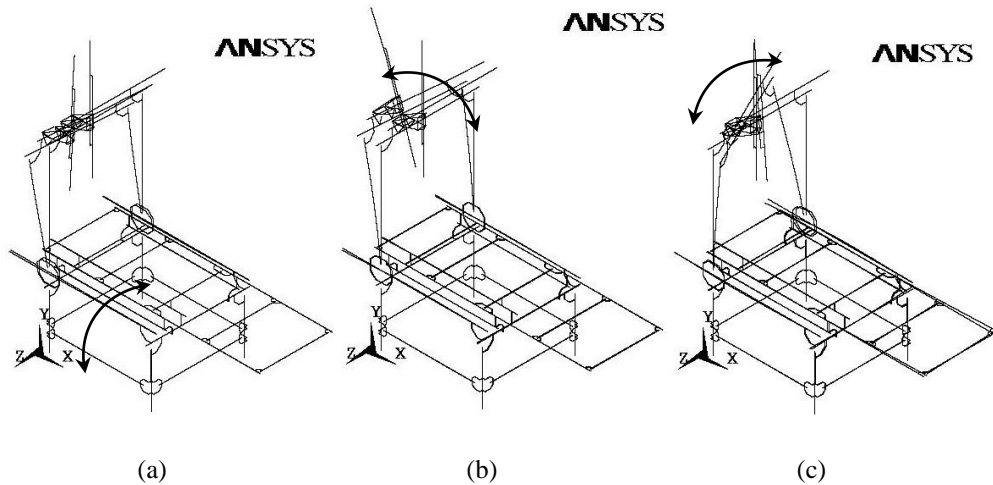
Figure 3.18 Mode-bx (a), Mode-bz (b), and Mode-ty (c) for $\mathbf{q_e}$=[700,200,400].

Simulation and experimental results show similar trend depending on the positions. As the rigidity of the system increases the natural frequencies increase.

It is also defined rigidity space of the system according to natural frequencies (f_{bx}, f_{bz} and f_{ty}) of the system. To demonstrate the rigidity space, numbers of 441 position vectors of the end point are defined. These position vectors are lie on yz- plane of the system. A Visual Basic program is prepared to obtain the natural frequencies from FEA. The program constructs ANSYS macro files which create finite element models according to position vectors. And then, the program is performed modal analyses by using these macro files in batch mode of ANSYS software. The rigidity spaces of the system are shown in Figure 3.19, 3.20 and 3.21.
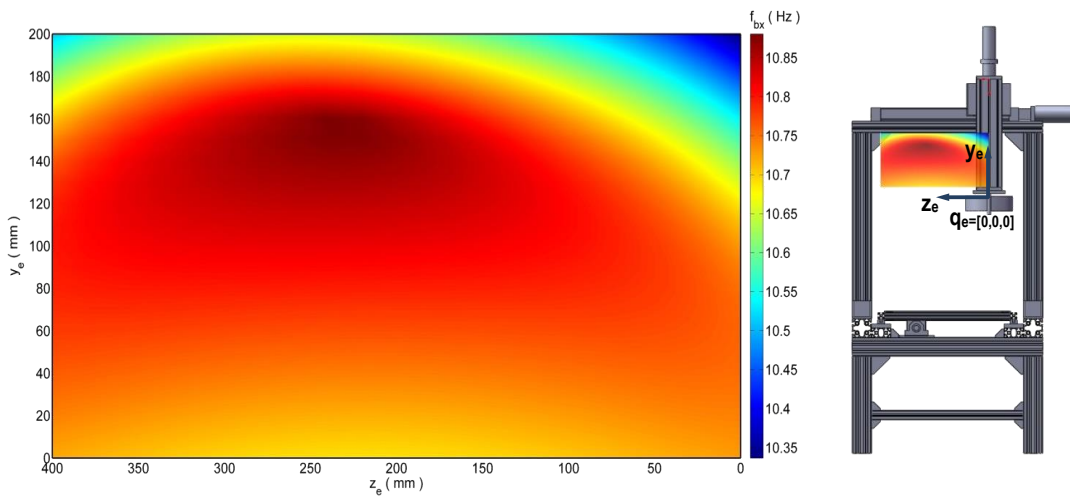
Figure 3.19 Rigidity space for f_{bx}.
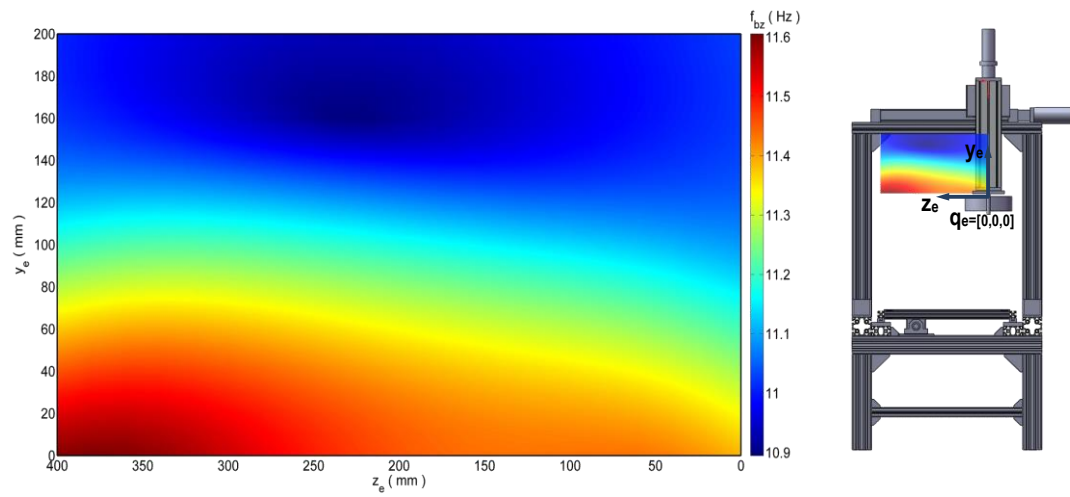
Figure 3.20 Rigidity space for f_{bz}.
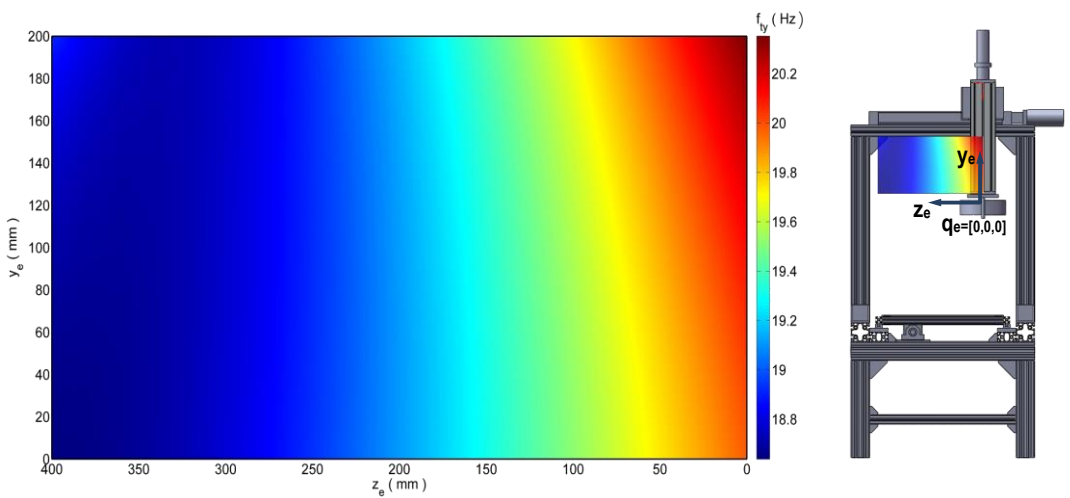
Figure 3.21Rigidity space for f_{ty}.

3.6.2 Static Analysis

The evaluation charts are given in Figure 3.22, 23, and 24 obtained from the static FEA results. The results are given for different end point locations, $\mathbf{q}_e$. The output quantities considered are listed in the charts. lz-car3-mx indicates that the output quantity of m_x for Car-3 of LM-z for example. The percentage values found are given and they are plotted as horizontal lines. A horizontal line is colored as green if the percentage less than 50%. It is colored as brown if the percentage is in the interval of 51-100%. It is colored as red if the percentage is above 100%. 50% and 100% values are shown as vertical lines.
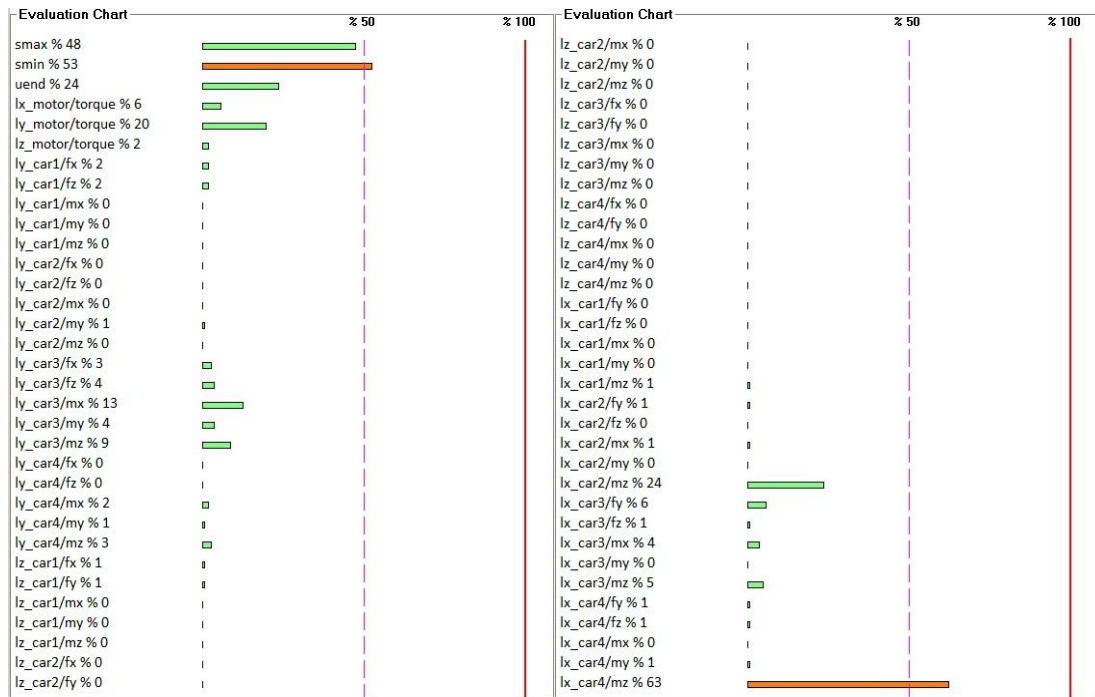
Figure 3.22 Evaluation chart for $\mathbf{q}_e$=[0,0,0] (Position-1).
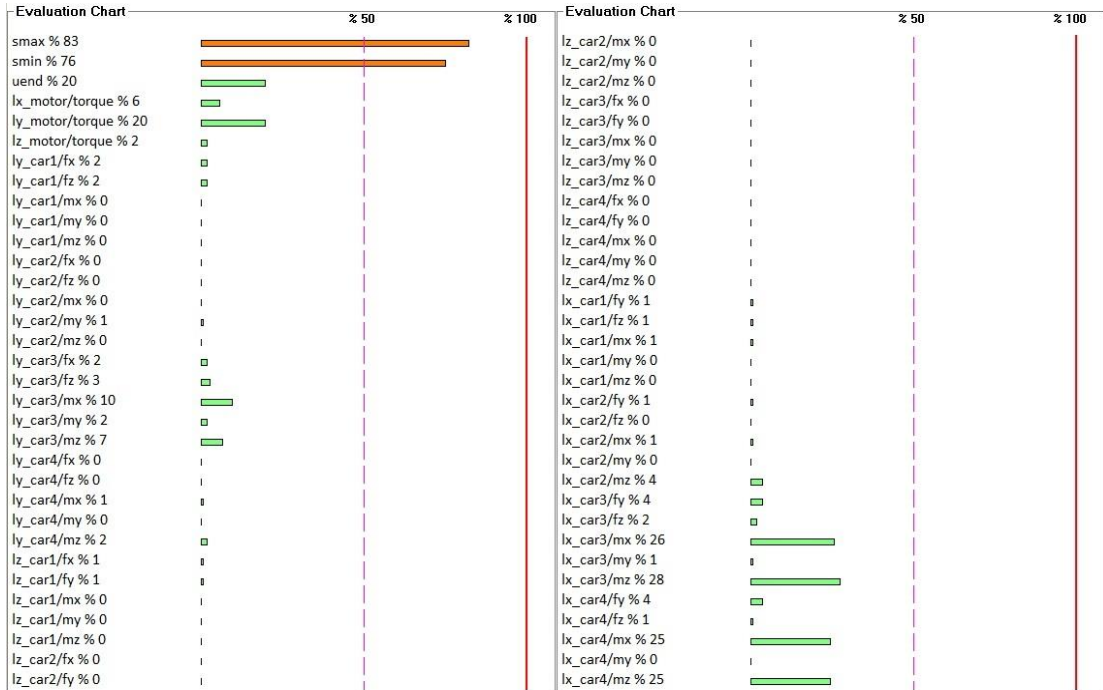
Figure 3.23 Evaluation chart for $\mathbf{q}_e$=[350,100,200] (Position-2).
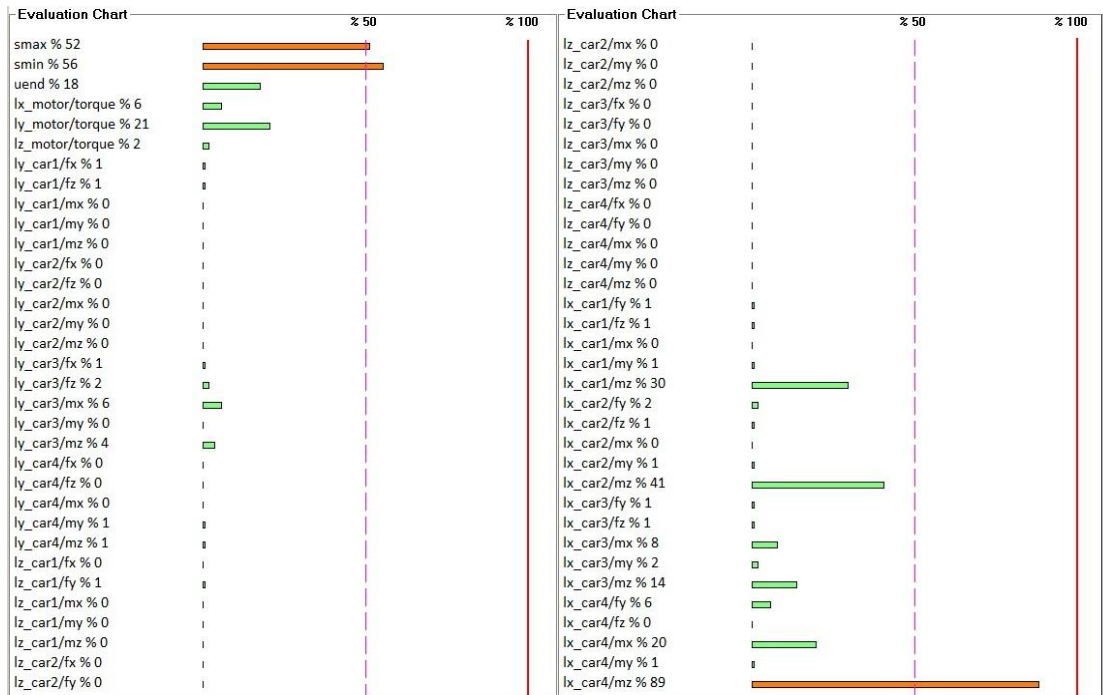
Figure 3.24 Evaluation chart for $\mathbf{q}_e$=[700,200,400] (Position-3).

The lower percentage for an output quantity indicates a longer life span. It is observed that as the end-point location changes the percentage values change. The percentages are different for different parts for a position. For example, ly-car3-mx has a percentage of 13; ly-car4-mz has a percentage value of 3 for Position-1 as seen in Figure 3.22. The percentage values also change when the end point position changes. For example, ly-car3-mx has a percentage of 13, 10, and 6 for Position-1, Position-2, and Position-3 as seen in Figure 3.22, 3.23, and 3.24, respectively.

CHAPTER FOUR

DYNAMIC ANALYSIS

4.1 Introduction

Vibrations occurred after moving of the axes and controls of vibrations are investigated in this chapter. To control the residual vibrations of LMS, trapezoidal motion profile is applied with open loop control. Experiments, finite element simulations and signal analysis method are conducted for the control purpose.

Vibrations are occurred along the period of the motion and after finished the motion due to inertia forces in flexible systems. Vibrations arisen after the motion is called residual vibrations. Residual vibrations significantly affect positioning achievement of the end point in flexible systems. If the magnitudes of the residual vibrations increase, steady state time is increase. Hence, positioning errors become the end point of the system. Decreasing of the residual vibrations is more important subject in flexible systems in terms of precision of the positioning.

Benosman & Le Vey (2004) presented a survey on control of residual vibrations at robots and flexible structures. Dynamic analysis of flexible robots investigated with classification of one axis, two axis and multi axis (Dwivedy & Eberhard, 2006). Active and passive control can apply for controlling of the residual vibrations (Preumont, 2002). Residual vibrations of flexible structures can decrease by changing motion commands with open loop control (Pereira , Trapero , Diaz , Feliu, 2012 ; Mimmi & Pennacchi, 2001 ; Shan, Liu & Sun, 2005). Diken & Alghamdi (2003) applied the control for controlling the residual vibrations on rotating an aluminum beam by using motion profile.

Dynamic behavior of structures can be determined by finite element models. There is need to construct detailed finite element model to obtain the dynamic response of the structures to real world external forces. Solution time is substantially long due to detailed finite element models containing numerous degrees of freedom.

Acquiring time of solution is important in terms of rapid design modifications. In addition to, these models require to large computer capacity to obtain dynamic responses of the structures.

Dynamic properties of the structures can also be acquired by the impulse response function between the excitation and response. Impulse response function sets the relation between the excitation and the response in time domain. If we know time history of the signal of the impulse response function (transfer function), we can predict the response caused by arbitrary excitation.

To explain impulse response approach with signal analysis, first two degrees of freedom system is taken into account. Therefore, applicable of this approach can be shown clearly on multi degrees of freedom system. And then dynamic analysis with finite element and the control of residual vibrations of LMS will examine with experiments and finite element simulations. Finally, impulse response approach will be applied to obtain the dynamic response of LMS.

4.2 Two Degrees of Freedom System

Two degrees of freedom spring-mass system is taken into account as an example. The system is indicated in Figure 4.1. The motion of the system is completely described by the coordinates $x_1(t)$ and $x_2(t)$, which define the positions of the masses m_1 and m_2 at any time t from respective equilibrium positions. The external forces $f_1(t)$ and $f_2(t)$ act on the masses m_1 and m_2 respectively.
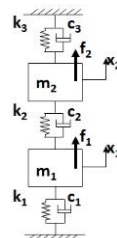
Figure 4.1 Two degrees of freedom system, where, $m_1=5.8$ kg and $m_2=3.2$ kg, $k_1=4325$ N/m, $k_2=3850$ N/m and $k_3=3500$ N/m, $c_1=37.2$ N.s/m, $c_2=33.5$ N.s/m and $c_3=32$ N.s/m.

After the kinetic and potential energies of the system considered are found, the equations of motion are obtained applying Lagrange equation and written in matrix format as follows;

$$\begin{bmatrix} m_1 & 0 \\ 0 & m_2 \end{bmatrix} \begin{Bmatrix} \ddot{x}_1 \\ \ddot{x}_2 \end{Bmatrix} + \begin{bmatrix} c_1 + c_2 & -c_2 \\ -c_2 & c_2 + c_3 \end{bmatrix} \begin{Bmatrix} \dot{x}_1 \\ \dot{x}_2 \end{Bmatrix} + \begin{bmatrix} k_1 + k_2 & -k_2 \\ -k_2 & k_2 + k_3 \end{bmatrix} \begin{Bmatrix} x_1 \\ x_2 \end{Bmatrix} = \begin{Bmatrix} f_1 \\ f_2 \end{Bmatrix} \quad (4.1)$$

It is necessary to solve the equations of motion to obtain the time history response of the system in Equation 4.1. The equations are linear ordinary differential equations. Several numerical methods are available for the solution of the equations. One of these methods is the Newmark numerical integration method. Time response of the system can also be obtained by using impulse response function method. Also, analytical solution can be used to find the time response of the system. In this example, analytical solution, Newmark integration method, impulse response function method and finite element results are compared with each other.

For the analytical solution, if the input is $f(t)=e^{st}$ and the response is $x(t)=H(s)e^{st}$. Applying the Laplace transform to Equation 4.1 by substituting numerical values and Equation 4.2 is obtained.

$$\begin{Bmatrix} X_1 \\ X_2 \end{Bmatrix} = \begin{bmatrix} \dfrac{160s^2 + 3275s + 367500}{D(s)} & \dfrac{1675s + 192500}{D(s)} \\ \dfrac{1675s + 192500}{D(s)} & \dfrac{290s^2 + 3535s + 408750}{D(s)} \end{bmatrix} \begin{Bmatrix} F_1 \\ F_2 \end{Bmatrix} \quad (4.2)$$

The transfer function between the input $F_1(s)$ and response $X_2(s)$ can be obtained as following,

$$X_2(s) = H_{21}(s) \cdot F_1(s) \quad (4.3)$$

$$D(s) = 928s^4 + 30307s^3 + 3614930s^2 + 39857875s + 2263187500$$

$$H_{21}(s) = \frac{1675s + 192500}{D(s)} \tag{4.4}$$

$x_2(t)$ can be obtained by taking inverse Laplace transform of $X_2(s)$. The impulse response of $x_2(t)$ is shown in Figure 4.2.
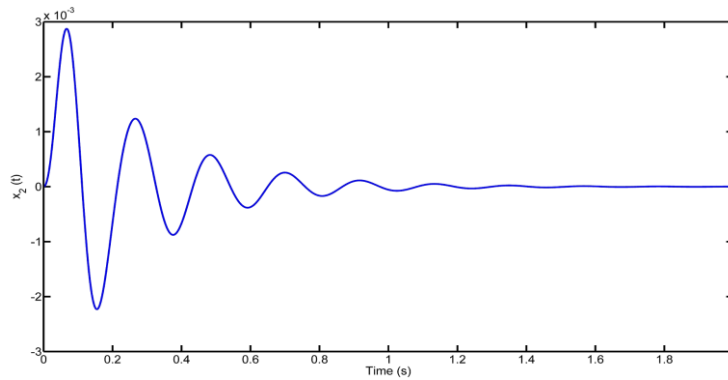
Figure 4.2 Impulse response of $x_2(t)$ from analytical solution.

Figure 4.3 shows a comparison between the impulse responses of $x_2(t)$ obtained from three different methods, while Figure 4.4 shows a zoomed view of the boxed region of the response plots.

Figure 4.3 Impulse responses of $x_2(t)$ with three different methods.

70
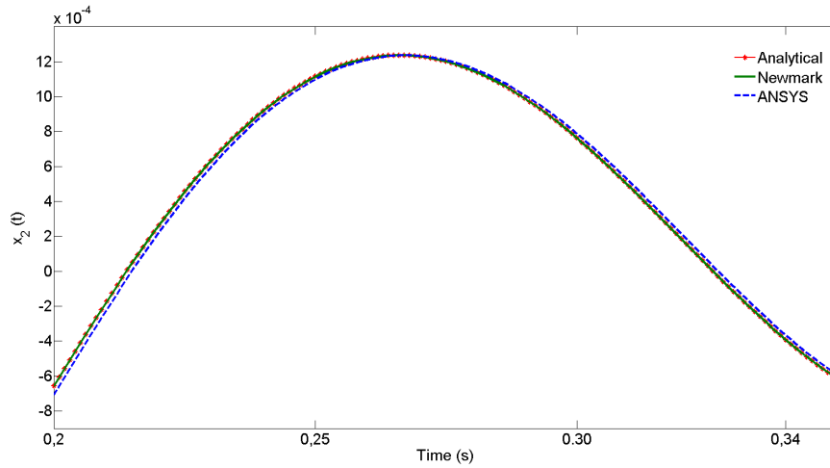
Figure 4.4 Zoomed view of impulse responses of $x_2(t)$ with three different methods.

The fast Fourier transform of Equation 4.3 gives

$$X_2(i\omega) = F_1(i\omega) \cdot H_{21}(i\omega) \tag{4.5}$$

Where $H_{21}(i\omega)$ is the frequency-response function (FRF). When $f_1(t)$ is an impulse force, the fast Fourier transform of $f_1(t)$ becomes $F_1(i\omega)=1$, and Equation 4.5 becomes

$$X_2(i\omega) = H_{21}(i\omega) \tag{4.6}$$

In other words, the fast Fourier transform of the response function $x_2(t)$ becomes the FRF when $f_1(t)$ is an impulse force. Therefore we can use samples of the impulse response to obtain response of arbitrary excitation for the system. The relationships between input f_1 and response x_2 are schematically shown in Figure 4.5.
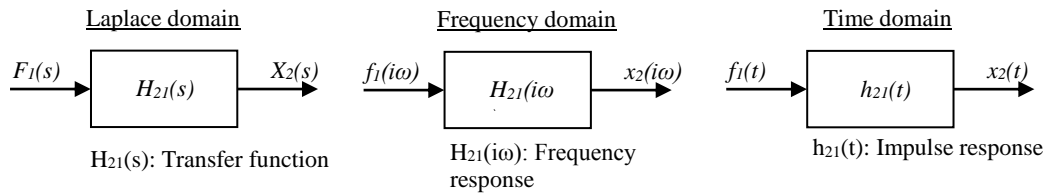
Figure 4.5 System input-response relationships in time and transformed domain.

We now consider the response of the system to an input force f_1 is given as in Figure 4.6. Time parameters of input f_1 is defined by $t=[t_a,t_c,t_d,t_s]$ and force

71

parameters is defined by $f_i=[F_a,F_d]$. t_i is given in second and f_i is given in Newton, unless otherwise stated.

The form of input f_1 is described by

$$
\begin{aligned}
f_1(t) &= 0 && \text{for} && t = 0 \\
&= F_a && \text{for} && 0 < t \le t_a \\
&= 0 && \text{for} && t_a < t \le t_a + t_c \\
&= F_d && \text{for} && t_a + t_c < t \le t_a + t_c + t_d \\
&= 0 && \text{for} && t_a + t_c + t_d < t \le t_s && (4.7)
\end{aligned}
$$
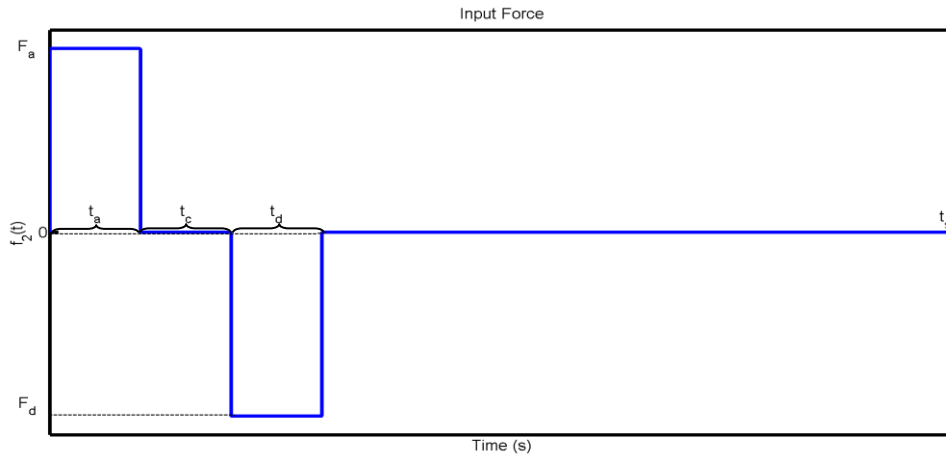
Figure 4.6 Input force $f_1(t)$.

We first make transient analysis to obtain time history of the impulse response $x_2(t)$ in ANSYS. After obtaining the samples of the response from ANSYS results, we prepare the samples of input force $f_1(t)$ with MATLAB code. The input parameters for $f_1(t)$ are chosen as $f_1=[100,-100]$, $t=[0.2,0.2,0.2,2]$. The time response of $x_2(t)$ is acquired according to procedure which is illustrated in Figure 4.7.
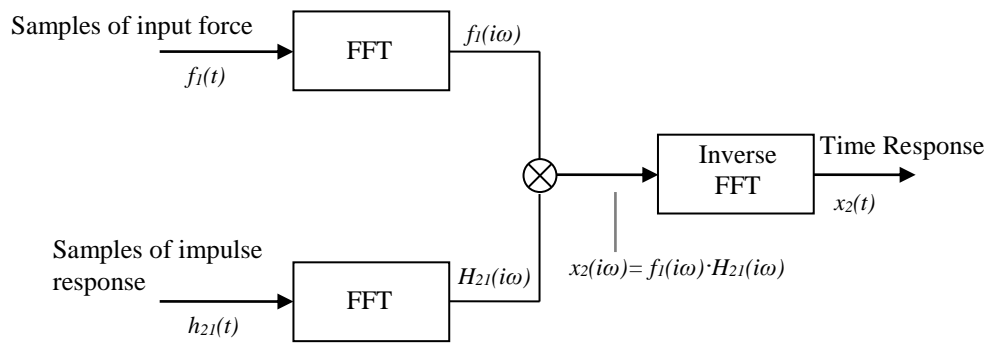
Figure 4.7 Obtaining time response procedure with signal analysis.

Figure 4.8 shows a comparison between time history responses of $x_2(t)$ obtained from three different methods. Figure 4.9 shows a zoomed view of the boxed region of the response plots.
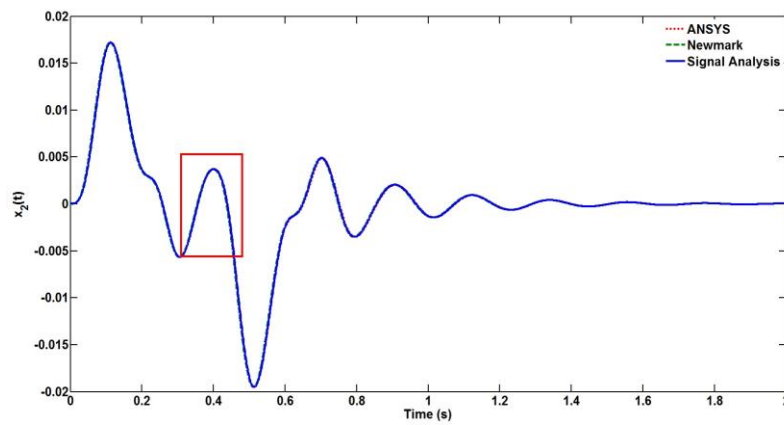
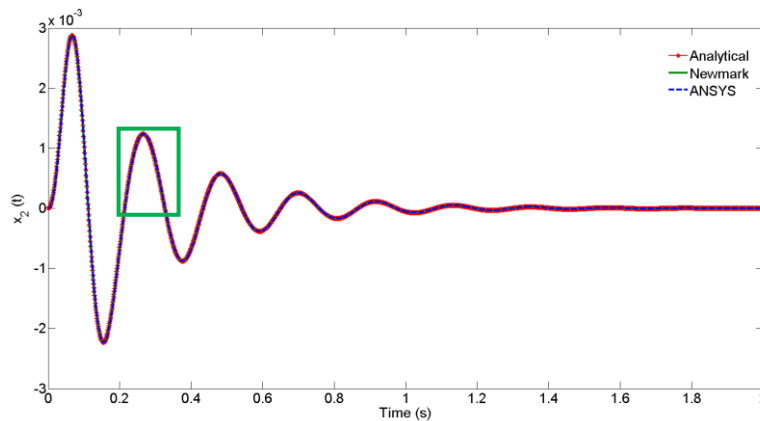Figure 4.8 Time history responses of $x_2(t)$ with three different methods.
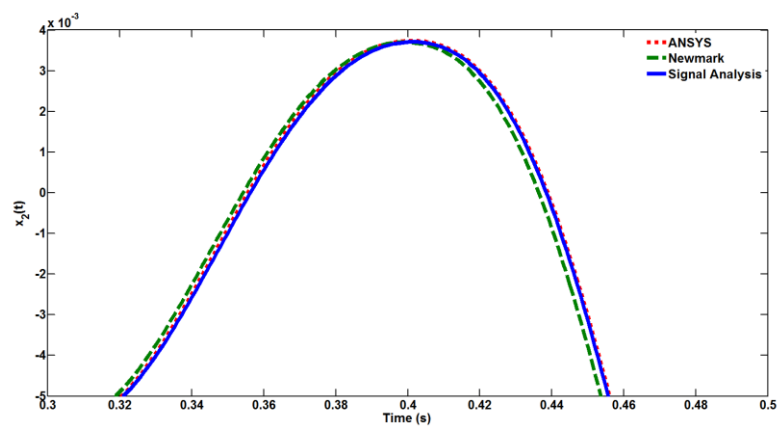

Figure 4.9 Zoomed view of time history responses of $x_2(t)$ with three different methods.

In Figure 4.9, the time history responses are clearly the same in all three different models. Thus, the impulse response function can be used to obtain the time history response of numerous degrees of freedom system rather than transient finite element analysis and the method is fast and simple.

4.3 Residual Vibration Control of Linear Motion System

To control the residual vibrations of LMS, trapezoidal velocity profile as seen in Figure 4.10 is applied with open loop control. Time parameters of velocity profile is defined by t=[t_a,t_c,t_d,t_m]. Where, t_a is acceleration time, t_c is constant velocity time, t_d is deceleration time, t_m is motion time.

In the studies about the control of residual vibrations reported that if t_d is selected to be equal to times of period which determined by first natural frequency for triangular and cycloidal velocity profile, the residual vibration control is satisfied (Ankarali & Diken ,1997; Diken & Alghamdi, 2003; Ankaralı , Mecitoğlu & Diken, 2012). Hence, time parameters of velocity profile can be determined according to information about system dynamics.
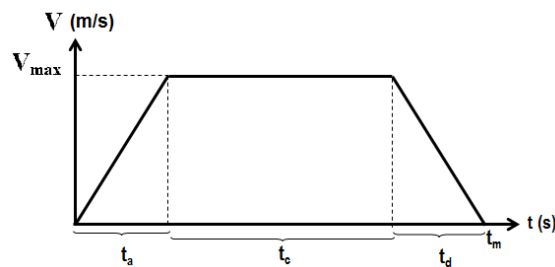
Figure 4.10 Trapezoidal motion profile.

The velocity profile is applied to z–axis (LM-z see Figure 3.4 Chapter three) both experiment and finite element analysis. t_a , t_d , t_c , t_m are described by

$$t_d = r_f \frac{1}{2 f_i}, \quad t_c = t_d, \quad t_a = t_m - t_c - t_d \tag{4.8}$$

Where, f_i (Hz) is natural frequency of the system and r_f indicates times of the half period which determined by natural frequency. f_i is chosen as f_{bx} =10.12 Hz (see Table 3.7 in Chapter three) in experiments due to z- axis motion is excited the bending vibration about the x- axis. f_i is chosen as f_{bx} =10.73 Hz for the transient finite element analysis in ANSYS.

The axes are driven with ADLINK/PCI-8366 control card. The velocity profile is given to servomotors with a developed VisualBASIC program which is used ADLINK-ActiveX components (ADLINK Technology Inc., 2012).

Motion is defined A position to B position (see Figure 4.11). Quantity of motion is 100 mm. Start position q_e=[0,0,100] at A point, finish position q_e=[0,0,0] at B point. Experiments are conducted for r_f=1, r_f=2. Acceleration signals are recorded at E point with wireless accelerometer sensor.
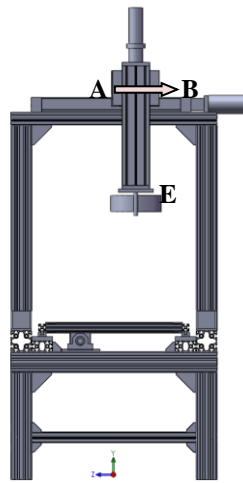
Figure 4.11 z- axis motion position.

In the finite element model, the trapezoidal velocity profile the same as the experiments is applied a point which is created approximately the center of mass of z − axis. Transient analyses are employed in ANSYS for r_f=1, r_f=2.

Recorded acceleration signals by experiments and time history of accelerations of E point which are obtained transient finite element results are shown in Figure 4.12

and residual vibrations are shown in Figure 4.13. The solution time of transient analysis is 2669 second in ANSYS. Solution time is given for Computer Type-1 (see Table 2.9 Chapter two).
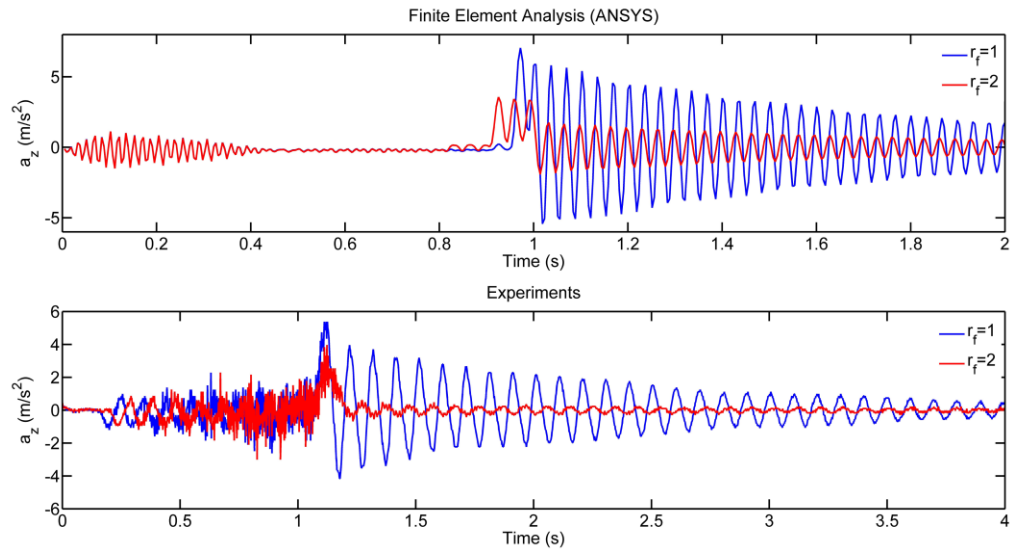
Figure 4.12 Recorded acceleration signals by experiments and time history of accelerations (ANSYS).
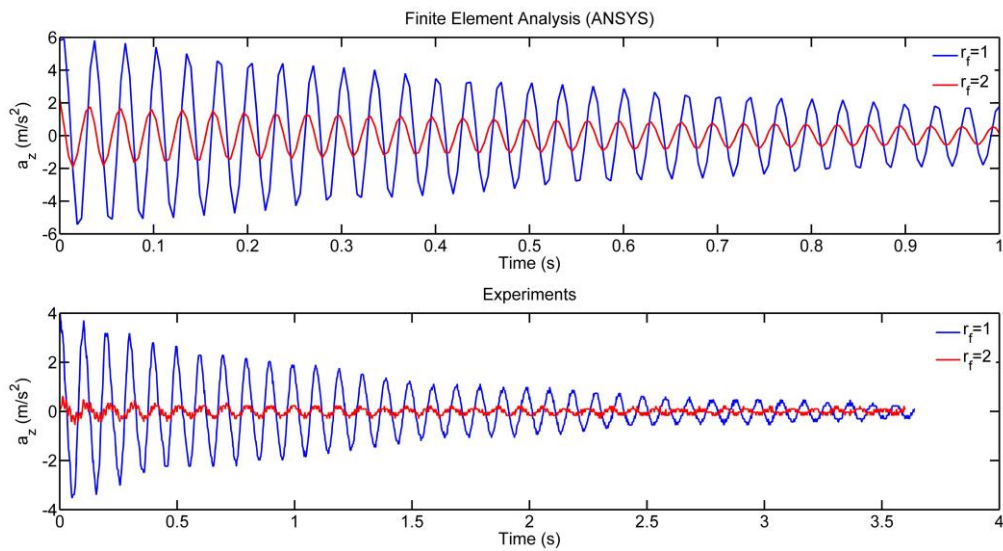
Figure 4.13 Residual vibrations.

According to the experimental results, vibration magnitudes of E point are decrease significantly. This decrement is also observed from finite element results.

76

Percentage differences between RMS values of residual vibrations are given in Table 4.1.

Table 4. 1 Comparison of residual vibration RMS values.

	r_f	a_z RMS	a_z % Decrement
Experiment	1	1.0916	87.04
	2	0.1415	
FEA	1	2.6251	68.84
	2	0.8180	

Percentage value of decrement in experiment is higher than percentage value of decrement in finite element results as seen in Table 4.1. This difference may be become from the assumptions in finite element model and boundary conditions. Decrements of vibration magnitudes are clearly observed with frequency spectrums of experimental residual vibrations as seen in Figure 4.14.
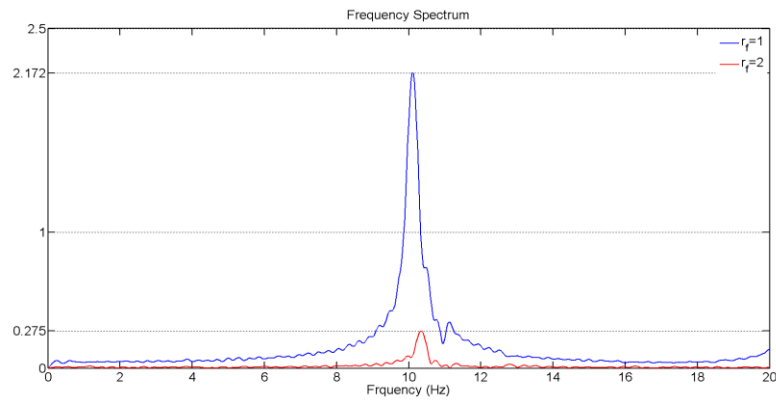
Figure 4.14 Frequency spectrums of residual vibrations.

As a result, open loop control is applied both experimental and simulation. The experiment results are good agreement with finite element analysis results.

4.4 Dynamic Responses of Linear Motion System with Signal Analysis

In this section, linear motion system is considered in terms of dynamic behavior. The method represented in Section 4.2 is used to obtain the dynamic response of the system.

To obtain the dynamic response of the system, firstly, impulse response of the system is obtained from ANSYS finite element model. The impulse response is obtained at position $\mathbf{q_e}$ =[0,0,0]. The impulse force is applied at E point (see Figure 4.15) in z- direction. The impulse time is taken as $dt=(1/f_{bx})/20$. Simulation time is 2 second. Finite element impulse response and its frequency spectrum are shown in Figure 4.16. Experimental response and its frequency response are shown in Figure 4.17. In the experiment, the sampling rate is 617 Hz. The system is excited by a hammer impact at E point in z- direction. Low-pass digital filter is used with cutoff frequency 25 Hz in MATLAB for frequency spectrums.
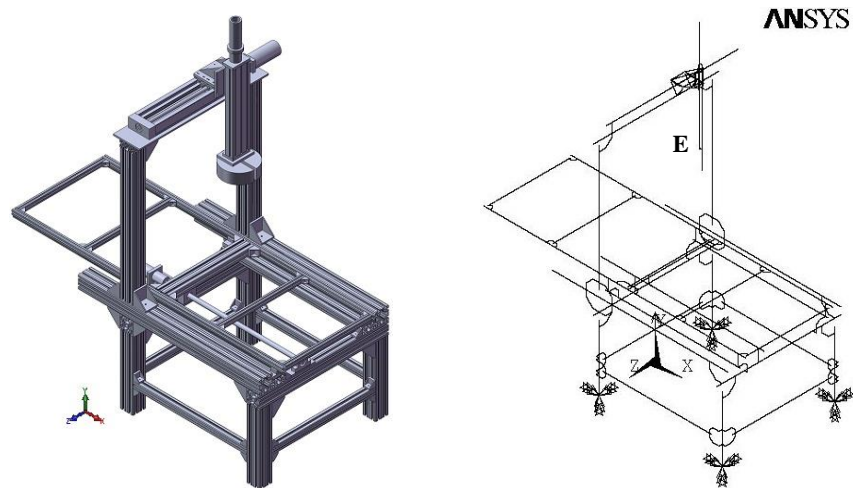
Figure 4.15 Position which is obtained impulse response.
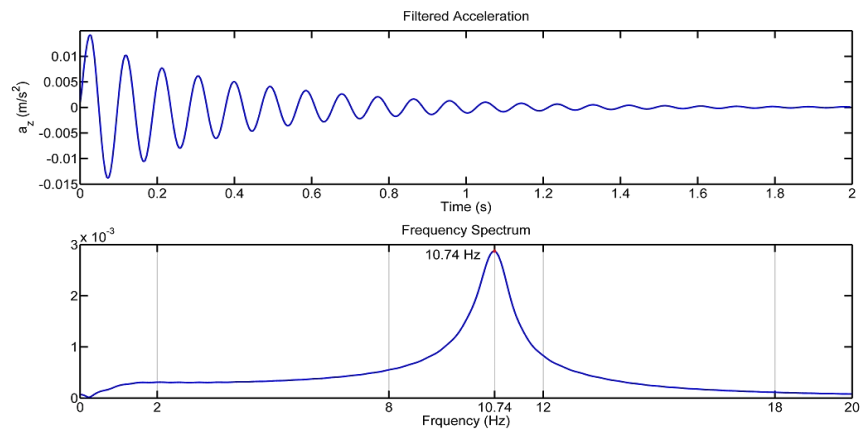
Figure 4.16 Impulse response and frequency spectrum from FEA.
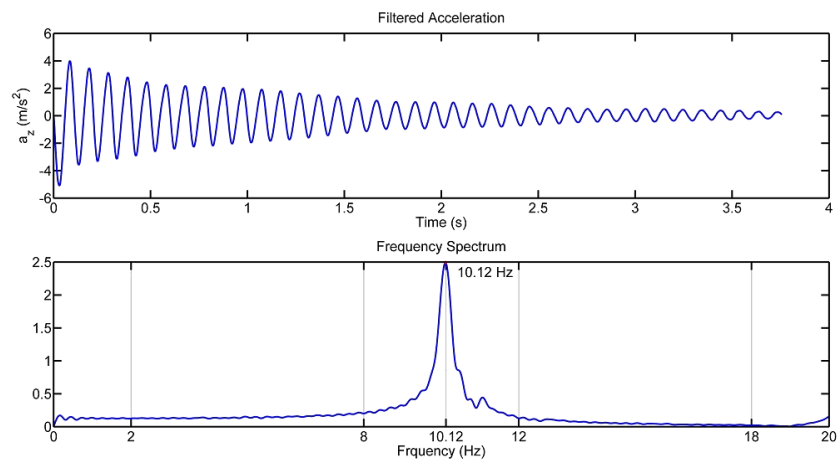
Figure 4.17 Impulse response and frequency spectrum from experiment.

The input parameters for an excitation force as seen in Figure 4.6 are chosen as $f_1=[100,-100]$, $t=[0.9068,0.0466.,0.0466,2]$. The acceleration response of E point (see Figure 4.15) in z- direction is acquired according to procedure which is illustrated in Figure 4.7. Also, the excitation force is applied at E point in z- direction for ANSYS transient analysis. The acceleration response of E point is obtained in ANSYS. Figure 4.18 shows comparison between transient response of signal analysis and ANSYS transient analysis. Transient finite element analysis solution time is1786 seconds in ANSYS. Signal analysis solution time is 0.13478 second. Solution time is given for Computer Type-1 (see Table 2.9 Chapter two). Figure 4.19 shows a zoomed view of the boxed region of the response plots.
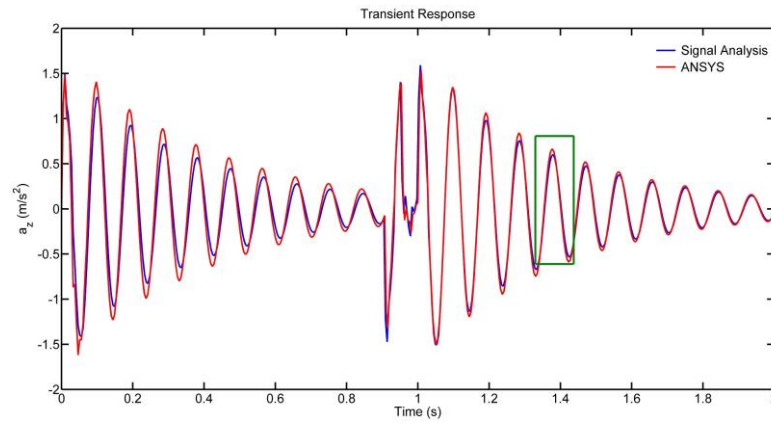
Figure 4.18 Comparison transient responses of E point acceleration.
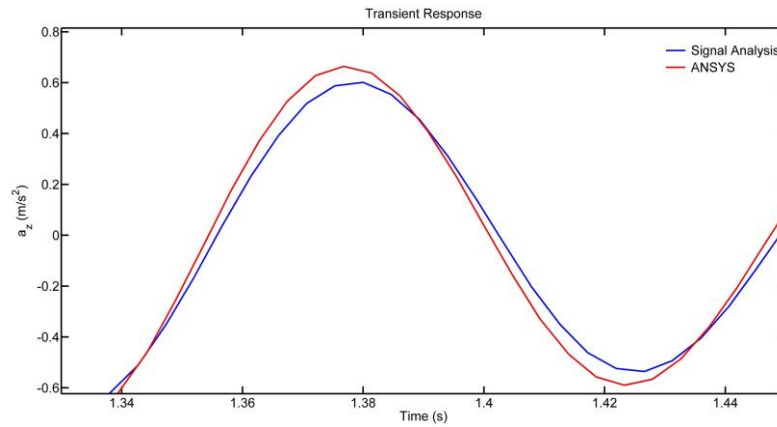
Figure 4.19 Zoomed view of transient responses of E point acceleration.

Signal analysis results are also obtained for the input parameters which are determined substituting numerical values $r_f=1$, $r_f=2$ in Equation 4.8 previous section. The results for $r_f=1$, $r_f=2$ values are depicted in Figure 4.19. Signal analysis solution time is 0.110291 second.
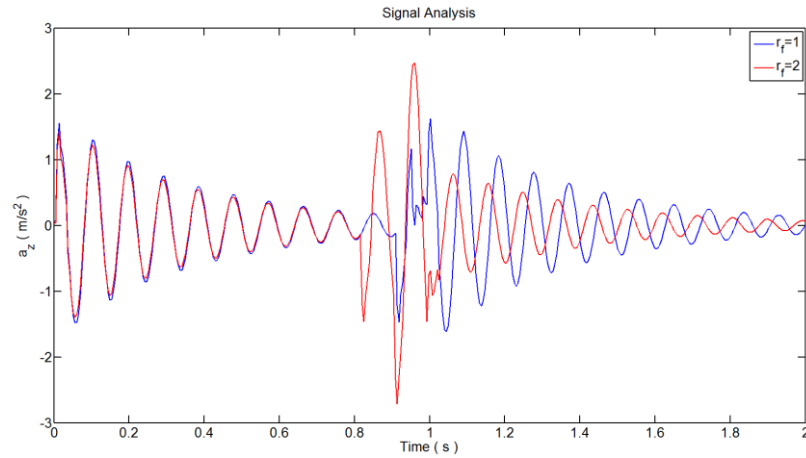
Figure 4.20 Signal analysis results for $r_f=1$, $r_f=2$.

As a conclusion, impulse response approach with signal analysis is applied for different input forces. The results which are given in Figure 4.20 shows parallel behavior to the results are given in Figure 4.13. In other word, decrements of residual vibrations are observed according to results in Figure 4.20 and Figure 4.14. Impulse response approach is fast and simple method according to comparison between ANSYS results and signal analysis results.

CHAPTER FIVE

CONCLUSIONS

Many machines run under dynamic working conditions. The main research area is the vibrations produced under dynamic conditions. The finite element method has been developed for modeling of realistic complex engineering systems. Structural modal parameters, such as natural frequencies, mode shapes can be determine by using finite element method.

In this thesis, the finite element analysis of a vertical machining center which constructed with modular aluminum profile systems is studied. Properly, the aluminum framing systems are extensively used in automation systems. They have the advantages such as shorter assembly time, fewer tools, flexible expansion and conversion, providing clean work environment, and reusable components.

A finite elements model of the vertical machining center is developed by using ANSYS parametric design language (APDL). A VisualBASIC program developed in this study uses a database to transfer the information about the system to the pre-processor of the FE-program. The same database is used to obtain solid models in SolidWorks by VisualBASIC commands.

Contribution of this thesis is a new approach for the finite element analysis of a vertical machining center which consists of linear motion systems (LMS) by beam elements. Proposed modeling approach not only aluminum structures but also can be applied steel structures. BEAM44 finite elements are used for modeling all parts of the system in ANSYS. In order to define connector elasticity, equivalent connector beams are obtained by using solid finite element results.

Vibration analysis results have been employed in ANSYS. However, there is need to validate accuracy of the finite element model. For this reason, experimental modal testing is carried out to measure the natural frequencies. And then, finite elements

model of the system is improved according to comparison between the finite elements analysis results and modal tests results.

Static analysis results have been employed in ANSYS. Evaluating charts are prepared by using the static analysis results obtained by ANSYS for further evaluations in developed VisualBASIC program. However, the values which are given in these charts are yet to be validated experimentally.

Vibrations are occurred along the period of the motion and after finished the motion due to inertia forces in flexible systems. Decreasing of the residual vibrations is more important subject in flexible systems in terms of precision of the positioning. Dynamic analyses of the system are employed in for the control purpose of residual vibrations. The trapezoidal motion profile is applied with open loop control. To validate the analyses, experiments are conducted. It is also, signal analysis method is used to predict the dynamic behavior of the system.

The future works in order to extend this study can be summarized as follows,

- Including the joint flexibilities between the moving parts in the linear motion systems proposed model, time dependent dynamics analysis can be improved.

- It will be useful to conduct an experimental study in order to check evaluating charts results.

- Controlling design can be added to this work in terms of high positioning accuracy.

- Drilling and milling processes are another interesting subject that can be examined by improving the finite element model proposed.

REFERENCES

Adlink PCI-8372+/8366+ cPCI-8312H SSCNET motion control card user's manual (2008). Retrieved August 31, 2012, from http://www.adlinktech.com/PD/marketing/Manual/PCI-8372++8366+/SSCNET_Series_Manual_50-1H001-1020_204.pdf

Akdağ, M. (2008). *Design and analysis of robot manipulators by integrated CAE procedures.* Ph.D. Thesis. İzmir: Dokuz Eylül University Graduate Scholl of Natural and Applied Sciences.

Akdağ, M., Karagülle, H. & Malgaca, L. (2012). An integrated approach for simulation of mechatronic systems applied to a hexapod robot. *Mathematics and Computers in Simulation*, *82* (5), 818-835.

Altintas, Y., Verl, A., Brecher, C., Uriarte, L. & Pritschow, G. (2011). Machine tool feed drives. *College International pour la Recherche en Productique Annals – Manufacturing Technology*, *60* (2), 779-796.

Ankarali, A., Diken, H. (1997). Vibration control of an elastic manipulator link, *Journal of Sound and Vibration, 204*(1), 162-170.

Ankaralı, A., Mecitoğlu, Z. & Diken, H. (2012). Response spectrum of a coupled flexible shaft-flexible beam system for cycloidal input motion, *Mechanism and Machine Theory, 47*, 89–102.

Bais, R.S., Gupta, A.K., Nakra, B.C. & Kundra, T.K. (2004). Studies in dynamic design of drilling machine using updated finite element models. *Mechanism and Machine Theory*, *39* (12), 1307-1320.

Bamberg, E. (2000). *Principles of rapid machine design*. Ph.D. Thesis. Massachusetts: Massachusetts Institute of Technology.

Benosman M., Le Vey G. (2004). Control of flexible manipulators: A survey. *Robotica 22*, 533-545.

Bosch Rexroth AG (2007). *Linear motion technology handbook.* Germany.

Chen, J.S., Huang, Y.K. & Cheng, C.C. (2004). Mechanical model and contouring analysis of high-speed ball-screw drive systems with compliance effect, *The International Journal of Advanced Manufacturing Technology*, *24* (3-4), 241–250.

Code of Federal Regulations (1986). *Published by the Office of the Federal Register National Archives and Records Administration.* Washington D.C: Retrieved February 29, 2012, from http://www.google.com.tr/books?id=oJw5AAAAIAAJ&printsec=frontcover&hl=tr&source=gbs_ge_summary_r&cad=0#v=onepage&q&f=false

Diken H., Alghamdi A. A. A. (2003). Residual vibration response spectra for a servomotor-driven flexible beam, *Journal of Mechanical Engineering Science*, *217* (5), 577-583.

Du, Z., Zhang, S. & Hong, M. (2010). Development of a multi-step measuring method for motion accuracy of NC machine tools based on cross grid encoder. *International Journal of Machine Tools & Manufacture*, *50* (3), 270-280.

Dwivedy S.K., Eberhard P. (2006). Dynamic analysis of flexible manipulators, a literature review, *Mechanism and Machine Theory, 41*, 749–777.

Garitaonandia, I, Fernandes & M.H., Albizuri. (2008). Dynamic model of a centerless grinding machine based on an updated FE model. *International Journal of Machine Tools & Manufacture*, *48* (7-8), 832-840.

Guan, Y., Ren, L., Sun, J. & Mu, D. (2010). Analysis and optimization of crossbeam of gantry machining center. *2nd International Conference on Information Engineering and Computer Science (ICIECS)*. Wuhan, China. Retrieved February 29, 2012, from http://ieeexplore.ieee.org/stamp/stamp.jsp?tp=&arnumber=5678295

History of numerical control (n.d.). Retrieved August 17, 2012, from http://www.losgatosmanufacturing.com/classes/handouts /history_of_numerical_control.pdf

Huang, D.T.Y, Lee, J.J. (2001). On obtaining machine tool stiffness by CAE. *International Journal of Machine Tools & Manufacture*, *41* (8), 1149-1163.

Hung, J.P., Lai, Y. L., Lin, C. Y. & Lo, T. L. (2011). Modeling the machining stability of a vertical machine under the influence of the preloaded linear guide. *International Journal of Machine Tools & Manufacture*, *51* (9), 731-739.

Kamalzadeh, A. (2008). *Precision control of high speed ball screw drives*. Ph.D. Thesis. Waterloo, Ontario, Canada: University Waterloo.

Karagülle, H., Malgaca, L. (2004). Analysis of end point vibrations of a two-link manipulator by integrated CAD/CAE procedures. *Finite Elements in Analysis and Design, 40* (15), 2049-2061.

Khim, G., Park, C. H., Shamoto, E. & Kim, S. W. (2011). Prediction and compensation of motion accuracy in a linear motion bearing table. *Precision Engineering*, *35* (3), 393-399.

Lee, S. W., Mayor, R. & Ni, J. (2006). Dynamic analysis of a mesoscale machine tool. *Journal of Manufacturing Science and Engineering*, *128* (1), 194-203.

Light, T.V., Gorlach, I.A. & Wiens, G.J. (2011). Dynamic modeling of a special purpose CNC machine. *Proceedings of the 15th WSEAS International Conference on System,* 207-213, Corfu Island, Greece. Retrieved January 01, 2012, from http://www.wseas.us/e-library/conferences/2011/Corfu/SYSTEMS/SYSTEMS-32.pdf.

Lin, C.Y., Hung, J.P. & Lo, T. L. (2010). Effect of preload of linear guides on dynamic characteristics of a vertical column-spindle system. *International Journal of Machine Tools & Manufacture*, *50* (8), 741-746.

Liu, G.R., Quek, S.S. (2003). *The finite element method: A practical course.* Oxford, Burlington: Elsevier Science Ltd.

Mahdavinejad, R. (2005). Finite element analysis of machine and workpiece instability in turning. *International Journal of Machine Tools & Manufacture*, *45* (7-8), 753-760.

Mimmi, G., Pennacchi, P. (2001) Pre-shaping motion input for a rotating flexible link, *International Journal of Solids and Structures,* 38, 2009-2023.

Ohta, H., Hayashi, E. (2000). Vibration of linear guideway type recirculating linear ball bearings. *Journal of Sound and Vibration*, *235*(5), 847-861.

Okwudire, C. (2005). *Finite element modeling of ballscrew feed drive systems for control purposes.* M.Sc. Thesis. Vancouver, Canada: The University of British Columbia.

Osborne, G.M. (2006). *Finite element concept modeling methodologies and software implementation for vehicle assemblies comprised of beam-like structural members.* Ph.D. Thesis. Louisville, Kentucky: Department of Mechanical Engineering University of Louisville.

Pham, D.T. (Ed.). (2008). *Theory and design of CNC systems*. London: Springer-Verlag London Limited.

Pereira E., Trapero J R., Diaz I. M. & Feliu V. (2012). Adaptive input shaping for single-link flexible manipulators using an algebraic identification, *Control Engineering Practice, 20*, 138–147.

Preumont A. (2002.) *Vibration control of active structures an introduction, Second ed*.: Kluwer Academic Publishers, Netherlands.

Rao, S.S. (1995). *Mechanical vibrations* (3rd ed.). Addison-Wesley Publishing Company.

Reynoso, A.G. (1985). *Structural dynamics model of a cartesian robot.* Ph.D. Thesis. Massachusetts: Massachusetts Institute of Technology.

Shan J., Liu H-T. & Sun D. (2005) Modified input shaping for a rotating single-link flexible manipulator, *Journal of Sound and Vibration*, *285*, 187–207.

Si, G.N., Yu, Y.Q. & Yang, J. X. (2010). Dynamic simulation of a multi-axis synchronous gantry machining center. *Second International Conference on Computer Modeling and Simulation*. 3, 95-98. Sanya, China. Retrieved February 29, 2012, from http://ieeexplore.ieee.org/stamp/stamp.jsp?tp=&arnumber=5421186.

Solidworks help documents (2007). Retrieved March 12, 2009, from http://help.solidworks.com/2010/English/SolidWorks/sldworks/LegacyHelp/Sldworks/Overview/StartPage.htm

Theory reference ANSYS release 12.1 (2009). Retrieved January 12, 2011, from http://www1.ansys.com/customer/content/documentation/121/ans_thry.pdf

Tizzard, A. (1994). *An Introduction to computer aided engineering*. England: McGraw-Hill Book Company Europe.

Varanasi, K. K., Nayfeh, S. A. (2004). The dynamics of lead-screw drives: Low-order modeling and experiments. *Journal of Dynamic Systems, Measurement, and Control, Transactions of the ASME, 126* (2) 388-396.

Vertical machining center patent. (1989). Retrieved August 17, 2012, from http://www.google.com/patents/US4797991?printsec=abstract&hl =tr#v=onepage&q&f=false

VisualBASIC 6.0 Help Documents (2011). Retrieved January 24, 2011, from http://msdn.microsoft.com/en-us/library/kehz1dz1%28v=vs.80%29.aspx

Weiwei, W. (2009). Finite element analysis of dynamic charateristic for the XK717 CNC milling machine. *International Conference on Measuring Technology and Mechatronics Automation.* 2, 803-805. Zhangjiajie, Hunan, China. Retrieved February 29, 2012, from http://ieeexplore.ieee.org/stamp/stamp.jsp?tp=&arnumber=5203554

Weule, H., Frank, T. (1999). Advantages and characteristics of a dynamic feeds axis with ball screw drive and driven nut. *College International pour la Recherche en Productique Annals – Manufacturing Technology. 48* (1), 303-306.

Wu, J.J. (2004). Finite element modeling and experimental modal testing of a three-dimensional framework. *International Journal of Mechanical Sciences, 46* (8), 1245-1266.

Xi, F., Qin, Z. (1998). An integrated approach for design and analysis of a fluid mixer. *Computer Aided Design*, *30* (13), 1037-1045.

Yi, Y.S., Kim, Y.Y., Choi, J.S., Yoo, J., Lee, D. J., Lee, S.W., et al. (2008). Dynamic analysis of a linear motion guide having rolling elements for precision positioning devices. *Journal of Mechanical Science and Technology*, *22* (1), 50-60.

Zaeh, M.F., Oertli, T. & Milberg, J. (2004). Finite element modelling of ball screw feed drive systems. *College International pour la Recherche en Productique Annals – Manufacturing Technology*, *53* (1), 289-292.

Zaeh, M., Siedl, D. (2007). A new method for simulation of machining performance by integrating finite element and multi-body simulation for machine tools, *College International pour la Recherche en Productique Annals – Manufacturing Technology*, *56* (1), 383-386.

Zhou, Y., Peng, F.Y. & Cao, X.H. (2011). Parameter sensitivity analysis of axial vibration for lead-screw feed drives with time-varying framework. *Mechanika*, *17*(5), 523-528.

APPENDICES

APPENDIX A1

A1. BEAM44 PROPERTIES OF USED PROFILE SECTIONS

The profiles are made of Al-6063-T6.

30X30


```
SECTION ID 1
DATA SUMMARY

Section Name
    =
Area
    = .316E-03
Iyy
    = .276E-07
Iyz
    = -.184E-15
Izz
    = .276E-07
Warping Constant
    = .811E-12
Torsion Constant
    = .343E-08
Centroid Y
    = .564E-11
Centroid Z
    = -.208E-10
Shear Center Y
    = -.502E-06
Shear Center Z
    = .506E-06
Shear Corr. YY
    = .298674
Shear Corr. YZ
    = -.131E-04
Shear Corr. ZZ
```

45X45L


```
SECTION ID 1
DATA SUMMARY

Section Name
    =
Area
    = .574E-03
Iyy
    = .110E-06
Iyz
    = -.509E-14
Izz
    = .110E-06
Warping Constant
    = .974E-11
Torsion Constant
    = .175E-07
Centroid Y
    = -.158E-08
Centroid Z
    = -.110E-07
Shear Center Y
    = .231E-06
Shear Center Z
    = -.137E-06
Shear Corr. YY
    = .24178
Shear Corr. YZ
    = .238E-04
Shear Corr. ZZ
```

91

45X90L


```
SECTION ID 1
DATA SUMMARY

Section Name
  =
Area
  = .001121
Iyy
  = .808E-06
Iyz
  = -.418E-13
Izz
  = .235E-06
Warping Constant
  = .724E-10
Torsion Constant
  = .128E-06
Centroid Y
  = .350E-08
Centroid Z
  = .239E-08
Shear Center Y
  = .682E-06
Shear Center Z
  = .792E-06
Shear Corr. YY
  = .308129
Shear Corr. YZ
  = -.303E-05
Shear Corr. ZZ
```

90X90


```
SECTION ID 1
DATA SUMMARY

Section Name
  =
Area
  = .003894
Iyy
  = .302E-05
Iyz
  = -.631E-12
Izz
  = .302E-05
Warping Constant
  = .113E-09
Torsion Constant
  = .153E-05
Centroid Y
  = -.493E-08
Centroid Z
  = .651E-09
Shear Center Y
  = .240E-06
Shear Center Z
  = .556E-06
Shear Corr. YY
  = .307422
Shear Corr. YZ
  = -.219E-04
Shear Corr. ZZ
  = .307426
```
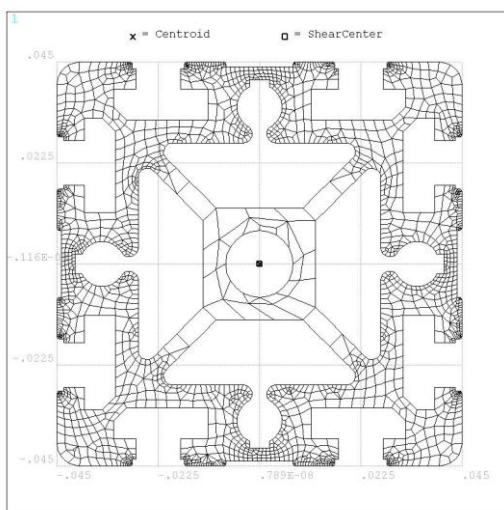
92

A1. EXPERIMENTAL RESULTS FOR DIFFERENT POSITIONS

$f=[f_{bx}, f_{bz}]$

q_e=[0,0,0], f=[10.12, 11.09]	q_e=[0,0,200], f=[10.30, 11.69]	q_e=[0,0,400], f=[10.30, 11.51]
q_e=[350,0,0], f=[10.30, 11.51]	q_e=[700,0,0], f=[10.36, 11.09]	q_e=[700,100,0],f=[10.60,11.69]
q_e=[700,100,200], f=[10.57, 12.14]	q_e= [700,100,400], f=[10.57, 12.02]	q_e=[350,100,200], f=[10.54, 12.11]

A1. FFT CODE FOR EXPERIMENTAL RESULTS

```matlab
clc;clear;close all

fcut=20;
tcut=1.238;
h=xlsread('D:\kr\matlab\M1t_1D\m1t_2a.csv');

fc=25;
ndata=h(:,1);[L,V]=size(ndata);


tdata=ndata(14:L,1);
xdata=h(14:L,4);
ydata=h(14:L,3);
zdata=h(14:L,2);


fs=617; % Sampling Frequency
nfft=1024*20;
ns=(L-14);dt=1/fs;ts=dt*(ns);t=0:dt:ts;nt=length(t)-1;


t1=find(t>=tcut);t1=t1(1);
t=t(t1:nt);t=t-tcut;

xdata=xdata(t1:nt);
ydata=ydata(t1:nt);
zdata=zdata(t1:nt);

xdata=xdata-mean(xdata);
ydata=ydata-mean(ydata);
zdata=zdata-mean(zdata);

xdata=[0;xdata];
ydata=[0;ydata];
zdata=[0;zdata];

t=[0,t];

%% Low Pass Filter
 fn=fs/2;     % Nyquist Frequency
 [b,a]=butter(2,fc/fn,'low');
 xdata=filter(b,a,xdata);
 ydata=filter(b,a,ydata);
 zdata=filter(b,a,zdata);
```

```matlab
%% Use FFT
h=zdata;
hf=fft(h,nfft);
ampl=abs(hf)*dt;
ampl=ampl(1:1+nfft/2);
fs=1/dt;df=fs/nfft;f=0:df:df*nfft/2;
f1=find(f>=fcut);f1=f1(1);
f=f(1:f1);
ampl=ampl(1:f1);
[i,j]=max(ampl);main_frequency=vpa(f(j),6)
mainFreqStr=num2str(f(j));
plot(f,ampl),xlabel('Frquency (Hz)')
hold on
plot(f(j),ampl(j),'r.', 'MarkerSize',15);
text(f(j)+0.25,ampl(j),['f = ',mainFreqStr,' Hz']);
```

A1. MATLAB CODE FOR TWO DEGREES OF FREEDOM SYSTEM

```matlab
%% Inputs
clc,clear;close all;

facel=100;
fdecel=-100;
tacel=0.2;
tconst=0.2;
tdecel=0.2;

m1=5.8;m2=3.2;c1=37.2;c2=33.5;c3=32;k1=4325;k2=3850;k3=3500
;
m=[m1,0;0,m2];c=[c1+c2,-c2;-c2,c2+c3];k=[k1+k2,-k2;-
k2,k2+k3];
dt=0.001;tson=2;t=0:dt:tson;ns=length(t);

%% Input Force Profile

f=0;tprev=0;
tt=tprev+dt:dt:tprev+tacel;n=length(tt);
ff=facel*ones(1,n);f=[f,ff];tprev=tprev+tacel;
tt=tprev+dt:dt:tprev+tconst;n=length(tt);
ff=facel*zeros(1,n);f=[f,ff];tprev=tprev+tconst;
tt=tprev+dt:dt:tprev+tdecel;n=length(tt);
ff=fdecel*ones(1,n);f=[f,ff];tprev=tprev+tdecel;
tt=tprev+dt:dt:tson;n=length(tt);
ff=fdecel*zeros(1,n);f=[f,ff];tprev=tprev+tdecel;

[s1,st1]=size(t);[s2,st2]=size(f);ns1=st1-st2;

for i=1:ns1
    if ns1==0
        f=[f];
    else
        f(st2+i)=0;
    end;
end;
fl=fopen('profil.txt','w');
fprintf(fl,'%f\r\n',f);fclose(fl);
plot(t,f);title('Excitation Force');
xlabel('Time (s)'),ylabel('F (N)');grid on

%% NEWMARK Integration
ms=m;cs=c;ks=k;f0=1;
gama=0.005;
tson2=tson+dt;
nb=2;nforce=1;nresp=2;
%----------------------------------------
```

```
alpha=0.25*(1+gama)^2;delta=0.5+gama;
a0=1/(alpha*dt^2);a1=delta/(alpha*dt);
a2=1/(alpha*dt);a3=1/(2*alpha)-1;
a4=delta/alpha-1;a5=(dt/2)*(delta/alpha-2);
a6=dt*(1-delta);a7=delta*dt;
t2=0:dt:tson2;ns2=length(t2);
u(1:nb,1:ns2)=0;u1(1:nb,1:ns2)=0;u2(1:nb,1:ns2)=0;
%---
mat1=a0*ms+a1*cs+ks;mat1=inv(mat1);
for n=2:1:ns2;
    fs(1:nb,1)=0;;if n==2;fs(nforce)=f0/dt;end
    up=u(1:nb,n-1);u1p=u1(1:nb,n-1);u2p=u2(1:nb,n-1);
    uc=fs+ms*(a0*up+a2*u1p+a3*u2p)+cs*(a1*up+a4*u1p+a5*u2p);
    uc=mat1*uc;
    u2c=a0*(uc-up)-a2*u1p-a3*u2p;
    u1c=u1p+a6*u2p+a7*u2c;
    u(1:nb,n)=uc;u1(1:nb,n)=u1c;u2(1:nb,n)=u2c;
end
h=u(nresp,1:ns2);h=h(1,2:ns2);
plot(t,h)
fl=fopen('impnmark.txt','w');
fprintf(fl,'%f\r\n',h);fclose(fl);

%% Impulse Response (Analytical Model)
n21=25*[67,7700];dh=[928,30307,3614930,39857875,2263187500]
;
ampl=1;
ampl=(2263187500/7700);
[r,p,kk]=residue(ampl*n21,dh);
r,p
a1=abs(2*r(2)),fi1=angle(r(2))
a2=abs(2*r(4)),fi2=angle(r(4))

h=587.9028*exp(-12.5674*t).*cos(51.8931*t+1.5643);
h=h+1053*exp(-3.7618*t).*cos(29.0054*t-1.5744);
h=h/ampl;
fl=fopen('impa.txt','w');
fprintf(fl,'%f\r\n',h);fclose(fl);
plot(t,h)

%% Signal Analysis (Impulse Response Approach)
h=load('impansys.txt');h=h(:,2);h=transpose(h);h=[0,h];
f=load('profil.txt');f=transpose(f);
ffth=fft(h);
fftf=fft(f);
fftx=ffth.*fftf;
x=dt*ifft(fftx);x=[x];
plot(t,x)
fl=fopen('trsfft.txt','w');
fprintf(fl,'%f\r\n',x);fclose(fl);
```

A1. TRANSIENT FINITE ELEMENT RESULTS OF LMS

FEA Results of E point

FEA Results of Center of Mass point z-Axis

FEA Results of Car-3 of z-Axis

FEA Results of Car-3 of z-Axis

FEA Results of Car-3 of z-Axis

100